Diarrheal Diseases Caused by Eukaryotic Microbes: From Murine Models to their Transcriptomes

By

Carolina Mendoza Cavazos

A dissertation submitted in partial fulfillment of

the requirements for the degree of

Doctor of Philosophy

(Microbiology)

at the

UNIVERSITY OF WISCONSIN-MADISON

2022

Date of final oral examination: 07/21/2022

The dissertation is approved by the following members of the Final Oral Committee:

Laura J. Knoll, Professor, Medical Microbiology and Immunology
Christina M. Hull, Professor, Biomolecular Chemistry
Federico E. Rey, Professor, Bacteriology
Phillip Newmark, Professor, Integrative Biology
Karthik Anantharaman, Assistant Professor, Bacteriology

Table of Contents

Acknowledgments

The work on this thesis was conducted by me and other scientists but it wouldn't be possible if the following people were not in my life. This thesis is dedicated to them.

To my advisor, who has portrayed what being a woman in science can look like. Laura, I appreciate how frank and real you are. I knew this was the lab for me a week in when you came in wearing sweatpants and we chatted about what science was interesting to me. Thank you for taking a chance on me, it has been an honor to be your first non-*Toxoplasma* graduate student.

To my family who has given me so much, including the privilege of making my own choices. To my parents, I love you both. Thank you for always being there. To my grandfather, si me gradué Tito! To the rest of my family, Mexican and Indian, it is the best to be called Mija/Beta by you, thank you for your unconditional support.

To my lab mates (current and former), you guys made the work easier and provided a safe space to be myself. You made my good days the best and my bad days a little better. Your scientific curiosity will stay with me forever. I love your weird quirks, your gossip, your pets, your kids, and above all your humor. You have been a great support system and I cannot wait to see what the future brings for you.

To my sister, who has taught me that social justice is everybody's responsibility. You have been an inspiration to become an active member of my community. It has been wonderful to see you grow from a pepina to the woman you are today. Dana, I have loved going through the DEI journey with you.

To my husband, who has been supportive, loving, and an absolute cheerleader through this journey. Thanks for always being in my corner, always reassuring me that I am strong, intelligent, and capable enough to earn this Ph.D. Thank you for giving me a space to be as vulnerable as I needed and for loving me as unconditionally as you do. Apu, I am so grateful I get to call you my life partner, you bring so much joy to my life.

Lastly, I dedicate this thesis to my mental health, which I struggled with a lot during graduate school. However, these struggles propelled a journey of self-reflection and healing. If you, the reader, think your mental health is struggling, please consider seeking help. Focusing on my mental health, attending therapy, and finding the medication to manage my depression were some of the best decisions I made in graduate school.

Chapter 1. Introduction

Entamoeba histolytica: Five facts about modeling a complex human disease in rodents

The text in this chapter is a reformatted version of a published article.

Citation

Mendoza Cavazos C, Knoll LJ (2020) ***Entamoeba histolytica*: Five facts about modeling a complex human disease in rodents**. PLoS Pathog 16(11): e1008950.

DOI link

Acknowledgments

Due to space limitations, we were unable to include all the work of colleagues but would like to thank them for their contributions to the *Entamoeba histolytica* field. We would also like to thank Sarah Wilson and Apoorva Maru for their critical read and editing of this manuscript.

Fact 1: Rodent models do not mimic the entire life cycle of E. histolytica

Entamoeba histolytica is an extracellular enteric eukaryotic parasite. Globally, an average of 500 million cases and 55,000 to 100,000 deaths are due to *E. histolytica* infection each year, primarily impacting the developing world (1, 2)). The world is widely unprepared for an outbreak of *E. histolytica* due to the lack of a vaccine and the use of a single drug type as treatment (reviewed in (3)). E. histolytica is the causative agent of the diarrheal disease known as amebiasis, but it can sometimes penetrate the intestinal wall, enter the circulation, and cause abscesses throughout the body, most commonly in the liver. *E. histolytica* has two main stages during its life cycle: the trophozoite and the cyst stage. The infectious agent is the cyst and is transmitted through the oral-fecal route via contaminated food or water. Animal models are not available for this stage interconversion, which is essential for disease propagation and pathogenesis. Excystation is the transition from the cyst form to the rapidly dividing trophozoite stage. Once a trophozoite, *E. histolytica* can either undergo invasive (5-10% of symptomatic infections) or non-invasive disease progression. As the parasite replicates during a non-invasive infection, it undergoes a second developmental change known as encystation, which involves the synthesis of a cyst wall to endure the exterior environment until a suitable host is encountered.

Because the cyst stage of *E. histolytica* cannot be induced in culture or rodents, *Entamoeba invadens* has served as an excellent model for the study of excystation and

encystation *in vitro*. Some examples of insights from the study of *E. invadens* include the identification of stage-specific promoters (4), cholesteryl sulfate impact on encystation efficiency (5), the negative regulation of encystation by Hsp90 *in vitro (6),* and the discovery of various transcription factor that regulate stage conversion (7, 8). A rodent model that produces *E. histolytica* cysts could be used to generate new treatments or vaccines for amebiasis by targeting parasite development. However, tremendous advances have been accomplished using the current infection model including vaccine development (reviewed in (9)), microbiota-parasite interactions (reviewed in (10)), host innate and adaptive immunity response to infection (reviewed in (11)), and molecular mechanisms responsible for tissue damage (reviewed in (12)).

Fact 2: Trophozoites can initiate infection in rodent models

A robust way to culture trophozoites has been developed in the laboratory setting (13) and has been the primary resource to perform in vivo infection. Trophozoites are surgically delivered into the target organ within the animal models. For intestinal studies, the trophozoites are injected into a surgically exposed cecum or an artificial colonic loop. While this procedure is invasive and bypasses the oral portion of the infection, the murine model has provided insight into many parasite-host interactions. These discoveries include, but are not limited to, alteration to Paneth cell function by *E. histolytica* infection (14), the genetic predisposition to disease progression due to host polymorphism in leptin receptors (15) or intergenic insertion previously linked to Inflammatory Bowel Disease (16), the ability to nibble on alive host cells (known as trogocytosis) (17), the discovery of pathogenicity of *Entamoeba moshkovskii* (18), and

microbiome mediated immune cell recruitment during *E. histolytica* infection (19, 20). To model invasive disease such as amoebic liver abscesses, trophozoites are delivered via intraportal inoculation to either hamsters or guinea pigs, (reviewed in (21)). Physiochemical factors encountered throughout the gastrointestinal tract can influence parasite development but are bypassed using these methodologies (22). To our knowledge, there are three studies conducted in the 1980s in which oral inoculation was performed with either cysts (23) or trophozoites (24, 25). *E. histolytica* strain SAW 408 trophozoites were orally inoculated into three types of rats, pre-treated with an antihistamine called cimetidine that blocks the production of stomach acid (24). The rats displayed the expected pathology in the intestinal tract 21 days post-infection. However, mice that were previously described as SAW 760 (Entamoeba dispar) or SAW 408 sensitive (26) did not display pathology by histology or shedding by wet mounts. A follow up study (27) tracked the health of rats 12 months after oral infection, concluding that infections can persist long-term. These studies highlight that rodents can be useful for studying the complex biology of E. histolytica but that more research is needed.

Fact 3: E. histolytica invasive disease can be modeled in rodents

E. histolytica disease outcomes range widely in humans: death, sepsis, liver abscesses, ulcers, dysentery, abdominal pain and mucoid diarrhea with occasional blood, and asymptomatic shedding. The fields focus on invasive disease is due to the pathogenicity of the trophozoite stage within the host, and the morbidity and mortality that invasive disease causes. One of the most widely used strains, HM-1: IMSS, was isolated from a

male patient admitted into a public hospital in Mexico City in 1967. Although the virulence of the initial isolate was high, this strain undergoes continuous culture passaging, so virulence has changed over the years. Some laboratories passage trophozoites through the cecum or liver of animal models to retain virulence (28, 29). Maintaining virulence in this strain has allowed modeling of invasive disease. Frontline researchers in the amebiasis community have contributed immeasurable knowledge using intestinal pathology and development of liver abscess as a measure of disease progression. Hamsters and guinea pigs are used for the study of invasive disease, especially for the development of liver abscesses, and are the preferred model for vaccine development (9). Various murine strains have been studied to determine what dictates susceptibility to *E. histolytica* infection, including but not limited to MUC2 knockouts to determine the effect of an induced dysbiosis state and infection outcome (30) and homozygous Lep^{ob} to determine the molecular mechanism by which leptin modulates mucosal protection (31). However, whether cysts are present in the feces is an outstanding question that has not been addressed.

Fact 4: Disease modeling in rodents has shown microbiome–host–parasite interactions

Recent literature suggests that the host microbiome is a modifier of disease outcome and parasite development. The microbiota serves as an immune response trainer (32), processor of carbon sources unavailable to the parasite (33), sustenance to the parasite via phagocytosis (34) can produce metabolites that inhibit encystation (35) and together with a healthy mucus barrier is the first line of defense against parasite

infection (reviewed in (36)). Moreover, the microbiota is required for *E. histolytica* pathogenicity, as germ free mice have an attenuated response to parasite infection (30). The importance of the microbiome is also observed in human cohorts and case studies, demonstrating a correlation between dysbiotic state, a well-known niche for opportunistic pathogens, and *E. histolytica* infection outcome (37, 38). Recently, the microbiome has been shown to have an effect on disease severity via the recruitment of neutrophils (19, 20). Additionally, halting of encystation has been observed in *E. invadens* via microbiome metabolites (35). The oral infection route is a modulator of disease progression and host immunological response, based on the impact pathogen delivery has in other parasites. For *Toxoplasma gondii,* immune murine knockout strains only displayed an increased susceptibility to infection when parasites were delivered through the natural route of infection (39). For *Trypanosoma cruzi,* oral versus gastrointestinal delivery of trypomastigotes display distinct patterns of disease progression in BALB/c mice (40). Lastly, vaccine administration factors are evidence of how the route of delivery of antigens can lead to distinct immune responses. For example, mucosal inoculation leading to IgA production (41). While bacterial microbiome changes have been correlated to various parasitic infections in numerous cohort studies (reviewed in (42)), it is unclear if the parasitic infection causes a state of dysbiosis or vice versa. Animals colonized with fixed microbial communities and orally challenged with either parasite stage will provide insight regarding the effect of the microbiome on parasite development.

Fact 5: Developing a rodent model that produced cysts would be beneficial for the parasitology field

Trophozoites are the metabolically active form of *E. histolytica* but the transmissible form is the cyst. These two forms of the parasites are quite different in terms of morphology, protein content, and ploidy (43, 44). Some scholars argue the field has moved beyond the lack of cyst stage as the current animal model induces disease and has provided a significant understanding of parasite virulence, host susceptibility, and disease progression (45). Currently, mechanisms for the induction of *E. histolytica* developmental changes and cyst production are not available. Researchers can obtain cysts from human patients in the clinical setting or non-human primates in captivity, which limits their access to most laboratories (46). Targeting parasite's developmental changes is a strategy that can result in transmission halting, as only the parasites that are equipped to surviving in the environment, protected by a cyst wall, are infectious to a new host. Approaches focused on encystation are being considered as potential avenues to decline transmission of enteric protozoa (reviewed in (47)). In the 1980s, wet mounts of fecal samples were routinely conducted (24). Today, there are some diagnostic methods for the identification of the cyst-like structures that are strain specific. The 1A4 antibody targets the Jacob2 lectin, while avoiding crossreactivity with xenic cultures of *Entamoeba dispar* isolates (48). Excystation attempts found histamine and glucose availability affect these metabolic processes (49). The most recent attempt to determine the presence of cysts used a colitis mouse model but found no cysts in tissue histology, cecum, or stool (50). Having a mouse model that produces infectious cysts that remain stable in storage would be beneficial for the parasitic community for

the following reasons: [1] reduces the number of animals used to maintain parasite virulence, [2] alleviates the need for the continuous passage of parasites in culture, [3] improves methods of detection for food safety, and patient diagnostics, [4] provides a new platform for anti-parasitic drug screening, and [5] allows for the study of the host response to developmental changes of the parasite. For drug screening and host immune response studies, a rodent model that can be orally challenged with either trophozoite or cyst stages of the parasite, while displaying invasive colitis would be the most useful. Particular challenges that would need to addressed are [1] consistency in the number or cysts used to initiate infection, [2] the extent of invasive disease, and [3] the number of cysts recovered from the colon or fecal samples.

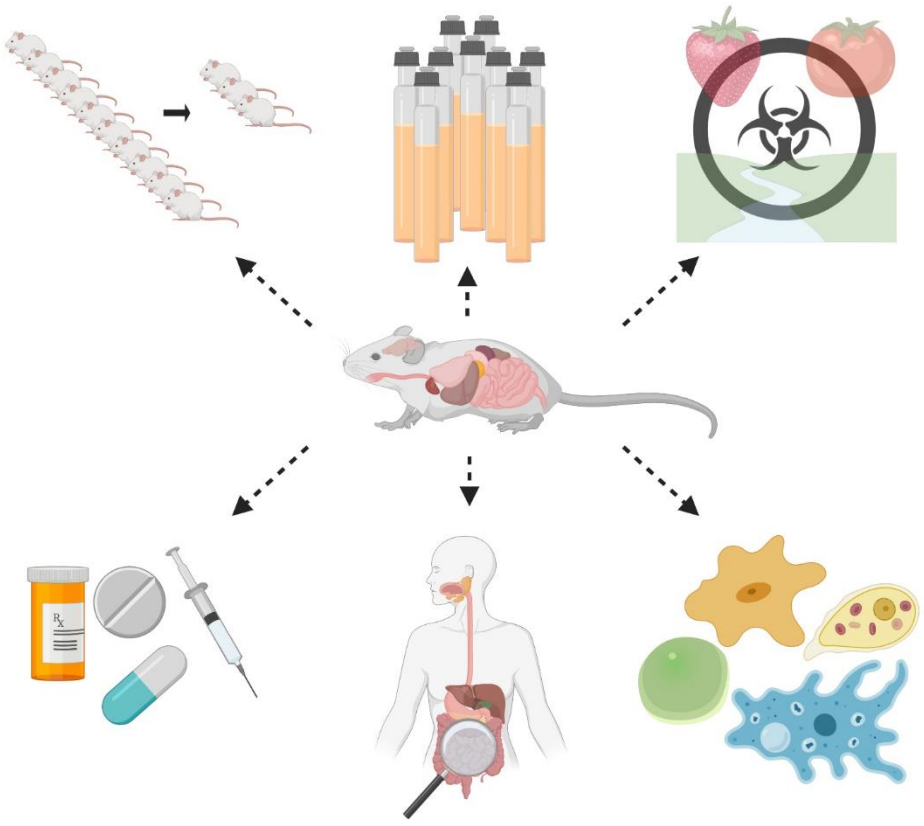

Figure 1: Ideal animal model that can support the full life cycle of *Entamoeba histolytica*. From top left to bottom right: [1] fewer animals used to maintain virulence [2] less need for continuous passaging [3] new detection methods for food safety and patient diagnostics [4] model for drug screening [5] focus on host response to developmental changes of the parasite *in vivo* [6] and could serve as potential model to pioneer *in vivo* studies of non-pathogenic protozoans. Figure created with BioRender.com

Why should we study diarrheal-causing microbial eukaryotes?

The text in this section is unpublished commentary on murine-specific eukaryotes used in the laboratory setting.

Citation

This a draft version for a PEARLS article suggested for PLOS ONE publication.

Acknowledgments

We would also like to thank Apoorva Maru for their critical read and editing of this manuscript.

As a racial minority, this question has always been hard to answer. 1) Simply because microbial eukaryotes are interesting. 2) Morally, because few and "rare" does not mean unimportant. A change of mindset is overdue for neglected diseases, and I invite the reader to reflect on why this mindset has prevailed for so long. 3) Practically, because we are neglecting the microbes' influence on the host, assuming there is no crosstalk between host and microbe is a disservice to animal research.

Microbial eukaryotes have proven to influence their host

In the last decade, nonpathogenic eukaryotes have been further explored. Microbial eukaryotes colonize the gut of healthy individuals (51, 52). However, modern medical practices have focused on eradicating all types of microbial eukaryotes regardless of the current health status of the host (53). These practices, combined with globalization, have decreased the eukaryotic colonization of individuals (52). The mammal gut environment is a habitat with very particular constants such as low oxygen, a constant warm temperature, and the constant physical force of peristalsis (54).

Nonetheless, several lineages have adapted to survive under these conditions. Based on the current approach, microbiome research is skewed towards bacterial communities alone, not considering microbial eukaryotes' presence or role (55). There are many reasons why microbial eukaryotic research is lagging compared to their prokaryotic counterpart. Sequencing platforms have been optimized for 16S, which is specific for bacterial genomes. Although 18S is a comparable target, all eukaryotes have such a gene. Thus, amplification of the host DNA and the diet components during sequencing

can mask the presence of microbial eukaryotes. Culturing methods are not optimal since there are no all-in-one media that is supportive of all protozoans, especially since they are not a monophyletic group. The field has heavily relied on population studies in terms prevalence and morbidity of microbial eukaryotes. The lack of a mouse model is another disadvantage that the field currently faces (56). Lastly, microbial eukaryotes have reduced diversity at deep phylogenetic levels and relative abundances compared to their bacterial counterpart. Nonetheless, the human gut is an ecosystem in which all the community members interact with one another and with the host. The research goal of various groups has focused on the advancement of the human microbiome field by exploring the cross-kingdom interactions between microbial eukaryotes and prokaryotes and their impact on health and disease (reviewed in (32, 42, 57, 58))

Microbial eukaryotes have been labeled as pathogenic or commensal in the past, which would suggest only the microbe is impacted by the host. Symbiotic relationships are a moving continuum that can ebb and flow throughout the length of the relationship. *Blastocystis* is a common microbial eukaryote that colonized humans (reviewed in (59)), which prevalence ranges widely among various regions of the world. Various cohort studies report a commensal role (51, 60) by acting as predators of highly abundant bacterial taxa and remodeling the bacterial richness and community evenness in a given microbiome (61). However, *Blastocystis* subtypes (ST1, ST2, ST3, ST4) are correlated with Inflammatory Bowel Disease (IBS) (62, 63). Most recently, *Blastocystis* colonization protected against chemically induced intestinal inflammation (64). There is an impact on the host by *Blastocystis*, whether beneficial or detrimental, remains to be debated by the field.

Murine models and their naturally occurring microbes

Murine models have been primordial for infectious disease research (65). The host microbiome has a profound impact on overall host health and response to disease. For example, murine models from different vendors can have drastically different microbiota (66), susceptibility to cancer (67), and other infectious diseases (68). In fact, a murine database catalogs the taxonomic profiling of a "healthy" gastrointestinal microbiome (69). However, fungi (55) and other eukaryotic microbes are overlooked in these studies.

Recently, the mycobiome's influence on host metabolism and fat deposition correlated with fungal colonization of various mouse vendors (70). The authors proposed that metabolites produced by naturally occurring fungi, like secondary bile acids, impact the host/microbiota. Another example is a commensal microbial eukaryote, *Tritrichomonas musculis*. *T. musculis* often colonizes the United States National Institute of Health (US-NIH) facilities (71). *T. musculis* activated the inflammasome of the intestinal epithelium, which triggers the host adaptive immune response (Th1 and Th17), resulting in anti-bacterial defense but overall intestinal inflammation (71). This naturally occurring colonization is especially interesting as routine checks for microbial eukaryotes are not as regular as their bacterial counterparts when sending or receiving animals. Screening is available by some commercial vendors upon request, with an added cost, and might not be a general practice.

The *Entamoeba* genus can infect an extensive host range

Below, I detail some reasons why I think studying the naturally occurring eukaryotic microbe, *Entamoeba,* can benefit global health at large. *Entamoeba* can live as a single cell in the aquatic sediments like *E. moshkovskii,* but in most cases is associated with a host intestinal tract (except for *E. gingivalis,* which colonizes the mouth (reviewed in (72)). *Entamoeba* can infect many vertebrates, such as non-human primates (73), reptiles (74), pigs (75-77), cattle (78), camels and sheep (79), goats (80), horses (81), deer (82, 83), elephants(84), and rodents(85) among many others. One of the possible factors that have allowed *Entamoeba* to thrive in many hosts is the presence of an extensive repertoire of bile acids in vertebrates (reviewed in (86)). Some of these infections are by *E. histolytica* and are presumed to be only carriers (87), while others are by the correspondent species and assumed to have evolved to be limited to their host. For example, cockroaches have complex microbiomes, and they harbor distinct *Entamoeba* ribosomal lineages (88). Nonetheless, the extensive host range indicates conservation of the mechanisms for colonization. Studying a murine-specific *Entamoeba* can aid the field advance research on the microbe's colonization and propagation.

Most of the *Entamoeba* incidence is not pathogenic

Various *Entamoeba* species colonize humans, but only *E. histolytica* is known for causing severe invasive disease. Estimations vary widely due to underreporting and the range of symptoms. According to the WHO, 500 million cases of *Entamoeba* disease occur globally (89). A recent meta-analysis used data from 110 studies spanning 47 countries and found the global prevalence to be 3.55% (90). *E. dispar* was responsible for 50% of the infections, followed by *E. histolytica* (32%) *E. moshkovskii* (10%), *E. gingivalis* (5%), *E. coli* (2%), *E. hartmanni* (1%), *E. polecki* (0.05%), *and E. nuttalli* (0.02%) (90). *E. dispar* has had some reports of pathogenicity (91), but for the most part, it is considered significantly less pathogenic than *E. histolytica*. This statistic is shocking; 250 million people would benefit from the study of less pathogenic species of *Entamoeba.*

Why *Entamoeba muris*?

The development model of choice for the *Entamoeba* field is *E. invadens*, a reptilian-specific pathogen. *E. invadens* helped determine *in vitro* cues that trigger developmental changes such as encystation and excystation (92). However, this model's biggest strength is its most significant drawback; this system lacks the host immune response. We must evaluate infection within a host to assess toxicology, side effects, and biological relevance., Thus, unless we are going to inject lizards, a murine model seems adequate to develop antiparasitic drugs and vaccine targets further. We

have genetic tools and have already developed knockout models to discern what immune responses could impact parasite replication or its developmental changes.

When studying *E. muris,* we are delimiting endemic parasite-host relationship but could be extrapolated to human health. We already have access to murine models, and there is no added effort to maintain *E. muris* once it colonizes a vivarium as mice are coprophagic animals (93).

Another advantage of a murine-specific microbe is that we can study the natural route of infection. *E. muris* has evolved to colonize mice via the oral-fecal route; instead of reinventing the proverbial wheel, we can harness what already works in nature. An argument can be made about how a natural colonizer is not pathogenic or will rarely cause invasive disease. My response to that argument is that the infection remains within the gastrointestinal tract in 90% of *E. histolytica* cases. If we encounter a cue that makes *Entamoeba muris* invasive in 10% of the cases, it would be the most representative model yet.

Lastly, suppose *E. muris* colonization has any effect on the host. In that case, it's essential to determine if such an effect is ubiquitous among an experimental population or if certain murine strains are more impacted than others. The presence of *E. muris* in one vivarium could be a confounding variable responsible for inconsistencies in experiments performed in different facilities. We could screen animals upon arrival at a vivarium facility. If desired, animals can be treated against *E. muris* using approved medication such as paromomycin. Alternatively, we could co-house uncolonized animals with colonized animals to ensure their microbiota, including *E muris*, is similar between experimental groups.

The situation is dire. There is no approved vaccine, no new drugs in the last 50 years, and no model mimics the infection suffered by 90% of patients worldwide. Infection with *Entamoeba* species decreases the quality of life even if death is not the outcome, studying less pathogenic *Entamoeba* can improve quality of life for millions of people, it is worth to explore.

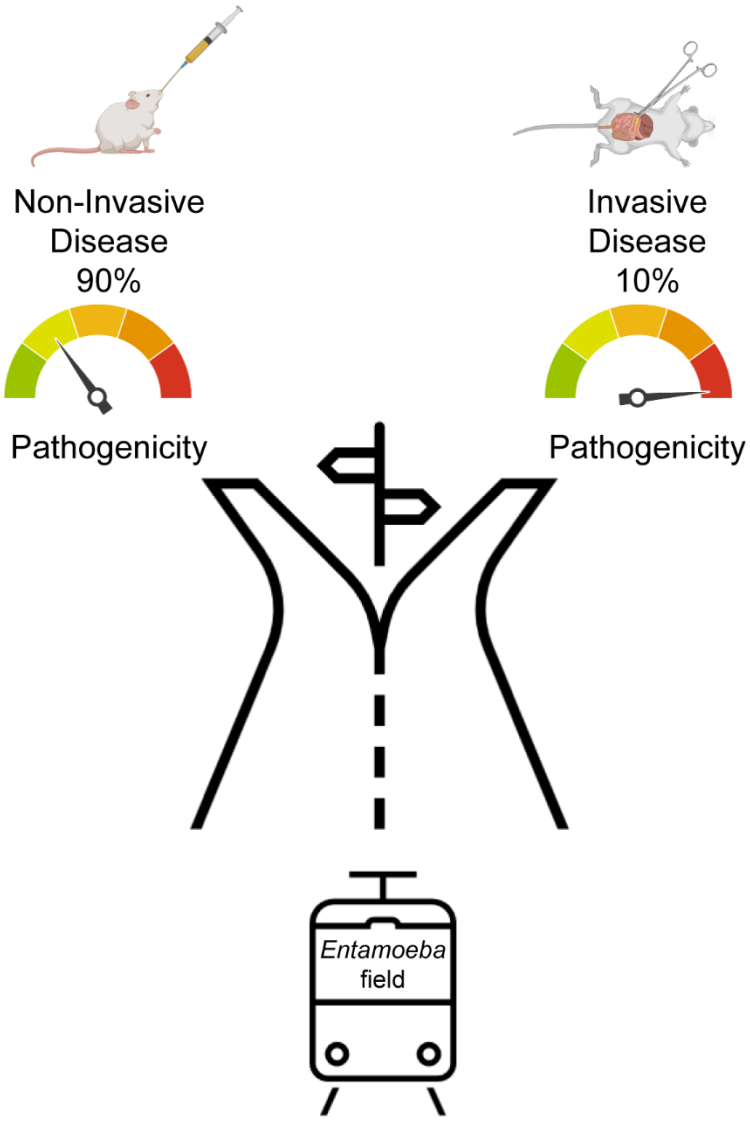

Figure 1: Types of disease pathology studied by *Entamoeba* researchers. Experimental infection has focused on invasive disease (right path) while non-invasive disease (left path) has been studied mostly in cohort population studies. In this review we propose to study noninvasive disease (left path) in animals using *Entamoeba muris*.

Chapter 2. *Cryptosporidium parvum*

Dual Transcriptomics to Determine Gamma Interferon-Independent Host Response to Intestinal *Cryptosporidium parvum* Infection

The text in this chapter is a reformatted version of a published article. Gallego-Lopez and Mendoza Cavazos contributed equally to this work; author order was determined alphabetically.

Citation

Gallego-Lopez* GM, **Mendoza Cavazos* C**, Tibabuzo Perdomo AM, Garfoot AL, O'Connor RM, Knoll LJ. **Dual transcriptomics to determine interferon-gamma independent host response to intestinal Cryptosporidium parvum infection.** Infect Immun. 2021 Dec 20:iai0063821. doi: 10.1128/iai.00638-21. Epub ahead of print. PMID: 34928716. DOI link

Authors' contributions

I, CMC, solely performed the transcriptomics analysis. I took raw reads and provided meaningful interpretations as well as data sharing with the public. My work resulted in manuscript's Figures 3 to Figure 7, all but two supplemental items (Figure 1 and Figure 7). Only the figures generated by my work are included in this chapter.

Design of experiments: GMGL, RMO & LJK. Conceptualization: RMO & LJK; RNA sequencing processing: CMC; RNA sequencing analytics: CMC; Funding acquisition:

RMO & LJK; Investigation: GMGL, CMC, AMTP; Methodology: GMGL, CMC, ALG, AMTP; Project administration: LJK. Resources: RMO & LJK; Supervision: LJK. Visualization: GMGL, CMC, AMTP; Writing: GMGL CMC; Writing – review & editing: CMC, ALG, AMTP, RMO and LJK. All authors read and approved the final manuscript.

Acknowledgments

We sincerely thank Bruno Martorelli Di Genova, Patrick Cervantes, and Carlos J. Ramirez for their lab assistance with IVIS and mice work. CMC would also like to thank Apoorva Maru for their critical read and proofreading of this manuscript.

Abstract

Animals with a chronic infection of the parasite *Toxoplasma gondii* are protected against lethal secondary infection with other pathogens. Our group previously determined that soluble *T. gondii* antigens (STAg) can mimic this protection and be used as a treatment against several lethal pathogens. Because treatments are limited for the parasite *Cryptosporidium parvum,* we tested STAg as a *C. parvum* therapeutic. We determined that STAg treatment reduced *C. parvum* Iowa II oocyst shedding in IFNγ-KO mice. Murine intestinal sections were then sequenced to define the IFNγ independent transcriptomic response to *C. parvum* infection. Gene Ontology and transcript abundance comparisons showed host immune response and metabolism changes. Transcripts for type I interferon responsive genes were more abundant in *C. parvum* infected mice treated with STAg. Comparisons between PBS or STAg treatments showed no significant differences in *C. parvum* gene expression. *C. parvum* transcript abundance was highest in the ileum and mucin-like glycoproteins and the GDP-fucose transporter were among the most abundant. These results will assist the field in determining both host- and parasite-directed future therapeutic targets.

Background

Cryptosporidium is an enteric, protozoan parasite of global distribution that causes the diarrheal disease, cryptosporidiosis. *C. parvum,* the most studied species of the 31 species of *Cryptosporidium* reported until now*,* can cause severe diarrhea in many species, including calves and humans (1). In human immunodeficiency virus (HIV)

infected patients and other immunocompromised individuals, *Cryptosporidium* causes a chronic, debilitating, and sometimes lethal diarrheal disease (2). Additionally, there is an association between *Cryptosporidium* and colorectal cancer (3–6) and recent studies have reported induction of digestive carcinoma in *Cryptosporidium* infected mice (7–9). Because there is neither a vaccine (10,11) nor effective therapeutics (12–14) to prevent and treat cryptosporidiosis in immunocompromised patients, characterization of protective immune responses and identification of new therapeutics are medical and veterinary imperatives.

C. parvum is transmitted via the oral-fecal route by consuming food or water contaminated with oocysts, the environmentally resistant stage of the parasite (15,16). Once inside the host, the oocyst releases sporozoites which invade epithelial cells of the gastrointestinal tract. The parasite undergoes several rounds of asexual replication before transitioning into sexual replication, all within gut enterocytes. Although the parasite is intracellular it remains extra-cytoplasmic, forming a feeder organelle by which it extracts nutrients from the host cell. Because of its very reduced metabolism, *Cryptosporidium* relies on the host cell for nucleotides (17,18), fatty acids (8,9), and glutaminolysis (21). The life cycle culminates in the production of oocysts that are released into the environment in the feces (17,22).

During *C. parvum* infection the cytokine interferon-gamma (IFNγ) plays a central role in controlling infection in both innate and cell-mediated immune response (23,24) through a variety of mechanisms. IFNγ inhibits parasite invasion, changes the intracellular iron

(Fe^{2+}) concentration in enterocytes that the parasite requires (25), and participates in the clearance of the parasite (24). Patients with IFNγ deficiency are more likely to develop chronic *C. parvum* infection (26). While wild-type mice are resistant to *C. parvum* infection, IFNγ-deficient mice are highly susceptible (23,27,28). Treatment of intact mice with IFNγ neutralizing antibodies renders these mice susceptible to *C. parvum* infection (29). IFNγ also induces up-regulation of the host enzyme indoleamine 2,3-deoxygenase (IDO), inducing tryptophan starvation (30) and killing the parasite. IFNγ is produced by natural killer (NK) cells (31), macrophages (32), and dendritic cells (33) in response to *Cryptosporidium* infection, and all these cell types have a protective role in the IFNγ-dependent innate immune response (34). Also, IFNγ plays a role in *Cryptosporidium* cell-mediated adaptive immune responses, inducing differentiation of naïve CD4 T cells to Th1 cells which secrete more IFNγ, produce IgG2 and promote cytotoxic T cell differentiation (24,29,35–37).

To identify novel *C. parvum* immune responses, we tested a non-infectious extract of soluble *Toxoplasma gondii* antigens (STAg) for efficacy against *C. parvum* infection. STAg was previously found to protect against viral, bacterial, and parasitic infections by induction of various innate immune responses. In mice infected with the avian influenza virus H5N1, STAg treatment reduced viral titers in the lungs, and induced a strong gamma interferon (IFNγ) response resulting in increased survival (38). STAg treatment was also able to prevent experimental cerebral malaria in mice challenged with *Plasmodium berghei* via induction of IL-12 and IFNγ and subsequent reduction of parasitemia (39). Additionally, STAg treatment provided resistance against *Listeria*

monocytogenes bacterial infection by reducing the bacterial burden in the spleen and liver by stimulation of TLR11 and promoting recruitment of Ly6C CCR2+ inflammatory monocytes (40).

Because STAg exhibited immunomodulatory activity protective against a variety of pathogens, for these studies, we tested STAg for anti-cryptosporidial activity. To mimic immunocompromised patients, we used IFNγ-knockout (IFNγ-KO) mice to define the IFNγ independent host response to *C. parvum*. Even in the absence of IFNγ, STAg treatment reduced *C. parvum* oocyst shedding, indicating that IFNγ independent immune responses were effective against the parasite. We were surprised by this IFNγ independence of STAg because it has been accepted that STAg elicits host defense via IL-12 mediated induction of IFNγ, a model that was consistent with our previous coinfection studies (38-40). To understand these novel IFNγ independence effects of STAg, we performed RNAseq on STAg-treated and *C. parvum*-infected intestinal tissue to identify components of the immune response responsible for reducing *C. parvum* oocyst shedding in an IFNγ independent manner.

Results

STAg treatment reduces the oocyst shedding in *C. parvum* infected IFNγ-KO mice.

To evaluate if STAg treatment would affect *C. parvum* infection, IFNγ-KO female mice were infected with $1x10^7$ *C. parvum* oocysts Iowa II strain by oral gavage then treated intraperitoneally with 1 mg STAg or PBS control on 1, 3, and 5 days post-infection (dpi). A seminal study previously showed that a lysate of uninfected host cells like human foreskin fibroblasts (HFF) is indistinguishable from the PBS control when testing induction of IFN-γ by *T. gondii* tachyzoites (41). Our previous work also showed that an HFF lysate treatment is analogous to the PBS control when testing the protective effect of STAg treatment against influenzas viral infection. Mice that were HFF treated had similar percent survival, viral titers, and tissue damage as those treated with PBS alone (38). Because HFFs were not seen to have a protective effect, we used PBS as the control for the RNA sequencing experiment. Fecal samples were collected every other day from day 0 to 14. Oocysts shedding over time was quantified by qPCR (18). We observed that STAg treatment significantly reduced oocyst shedding compared with the PBS treated group, indicating that STAg has a therapeutic or immunomodulatory effect against *C. parvum* infection (Experiment 1, Fig 1A, $p = 0.020$). The experiment was repeated with IFNγ-KO mice infected with $1x10^5$ Nano luciferase (Nluc) *C. parvum* oocysts Iowa II strain and oocyst shedding over time was quantified by NLuc expression (43). STAg treatment again significantly reduced the oocyst shedding (Experiment 2, Fig 1B; $p = 0.034$) confirming our first results (Fig 1A). There was a slight difference in

the peak of oocyst shedding between the two experiments, with the peak of shedding at day 7 for experiment 1 and day 9 for experiment 2. Perhaps the addition of the luciferase gene results in a delay of oocyst shedding. Regardless, from these two independent experiments, we concluded that STAg treatment reduces *C. parvum* oocyst shedding in the absence of IFNγ.

Murine intestinal sections were sequenced to determine the interferon-gamma independent transcriptomic response to *C. parvum* infection

To understand the IFNγ-independent mechanism by which STAg reduces *C. parvum* oocyst shedding, we wanted to perform transcriptomic analysis of the host. However, we also wanted to simultaneously obtain *C. parvum* transcripts, so we visualized infection in the entire intestinal tract before we selected a section to sequence. We infected IFNγ-KO female mice with NLuc *C. parvum* and visualized the parasites throughout the mouse intestinal tract using an *in vivo* imaging system (IVIS). Using this technique, Nluc *C. parvum* was localized mainly in the cecum and ileum at 9 dpi (Fig 1C), so these were the sections we chose to sequence.

To investigate the changes in the transcriptome attributable to STAg during *C. parvum* infection, mice were infected, treated and samples collected as shown in Fig 2A.

Infected mice treated with PBS shed more oocysts than STAg treated infected mice (Experiment 3, Fig 2B, $p = 0.049$), indicating that results in this experiment were analogous to experiments shown in Fig 1. As *C. parvum* infects and replicates in enterocytes (15,44,45), we collected the epithelial cell layer in the ileum and caecum for

transcriptomic analysis. This methodology allowed us to remove the mucus layer and to concentrate the parasite transcriptome relative to the host transcriptome. We evaluated these samples by qPCR for *C. parvum* 18S rRNA to determine parasitemia levels. We found that day 9 had significantly more *C. parvum* 18S rRNA than day 6 (Figs 2C and S1), so we sequenced day 9 samples. Raw reads were processed and analyzed for differential expression and gene ontology enrichment (Fig 2D and Table S1).

Table S1: Percent of uniquely mapped reads per genome.

Sample	Treatment	Reads (Millions)	*Mus musculus*	*Cryptosporidium parvum*
Mouse 1-ILEUM	PBS	84.92	81.38 %	N/A
Mouse 2-ILEUM	PBS	74.73	83.62 %	N/A
Mouse 3-ILEUM	PBS	75.19	80.65 %	N/A
Mouse 4-ILEUM	STAg	77.68	84.32 %	N/A
Mouse 5-ILEUM	STAg	75.48	79.29 %	N/A
Mouse 6-ILEUM	STAg	74.67	79.55 %	N/A
Mouse 7-ILEUM	STAg	93.03	76.66 %	2.02 %
Mouse 8-ILEUM	STAg	86.43	78.56 %	1.89 %
Mouse 9-ILEUM	STAg	74.11	76.17 %	3.14 %
Mouse 10-ILEUM	PBS	73.84	78.60 %	1.21 %
Mouse 11-ILEUM	PBS	88.92	75.48 %	1.66 %
Mouse 12-ILEUM	PBS	66.93	72.71 %	5.56 %
Mouse 1-CECUM	PBS	83.87	82.43 %	N/A
Mouse 2-CECUM	PBS	84.09	82.34 %	N/A
Mouse 3-CECUM	PBS	80.34	78.22 %	N/A
Mouse 4-CECUM	STAg	72.90	76.92 %	N/A
Mouse 5-CECUM	STAg	87.02	76.53 %	N/A
Mouse 6-CECUM	STAg	67.14	76.14 %	N/A
Mouse 7-CECUM	STAg	76.48	74.12 %	0.86 %
Mouse 8-CECUM	STAg	72.64	75.07 %	0.37 %
Mouse 9-CECUM	STAg	73.65	76.08 %	0.18 %
Mouse 10-CECUM	PBS	78.48	81.48 %	0.19 %
Mouse 11-CECUM	PBS	86.73	79.28 %	0.27 %
Mouse 12-CECUM	PBS	70.66	76.75 %	0.12 %

Intestinal transcriptomic response to *C. parvum* Iowa II oral challenge is the most prominent in the host's ileum.

A total of 12 differential gene expression comparisons between tissues, treatments, and infection status were conducted for *Mus musculus* (Table S2) and *C. parvum* Iowa II

(Table S3) transcripts. Principal Component Analysis (PCA) was used to visually compare the ileal and cecal transcriptomes of mice treated with STAg or PBS with and without *C. parvum* infection (Fig 3). Clustering of normalized values calculated by DESeq2 indicates a clear separation between ileal and cecal samples. Ileal samples from STAg treated animals (n=6, n=3 per infection group), clustered by infection status (Fig 3, right side). One of the ileal samples from the PBS treated infected group does not cluster with the other infected samples, likely due to the percent of reads mapped to the *C. parvum* Iowa II genome (5.56% vs 1.21% and 1.66%). The cecal samples did not cluster significantly based on infection or treatment.

In terms of the host transcriptomic response to infection and STAg treatment, we observed a low number of differentially expressed genes (DEGs) when comparing the

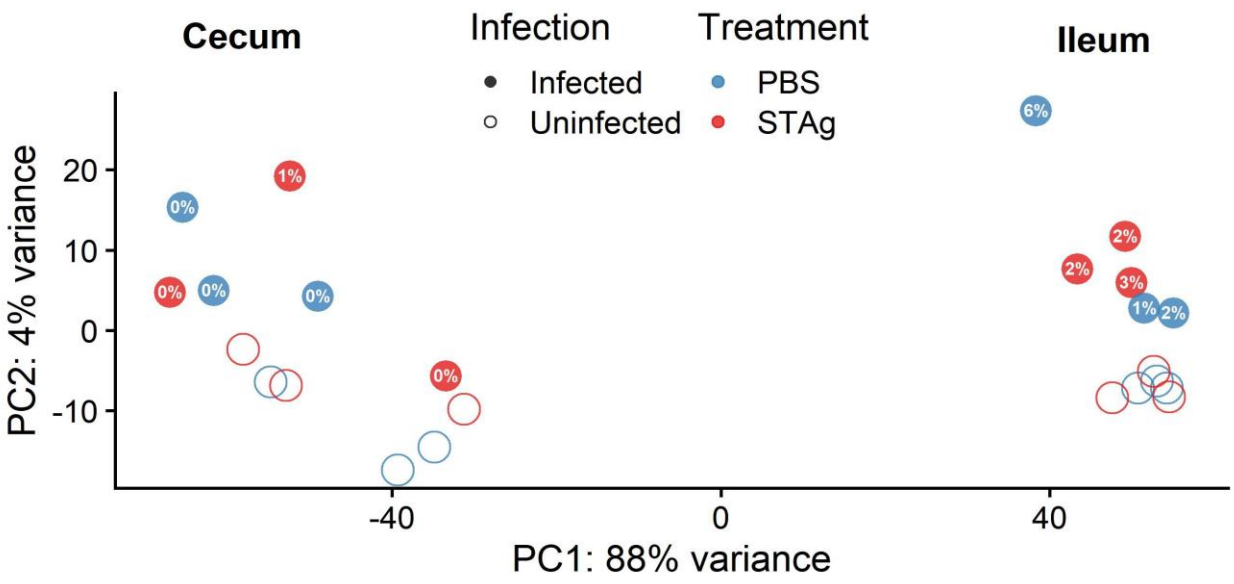

Figure 3. Principal Component Analysis (PCA) of ileum and cecum samples. PCA plot from normalized values calculated by DESeq2. Mapping of the cecum and ileum intestinal section to *Mus musculus* genome. Symbol filling represents *C. parvum* Iowa II infection status: Uninfected (open); Infected (filled). Symbol color represents treatment: control treatment PBS (blue); Soluble *T. gondii* antigen, STAg (red). The text within each individual mice corresponds to the percent of reads uniquely mapped to the *C. parvum* Iowa II genome up to one significant figure, for a more detailed mapped percentage see Table S1.

PBS and STAg treatment. In the ileum of infected animals, STAg treatment had 13 significant DEGs compared to PBS treatment. However, in the cecum of infected mice, STAg treatment had only 2 DEGs compared to PBS treatment (Fig 4A, Table S2 comparisons 1-4). Only a single gene, Myosin Binding Protein C2 (Mybpc2), is shared between comparisons 1 and 2 (Fig 4A), highlighting that it is less abundant with STAg treatment with or without infection.

Table S2: Host all possible comparisons between tissue, treatment, and infection status

	Group 1			Group 2			
Comparison	Tissue	Infection	Treatment	Tissue	Infection	Treatment	File Name (.csv)
1	Ileum	Infected	STAg	Ileum	Infected	PBS	Supplemental file 1
2	Ileum	Uninfected	STAg	Ileum	Uninfected	PBS	Supplemental file 2
3	Cecum	Infected	STAg	Cecum	Infected	PBS	Supplemental file 3
4	Cecum	Uninfected	STAg	Cecum	Uninfected	PBS	Supplemental file 4
5	Ileum	Infected	STAg	Ileum	Uninfected	STAg	Supplemental file 5
6	Ileum	Infected	PBS	Ileum	Uninfected	PBS	Supplemental file 6
7	Cecum	Infected	STAg	Cecum	Uninfected	STAg	Supplemental file 7
8	Cecum	Infected	PBS	Cecum	Uninfected	PBS	Supplemental file 8

Table S3: *C. parvum* all possible comparisons between tissue and treatment

	Group 1		Group 2		
Comparison	Tissue	Treatment	Tissue	Treatment	File Name (.xlsx)
9	Ileum	STAg	Cecum	STAg	Supplemental file 10, tab 1
10	Ileum	PBS	Cecum	PBS	Supplemental file 10, tab 2
11	Ileum	STAg	Ileum	PBS	Supplemental file 10, tab 3
12	Cecum	STAg	Cecum	PBS	Supplemental file 10, tab 4

In contrast, when we compared the impact of infection, we found the highest number of DEGS. (Fig 4B, Table S2 comparisons 5-8). As the host cell responds to infection it was expected to have a transcriptomic effect. Whether STAg or PBS treated, more than

100 genes were significantly differentially expressed within the ileum (Fig 4B) between infected and uninfected animals. Within the STAg treated mice, a total of 129 genes for ileum (Fig S2C) and 78 for the cecum (Fig S2D) were classified as differentially expressed. Out of those 129 genes within the ileum of STAg treated mice, 100 were exclusive to the ileum (Fig 4B). Out of 78 cecal DEGs between infected and uninfected STAg treated mice (Fig 4B), 61 were exclusive to the cecum of STAg treated animals, 7 were shared with the ileum of STAg treated mice. The remaining 10 genes were not exclusive to STAg treatment and shared with PBS treated groups: 5 ileum PBS and 5 cecum PBS treated groups (Fig 4B). Only 2 genes were shared between every single comparison when treatment was maintained constant, and infection status was compared: Keratin 13 (Krt13) and Cytosolic phospholipase A2 gamma (Pla2g4c). Krt13 and Pla2g4c are more abundant in infected mice regardless of treatment status. In the rest of the comparisons, only a low number of transcripts were shared (Fig 4A). PBS treatment allowed us to observe the natural IFNγ independent host responses. Seven genes are exclusive to these control infections (Fig S3A).

Overall, the number of DEGs was higher for the ileum (Fig 4B, S2A, and S2C) than for the cecum (Fig 4B, S2B, and S2D). These results are not due to unmapped reads, as we observed, on average, ~79% of the reads of both tissues to be uniquely mapped to the host genome. Because the percentage of reads mapped to the *C. parvum* Iowa II genome is considerably higher in the ileum than the cecum (Fig 3 and Table S1), it is

not surprising that this tissue had the highest number of significant DEGs regardless of treatment.

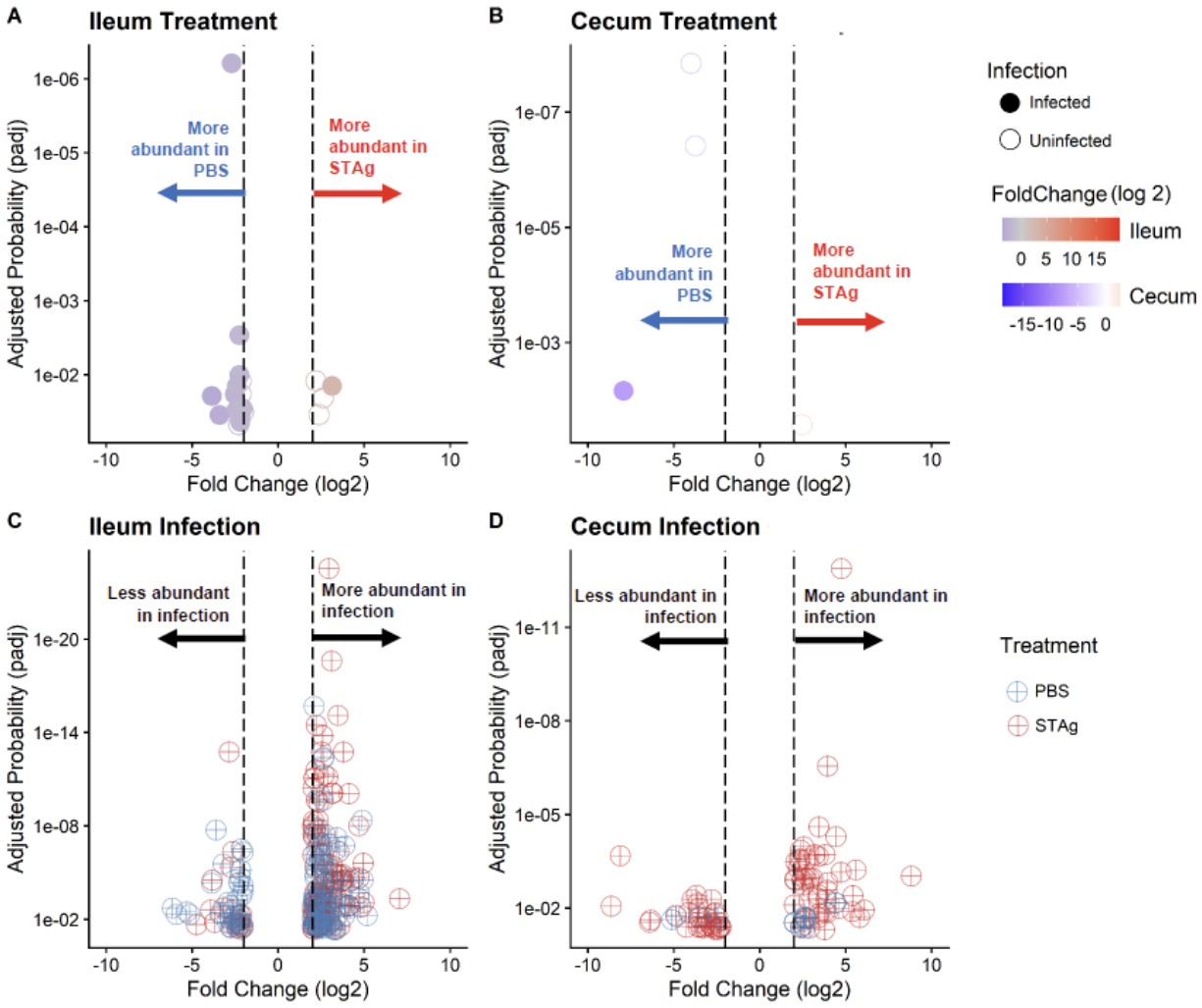

Figure S3. Host Differential expressed genes by treatment (A and B), infectious status (C and D), and tissue (Ileum: A and C, Cecum: B and D). Only significant DEGs are shown. DEGs, represented by a circle, had a < 0.05 padj value and a > 2 absolute log2fold change (dashed vertical line). Not pictured in these volcano plots due to limited space are: 2310069B03Rik_1 (log 2-fold change= 19.54 (A) and -18.64 (C)) and Entpd4 (log 2-fold change= -19.40 (B) and -23.14 (D)). Treatment is represented by color (PBS=blue, STAG=red). Open circles represent uninfected animals while filled circles indicate infected animals. (A and B). Color scale represents the fold change (log 2), the higher the absolute value of the fold change (log 2), the darker the color (A and B). DEGs that were determined to be significant in more than one comparison are represented by overlapping regions of circles in the Venn diagram (Figure 4 and Fig S2) but are not presented in these volcano plots.

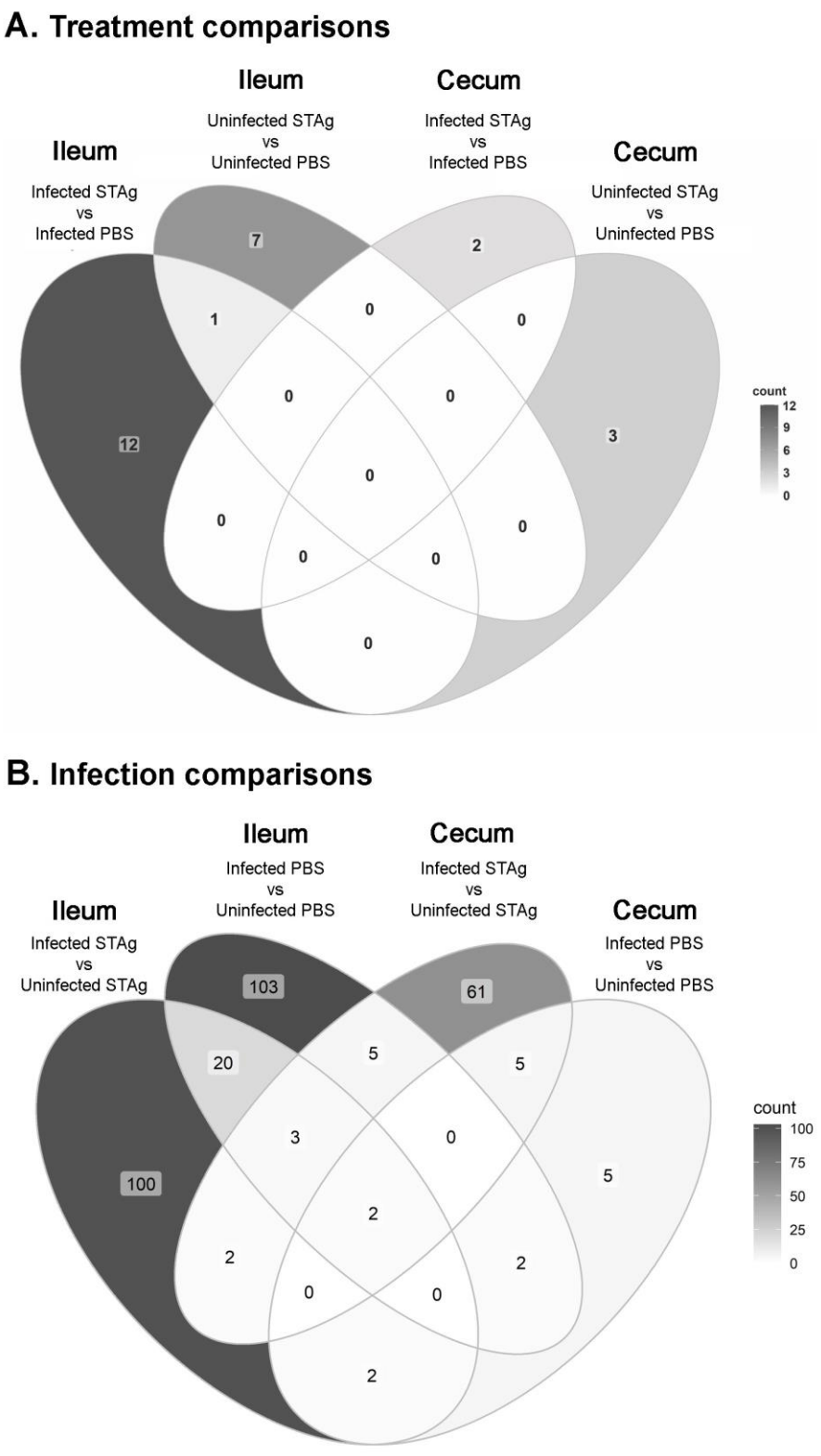

Figure 4 Host differentially expressed genes when comparing treatment (A) and infection (B) Color scale represents a higher number of DEGs as darker shades of grey.

Gene Ontology analysis shows differentially expressed immune response to *C. parvum* infection based on treatment

To further explore the transcriptomic response to *C. parvum* Iowa II infection and STAg treatment, we used Gene Ontology (GO) enrichment analysis through the Database for Annotation, Visualization, and Integrated Discovery (DAVID), v6.8 (46,47). Genes that were differentially expressed between infected and uninfected mice while PBS or STAg treated (comparisons 5-8 in Table S2) were analyzed for enrichment of three GO term categories: cellular component (Fig S4), molecular function (Fig S5), and biological process (Fig 5). In comparison to the cecum of uninfected STAg treated mice, the cecum of infected STAg treated mice were enriched for cellular component GO terms skewed towards the periphery of the host cells: host membrane (GO:0016020), extracellular space (GO:0005615), and extracellular region (GO:0005576) when comparing infection status (Fig S4). In the ileum of infected-STAg treated mice, as compared to the uninfected-STAg treated mice, DEGs were associated with the mitochondrion (GO: 0005739), the extracellular region (GO:0005576), and the endoplasmic reticulum (GO:0005783) (Fig S4). Cellular component GO-terms had the highest level of enrichment for the cecum samples from STAg treated animals, which was not observed in the biological process or molecular function GO terms (Fig S5 and Fig 5). Due to the localization of the parasite on the periphery of the host cell, it is encouraging that we observe GO terms that are related to the extracellular space and cellular trafficking when comparing infection. We observed major enrichment of molecular function GO terms related to purine metabolism and RNA binding in the ileum

of mice infected and STAg treated, which was not observed in the ileum of mice that were PBS treated (Fig S5).

As expected, the biological process GO terms showed enrichment for host immunity in the ileum of mice treated with STAg (Fig 5). As we tested our hypothesis in IFNγ-KO mice, we expected the signaling to be IFNγ independent. The innate immune response was significantly associated with type I interferon response, including IFN-alpha signaling (GO:0035457), response to IFN-beta signaling (GO:0035458), downstream targets like defense response to virus (GO:0051607), and response to virus (GO: 0009615) (Fig 5).

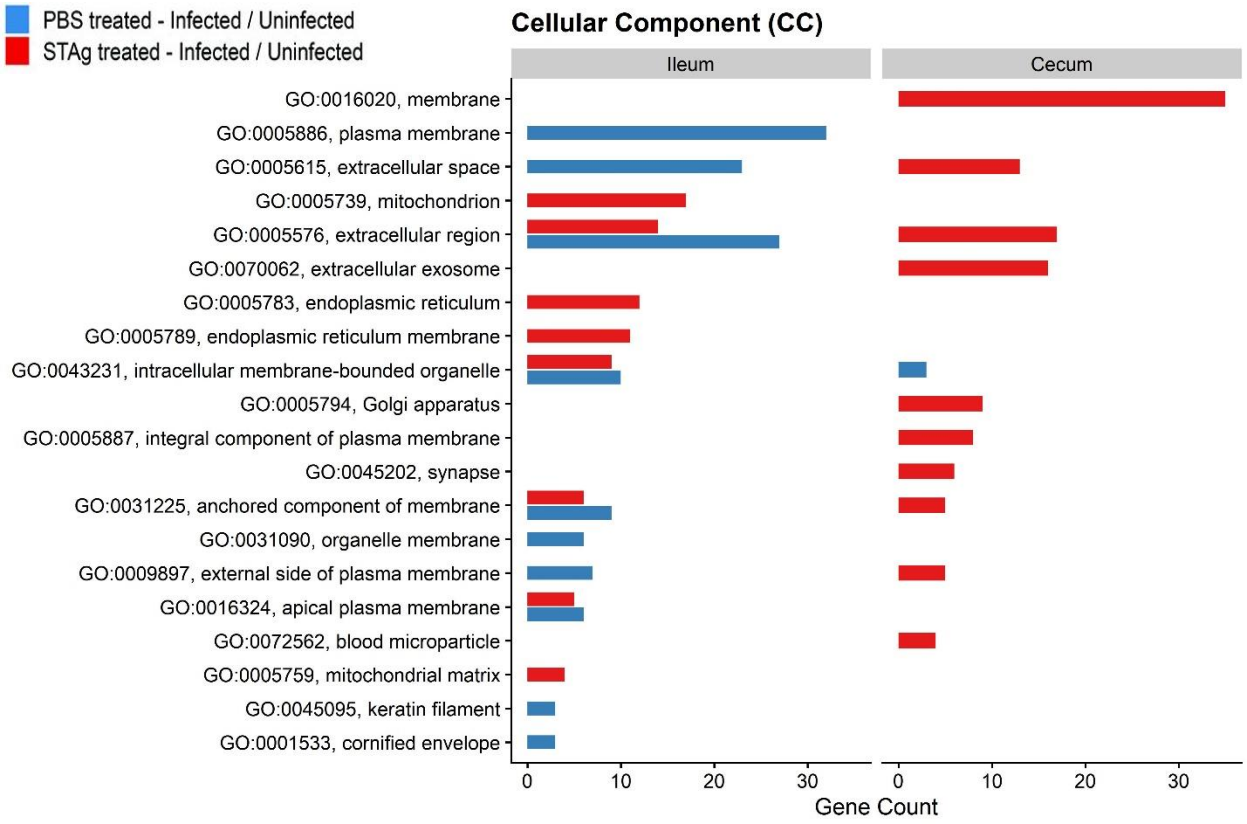

Figure S4. Host gene ontology (GO) of cellular component (CC)) in STAg and PBS treated mice. Differentially expressed genes (DEGs) in comparisons 1-2 and 3-5 were analyzed for gene ontology enrichment of cellular component (CC) using the Database for Annotation, Visualization, and Integrated Discovery (DAVID, v6.8). Only GO terms populated by 3 or more DEGs were included in these visualizations ($p < 0.05$). Bar filling color represents treatment: control treatment PBS (blue); Soluble T. gondii antigen, STAg (red).

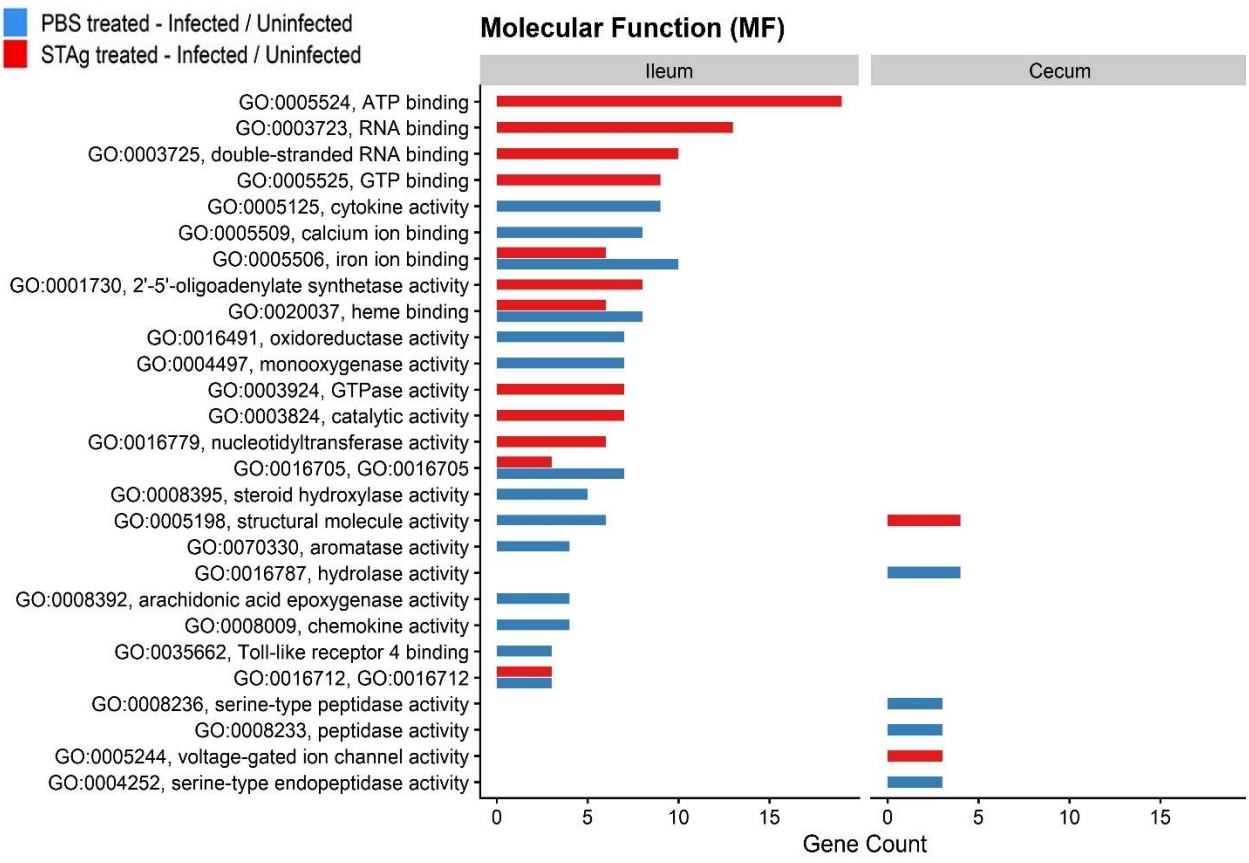

Figure S5. Host gene ontology (GO) of molecular function (MF) in STAg and PBS treated mice. Differentially expressed genes (DEGs) in comparisons 1-2 and 3-5 were used for gene ontology enrichment of molecular function (MF) using the Database for Annotation, Visualization, and Integrated Discovery (DAVID, v6.8). Only GO terms populated by 3 or more DEGs were included in these visualizations ($p < 0.05$). Bar filling color represents treatment: control treatment PBS (blue); Soluble T. gondii antigen, STAg (red).

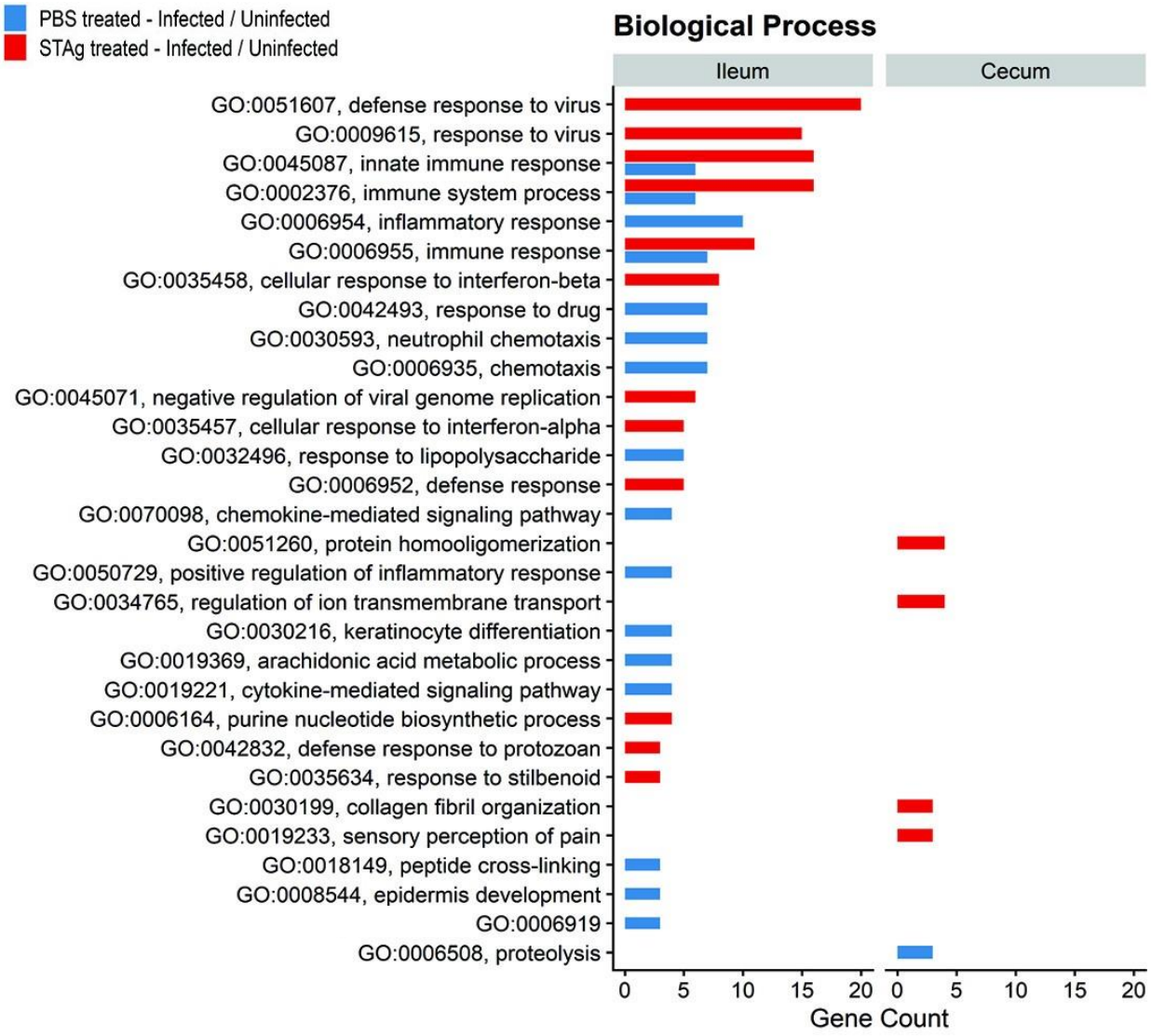

Figure 5. Host gene ontology (GO) of biological process (BP) in STAg and PBS treated mice. Differentially expressed genes (DEGs) in comparisons 5-8 were analyzed for gene ontology enrichment of biological process (BP)**,** using the Database for Annotation, Visualization, and Integrated Discovery (DAVID, v6.8). Only GO terms populated by 3 or more DEGs were included in these visualizations ($p < 0.05$). Bar filling color represents treatment: control treatment PBS (blue); Soluble *T. gondii* antigen, STAg (red). GO:0006919 stands for "activation of cysteine-type endopeptidase activity involved in apoptotic process".

Transcript abundance comparisons show immune response and host metabolism changes

As the DEGs in the cecum were highly variable among biological replicates, we focused on ileal samples for further analysis. To compare the abundance of these significant genes across the 6 biological replicates per treatment group, we generated heatmaps charting the normalized reads per animal (Fig 6A and S6). We found 37 genes related to IFN type I in mice infected and treated with STAg (Table 1 and Fig 6A) but not present in mice infected and treated with PBS (Fig S6). Among them were eight oligoadenylate synthetase (OAS) genes, the DDx60 (48), the Dhx58 also known as Lpg2 (49), Mtx2, Tap1, Trim 30a-b-c, the ubiquitin-specific peptidase 18, seven interferon-induced proteins, the Immunity-related GTPase, the immunity-related

GTPase family M member 1 and 2; and the Ring finger proteins 213 and 225 (50,51). Similarly, 6 members of the Schlafen gene family (SLFN) were present in higher abundance in STAg treated infected mice versus STAg treated uninfected mice (Comparison 5 and Table 1). To evaluate type I interferon responses earlier in infection, we examined the abundance of interferon induced protein 44 (IFI44) and OAS-3 at 6 and 9 dpi by qPCR. As expected, IFI44 and OAS-3 were significantly more abundant in infected STAg treated mice vs uninfected at 9 dpi, but the expression differences were not significant at 6 dpi (Fig S7).

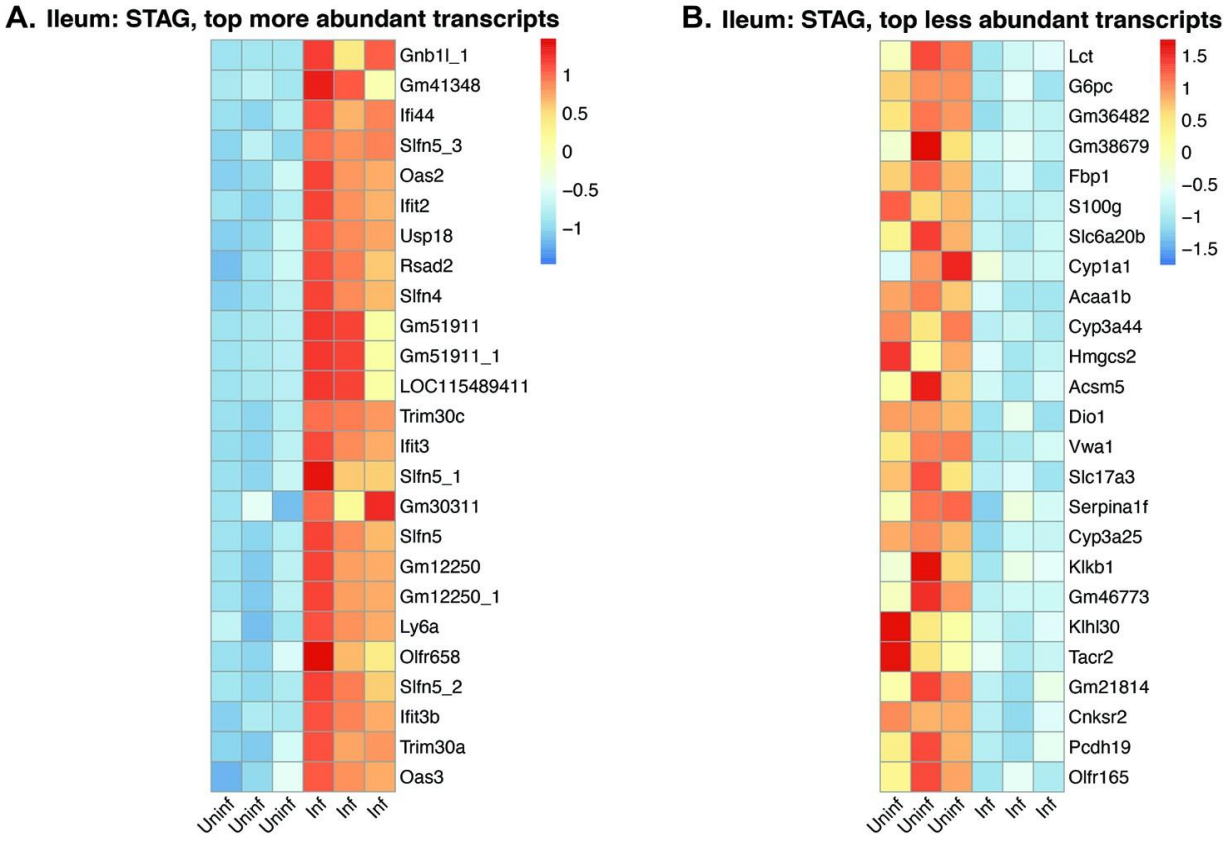

Figure 6: Heatmap of differentially expressed genes in the ileum of mice treated with STAg (comparison 5). The top 25 more **(A)** and less **(B)** abundant transcripts (ranked by log2 fold change). Each column represents a biological replicate.

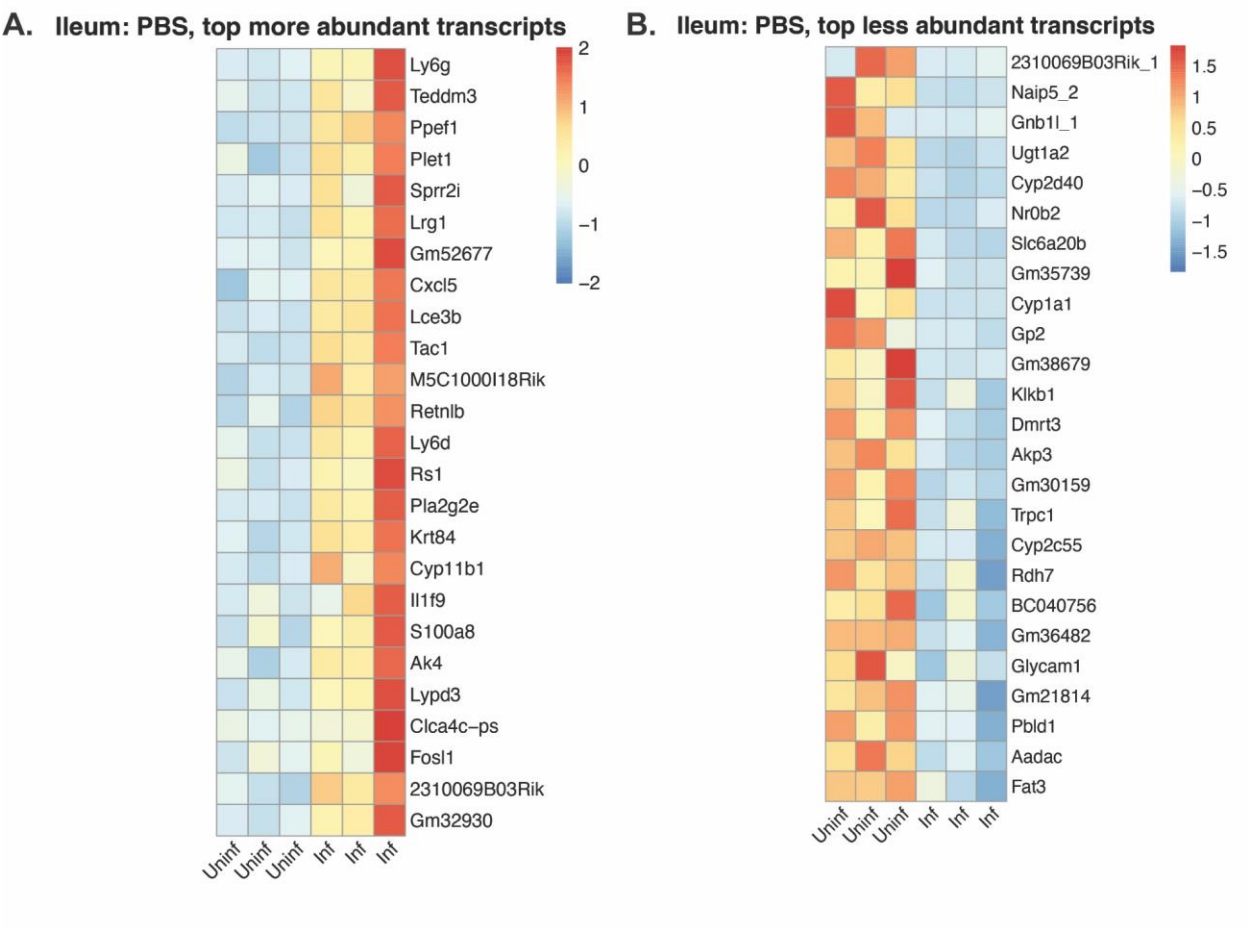

Figure S6. Heatmap of host differentially expressed genes in the ileum of mice treated with PBS. **(A)** The top 25 more and **(B)** less abundant transcripts in ileum treated with PBS; The color scale was determined by log2 fold change in Infected and non-infected mice. Each column represents a biological replicate.

Table 1. Transcripts associated with IFN type I present in the ileum of STAg-treated mice (infected vs uninfected)

Gene ID	Log_2 fold change	Gene name
Ddx60	2.45	DEAD (Asp-Glu-Ala-Asp) box polypeptide 60
Dhx58	2.82	DEXH (Asp-Glu-X-His) box polypeptide 58
Ifi204	3.09	Interferon-activated gene 204
Ifi44	4.95	Interferon-induced protein 44
Ifit1	2.55	Interferon-induced protein with tetratricopeptide repeats 1
Ifit1bl1	2.53	Interferon-induced protein with tetratricopeptide repeats 1B like 1
Ifit2	4.68	Interferon-induced protein with tetratricopeptide repeats 2
Ifit3	3.76	Interferon-induced protein with tetratricopeptide repeats 3
Ifit3b	3.48	Interferon-induced protein with tetratricopeptide repeats 3B
Igtp	3.22	Interferon-g-induced GTPase
Irgm1	2.13	Immunity-related GTPase family M member 1
Irgm2	2.18	Immunity-related GTPase family M member 2
Mx2	3.17	MX dynamin-like GTPase 2
Oas1a	2.47	2'-5' oligoadenylate synthetase 1[a]
Oas1b	2.88	2'-5' oligoadenylate synthetase 1B
Oas1g	2.54	2'-5' oligoadenylate synthetase 1G
Oas1h	2.74	2'-5' oligoadenylate synthetase 1H
Oas2	4.70	2'-5' oligoadenylate synthetase 2
Oas3	3.39	2'-5' oligoadenylate synthetase 3
Oasl1	2.06	2'-5' oligoadenylate synthetase-like 1
Oasl2	2.75	2'-5' oligoadenylate synthetase-like 2
Rnf213	2.11	Ring finger protein 213
Rnf225	2.33	Ring finger protein 225
Slfn1	3.16	Schlafen 1
Slfn10-ps_3	2.49	Schlafen 10, Pseudogene
Slfn2	2.52	Schlafen 2
Slfn4	4.11	Schlafen 4
Slfn5	3.72	Schlafen 5
Slfn5_1	3.74	Schlafen 5_1
Slfn5_2	3.53	Schlafen 5_2
Slfn5_3	4.82	Schlafen 5_3
Tap1	2.10	Transporter 1, ATP-binding cassette, subfamily B (MDR/TAP)
Trim30a	3.48	Tripartite motif-containing 30A
Trim30b	2.26	Tripartite motif-containing 30B
Trim 30c	3.80	Tripartite motif-containing 30B
Usp18	4.41	Ubiquitin-specific peptidase 18

Curiously, 2 transcripts related to gluconeogenesis were identified in lower abundance in the ileum of infected and STAg treated mice when compared to their uninfected counterparts (Fig 6B), Glucose-6-Phosphatase Catalytic Subunit (G6pc), and Fructose 1,6-bisphosphatase (Fbp1). There have been sporadic reports that juvenile animals (52) or senior human hosts (53) with *C. parvum* infection seem to have a lower tolerance for lactose, and we are the first to observe lactase (Lct) transcript to be in lower abundance in infected mice (Fig 6B). In the PBS-treated mice, transcripts for G6pc, Fbp1, and Lct were also less abundant, but they did not achieve the set threshold limits. For Fbp1, the log2 fold change was -1.8 and for Lct, the log2 fold change was -1.9. While G6pc did make the -2 log change cutoff (-2.7), due to variability, G6pc did not meet the padj threshold ($p = 0.07$). To evaluate these metabolic changes earlier during infection, we examined the abundance of Fbp1 and Lct at 6 and 9 dpi by qPCR. While Fbp1 was significantly lower in infected animals at 9 dpi, the differences were not significant at 6 dpi (Fig S7). Lct trended lower in infected animals at 9 dpi, but no differences were seen at 6 dpi (Fig S7). These results suggest that infection with *C. parvum* may modulate host carbohydrate metabolism away from gluconeogenesis and disaccharides like lactose during the infection peak. It will be interesting to further investigate if *C. parvum* infection reduces the expression of these enzymes in other hosts or *in vitro* models. While comparing the PBS and STAg treatments within infected animals we observed 13 DEGs (Fig 4A). STAg treated mice have a lower abundance of Interleukin 10 (IL-10), chemokine 4 (Ccl4), Prostaglandin E Receptor 3 (Ptger3), granzyme B(Gzmb), granzyme K (Gzmk), keratine 14 (Krt14), and others when compared to PBS treatment

(Fig 7). These results highlight that STAg treatment reduced the abundance of some inflammatory responses elicited by *C. parvum.*

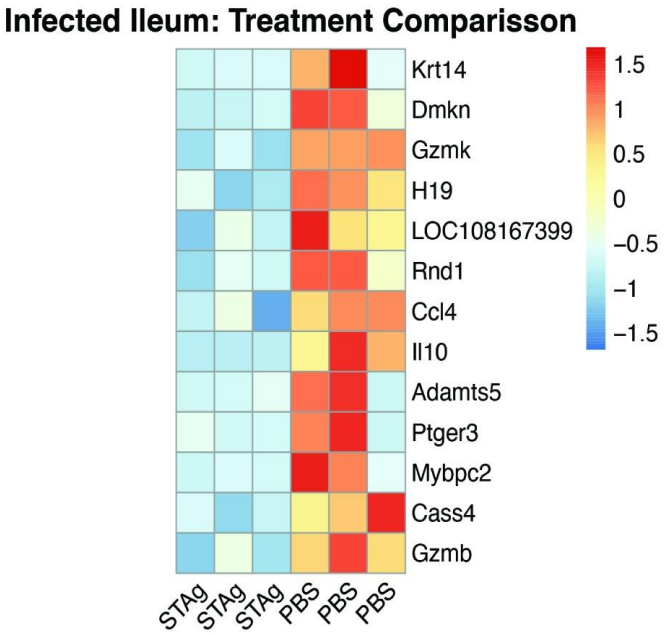

Figure 7: Heatmap of differentially expressed genes in the ileum of infected mice treated with STAg or PBS. 13 genes (ranked by log2 fold change) were found to be differentially expressed in the ileum between infected mice treated with PBS or STAg. Each column represents a biological replicate.

C. parvum transcript analysis shows no significant differences in gene expression between PBS or STAg treatments

An analysis was conducted to determine if STAg treatment had any effect on the transcriptome of *C. parvum* (Table S3). When a PCA exploration for reads that were aligned to the *C. parvum* Iowa II genome was conducted, we observed clustering of the ileum, but not the cecum samples (Fig S8). The percentage of uniquely mapped reads to the *C. parvum* Iowa II genome was significantly lower when compared to host

mapping, a result that we were expecting according to other similar studies (54). On average per sample, the ileum had more transcripts that mapped to the *C. parvum* Iowa II genome than the cecum (Table S1). Differential expression analysis of the parasite transcriptome was performed in the same manner as for the host transcriptome but there were no significant differentially expressed genes between PBS and STAg treated samples. These results indicate that the effect of STAg to lower *C. parvum* oocyst shedding was more likely due to changing the host immune response than a direct effect on the parasite. The most abundant *C. parvum* Iowa II transcripts within the ileum, are listed in Tables 2 and 3. The presence of transcripts encoding the *Cryptosporidium* mucin-like glycoproteins (55) such as cpMuc5 (cgd2_430)(56), cpMuc7 (cgd2_450), and cpMuc3 (cgd2_410) were observed in STAg-treated animals (Table 2) and gp40 and the mucin cgd7_4020 in PBS-treated animals (Table 3). For both treatments, the parasite GDPfucose transporter (CGD3_500) was among the top 10 most abundant transcripts,

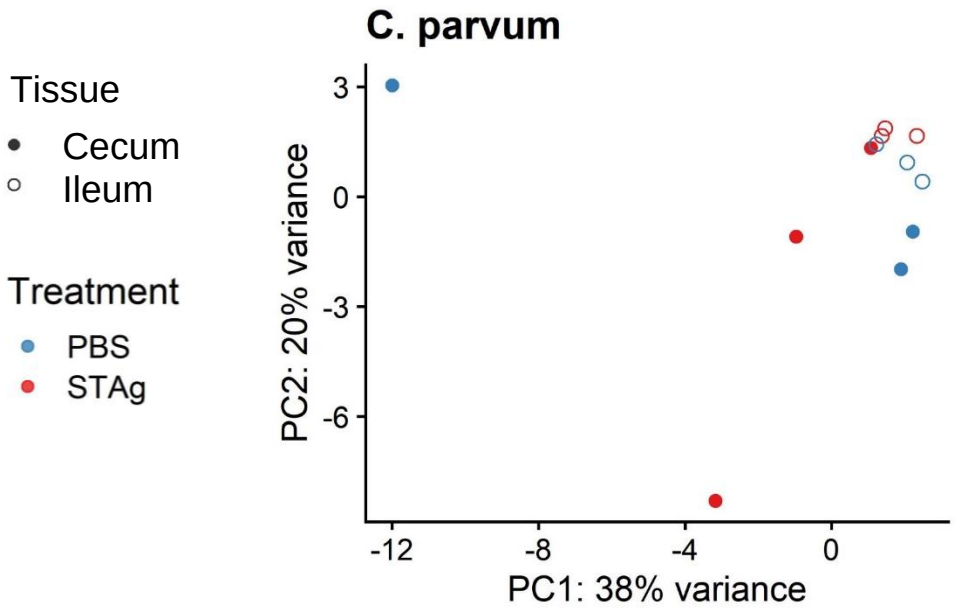

Figure S8: Principal Component Analysis (PCA) of mapping of ileum and cecum samples to the *Cryptosporidium parvum* Iowa II genome. PCA plot from normalized values calculated by DESeq2. Symbol filling represents host tissue: ileum (open); cecum (filled). Symbol color represents treatment: control treatment PBS (blue); Soluble T. gondii antigen, STAg (red).

Table 1. Transcripts associated with IFN type I present in the ileum of STAg-treated mice (infected vs uninfected)

Gene ID	Log_2 fold change	Gene name
Ddx60	2.45	DEAD (Asp-Glu-Ala-Asp) box polypeptide 60
Dhx58	2.82	DEXH (Asp-Glu-X-His) box polypeptide 58
Ifi204	3.09	Interferon-activated gene 204
Ifi44	4.95	Interferon-induced protein 44
Ifit1	2.55	Interferon-induced protein with tetratricopeptide repeats 1
Ifit1bl1	2.53	Interferon-induced protein with tetratricopeptide repeats 1B like 1
Ifit2	4.68	Interferon-induced protein with tetratricopeptide repeats 2
Ifit3	3.76	Interferon-induced protein with tetratricopeptide repeats 3
Ifit3b	3.48	Interferon-induced protein with tetratricopeptide repeats 3B
Igtp	3.22	Interferon-g-induced GTPase
Irgm1	2.13	Immunity-related GTPase family M member 1
Irgm2	2.18	Immunity-related GTPase family M member 2
Mx2	3.17	MX dynamin-like GTPase 2
Oas1a	2.47	2'-5' oligoadenylate synthetase 1[a]
Oas1b	2.88	2'-5' oligoadenylate synthetase 1B
Oas1g	2.54	2'-5' oligoadenylate synthetase 1G
Oas1h	2.74	2'-5' oligoadenylate synthetase 1H
Oas2	4.70	2'-5' oligoadenylate synthetase 2
Oas3	3.39	2'-5' oligoadenylate synthetase 3
Oasl1	2.06	2'-5' oligoadenylate synthetase-like 1
Oasl2	2.75	2'-5' oligoadenylate synthetase-like 2
Rnf213	2.11	Ring finger protein 213
Rnf225	2.33	Ring finger protein 225
Slfn1	3.16	Schlafen 1
Slfn10-ps_3	2.49	Schlafen 10, Pseudogene
Slfn2	2.52	Schlafen 2
Slfn4	4.11	Schlafen 4
Slfn5	3.72	Schlafen 5
Slfn5_1	3.74	Schlafen 5_1
Slfn5_2	3.53	Schlafen 5_2
Slfn5_3	4.82	Schlafen 5_3
Tap1	2.10	Transporter 1, ATP-binding cassette, subfamily B (MDR/TAP)
Trim30a	3.48	Tripartite motif-containing 30A
Trim30b	2.26	Tripartite motif-containing 30B
Trim 30c	3.80	Tripartite motif-containing 30B
Usp18	4.41	Ubiquitin-specific peptidase 18

Table 2 Top 10 more abundant C. parvum transcripts in STAg-treated ileum

	CryptoDB ID	Transcript name	Average counts	Counts for: Mouse 1	Mouse 2	Mouse 3
1	cgd6_10	Proteophosphoglycan	5938	4943	5784	7088
2	cgd4_3630	Cross-beta structure silk protein 1	3007	2621	3043	3357
3	cgd2_410	Signal peptide-containing protein-Mucin 3	2099	1659	1984	2654
4	cgd6_1070	Uncharacterized protein	1989	1747	1975	2246
5	cgd4_3410	RNA recognition motif/WW Domain-containing protein	1877	1515	1837	2281
6	cgd3_550	Major Facilitator Superfamily	1875	1612	1687	2327
7	cgd3_500	GDP-fucose transporter	1582	1306	1596	1844
8	cgd2_430	Signal peptide-containing Protein-cpMUC5	1567	1424	1591	1687
9	cgd8_550	Uncharacterized protein	1512	1239	1542	1755
10	cgd2_450	Signal peptide-containing protein-cPMUC7 CIPW_000002748	1447	1286	1485	1569

Table 3 Top 10 more abundant C. parvum transcripts in PBS-treated ileum

	CryptoDB_ID	Transcript name	Average counts	Counts for: Mouse 1	Mouse 2	Mouse 3
1	cgd6_1080	Glycoprotein gp40	50,954	20891	34483	97488
2	cgd2_1373	Unspecified product	23,847	17477	15032	39033
3	cgd6_3990	Elongation factor 1-alpha	22,218	9455	15754	41446
4	cgd8_3520	Uncharacterized secreted protein	21,677	9928	16857	38247
5	cgd5_1470	Nucleoside diphosphate kinase	17,366	7388	12296	32415
6	cgd7_4020	Cryptosporidial mucin	16,472	6621	12245	30549
7	cgd1_3810	Uncharacterized protein	16,058	7149	12082	28944
8	cgd3_510	GDP-fucose transporter	14,106	6146	10245	25928
9	cgd5_3160	Actin	13,058	5118	8647	25408
10	cgd6_5410	Uncharacterized secreted protein	11,013	5104	8578	19357

Discussion

While nitazoxanide has some efficacy in immune-competent adults, it is not effective in severely immunocompromised patients (57–59) highlighting the need to develop interventions effective in the absence of normal immune responses. To mimic the human immune-compromised state, we used IFNγ-KO mice to define the IFNγ independent host response to *C. parvum*. We found that STAg treatment reduced *C. parvum* infection in IFNγ-KO mice (Fig 1) and performed transcriptomic analysis to determine this novel IFNγ-independent mechanism of STAg treatment. IFNγ-KO mice have a higher number of significant DEGs when comparing infection within a tissue

whether treated with PBS or STAg (Fig 4B), suggesting that treatment alone is not sufficient to elicit a host gene expression change. *C. parvum* infection likely acts synergistically with STAg treatment to elicit the type I interferon immune response. It is interesting that the intestinal parasitemia as measured by qPCR of *C. parvum* 18S rRNA was not reduced by STAg treatment (Fig 2C), but the shedding was (Fig 2B). Perhaps the host response elicited by STAg is preferentially targeting oocyst shedding and not parasite replication. However, the difference could also be due to the nature of the two assays. While the luciferase assay will detect only viable parasites that are expressing the nanoluc reporter, the qPCR assay detects viable and dying/dead parasites prior to the degradation of their genomic DNA.

Most of the DEGs in the ileum were classified as belonging to the type I interferon response and its downstream effectors, typically known for their anti-viral activity (Table 1 and Fig 6A). IFNs are a multigenic family of cytokines that regulate different aspects of the immune response. There are three classes of IFN: type I, II, and III, which recognize distinct receptors on cell membranes (60). IFN signaling induces transcription of hundreds of IFN-stimulated genes that further the immune response against viral infection. The IFN type I response is essential in the immune response against viruses (61) but its role in *Cryptosporidium* infection has been poorly characterized. In 2009, Barack *et al*. were the first to describe the IFN type I response to *Cryptosporidium* infection in human and mice enterocytes in vitro (62). Upregulation of long-non coding

RNAs influences the IFN type I response to *C. parvum* in an in vitro murine model (51). IFN type I genes were upregulated in lung organoids microinjected with oocysts at 72 hours post-injection (63). Our study is the second *in vivo* transcriptome analysis to report more abundant IFN type I transcripts during *C. parvum* infection.

Among the IFN-stimulated genes, we found in high abundance eight oligoadenylate synthetase (OAS) and six Schlafen genes in infected and STAg treated mice (Table 1). OASs synthesize short oligomers that activate RNAse L to cleave cellular and viral RNAs (64,65), participate in apoptosis, and control cellular growth (66). There are at least a dozen OAS proteins in mice and four in humans. OAS-like proteins consist of one OAS domain and two ubiquitin-repeat domains (UBL). Humans have one OAS-like protein, while mice have two OAS-like proteins OASL1 and OASL2. Murine OASL1 has a context-dependent role in the anti-viral response; in the early stages of infection, it forms stress granules trapping viral RNAs, but in later stages of infection, it downregulates the IFN response (61,64,67). The murine Schlafen family has 9 proteins with 5 human homologs. Schlafen proteins have been described to have many potential roles in cell processes, including but not limited to cell differentiation, inhibition of anchorage-independent growth, and regulation of the immune response (68,69). SLFN2 has been shown to regulate type I interferon response via the NF-κβ pathway (70). SLFN3 and its human analog SLFN12 are critical in regulating intestinal epithelial differentiation (43,44). Of this family, the most abundant transcript in our transcriptomic dataset was Schlafen 4 (Slfn4) (71). A previous study has shown in SLFN4 overexpressing mice a reduction in the recruitment of inflammatory macrophages,

suggesting SLFN4 as a negative regulator of monocytopoiesis (72). It will be interesting to further explore the relationship between SLFN4 and *C. parvum* infection.

Using GO enrichment analysis, we found an enrichment of immunological terms downstream of IFNα/β signaling (Fig 6). Curiously, no change in IFNα/β transcript abundance was observed. This change in the abundance of the effectors versus the signaling molecules themselves is probably due to the late time point selected. We chose the 9 dpi timepoint to coincide with the peak *C. parvum* Iowa II oocysts shedding to maximize the number of *C. parvum* transcripts in the datasets (Fig 2C and Fig S1).

Future experiments will analyze the IFNα/β signaling pathways throughout the time course of infection to determine the level of protection type I signaling confers against *C. parvum* infection.

STAg treated mice had a lower abundance of IL-10 (Fig 7). IL-10 is an anti-inflammatory cytokine, its role is to modulate a balance between pathology and protection against a rampant immune response (73,74). IL-10 is elevated in the stool of *Cryptosporidium* infected Haitian children (73) as well as in patients co-infected with *C. parvum* and HIV (75). In animal models, IL-10 knockout mice are more resistant to *C. parvum* infection (76), but anti-IL-10 antibody treatment in calves does not reduce *C. parvum* shedding (77). We did not see significant differences in serum IL-10 levels between treatment groups at either day (Fig S9). There are likely differences between localized/tissue

responses and cytokines in serum. We have seen this phenomenon before with *Eimeria* intestinal infection and the IL-10 response (78).

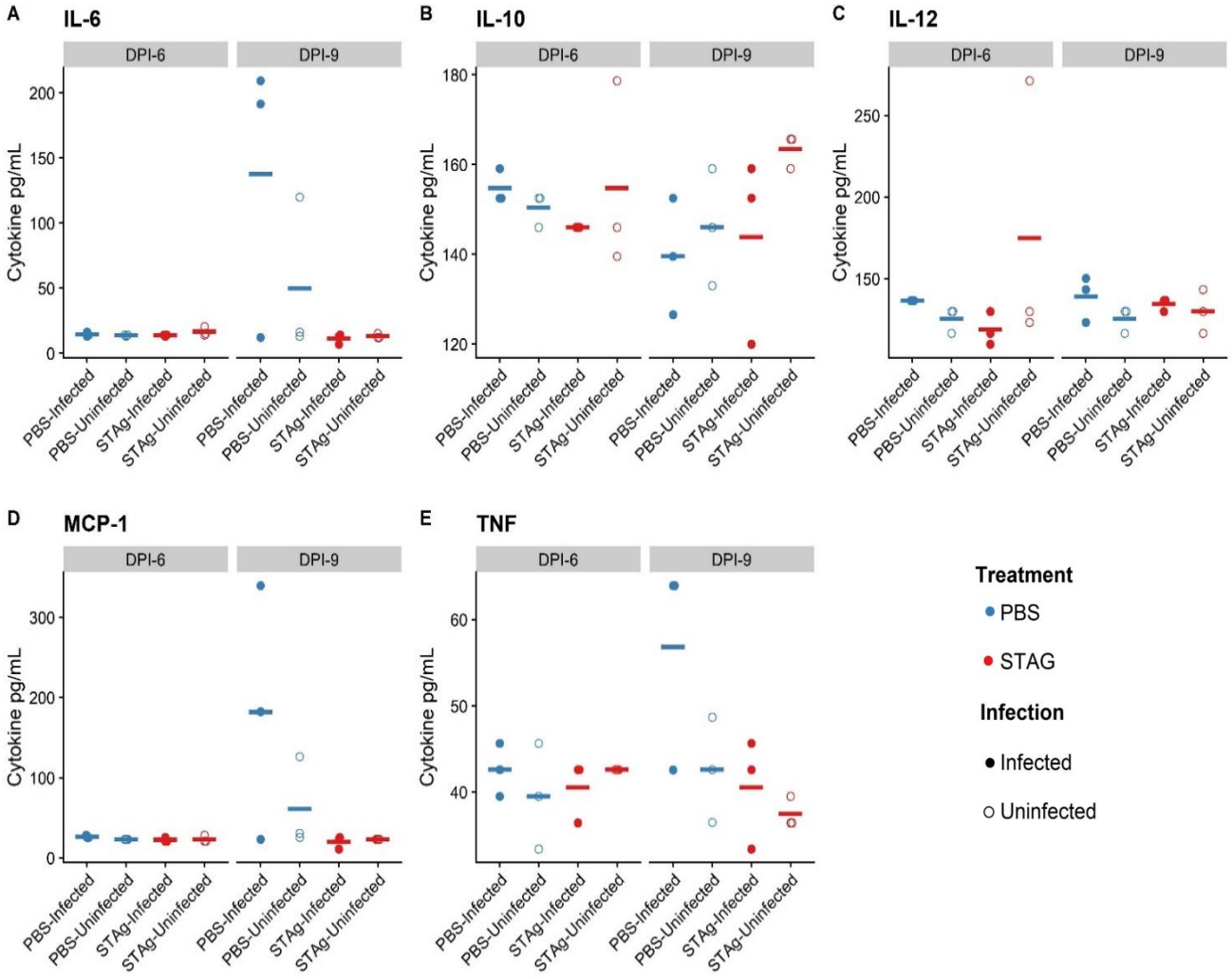

Figure S9. Cytokine levels in mice sera (Experiment 3). Serum was collected from mice euthanized 6 and 9 dpi. Cytokine levels of IL-6, IL-10, IL-12, TNF, and MCP1 were determined using an inflammation cytokine bead array kit (Biosciences). ANOVA testing was used to calculate significance between treatment groups as well as within the same treatment group across dpi. No significant differences were observed.

STAg treated mice also had a lower abundance of Ccl4, the prostaglandin receptor Ptger3, and granzymes B and K (Fig 7), which have all previously been implicated in *Cryptosporidium* infection. Ccl4 is a chemokine independent of IFNγ, whose expression

level increases during *C. parvum* infection when compared to control mice (33). While the differences in prostaglandin receptors have not previously been seen, high levels of prostaglandins have been observed in *C. parvum* infection, which leads to increased mucosal activity and downregulation of inflammatory cytokine production (79,80). Granzymes induced by NK cells or CD8+ cytotoxic T cells (81) have been found in high abundance in mice and humans infected with *Cryptosporidium*, inducing cell death and cytolysis of infected epithelial cells. They are also associated with apoptosis and colon lesions in AIDS patients co-infected with *Cryptosporidium* (82–85).

Even though we could not assess *C. parvum* differential expression, we report the most abundant *C. parvum* transcripts within the ileum. Among those transcripts, we found the GDP-fucose transporter (CGD3_500) to be abundant in our infected animals, regardless of treatment. In other apicomplexan parasites like *Toxoplasma gondii,* O-fucosylated glycoproteins can form assemblies that are associated with nuclear pore complexes (86). For both *T. gondii* and *Plasmodium falciparum,* O-fucosylation of thrombospondinlike repeats is required for processing proteins relevant to host cell invasion (87,88).

We also found transcripts for parasite mucins in high abundance. Mucins are glycoproteins that have an amino acid composition consisting of 20 to 55% serine, threonine, and proline residues, with extensive chains of O-linked carbohydrates (55) forming homo-oligomers. Mucins have been reported both in the host and in some

gastrointestinal parasites. *Cryptosporidium's* mucins are important for attachment and invasion to the host cell (55) or evasion of the host immune system (89). Many essential *Cryptosporidium* proteins are mucin-like proteins such as gp40/15 (90), cpClec, gp30, and gp900 (91). There is a genetic locus of seven mucins denominated cpMuc1-7, which suggests that these seven mucins are regulated and expressed in a coordinated fashion with a role in the same biological processes (55). C*ryptosporidium* mucins have high polymorphism between species and genotypes, which suggests gene products might be important virulence determinants subject to immune pressure (55). Recently, it has been published that mucins play a role in tissue tropism between gastric and intestinal *Cryptosporidium* species and also determine differences in host range among *Cryptosporidium* species (92,93). Further investigation is required for the validation of the differential expression of *C. parvum* transcriptomic response to STAg treatment.

We did not find significant differences in transcript abundances when comparing STAg vs PBS treatment. It is possible that STAg treatment only affects the host transcriptome while the parasite transcriptome remains unaffected. This lack of differential *C. parvum* expression could also be due to the limitations of coverage and sequence depth of our study. There was a significantly higher mapping of *C. parvum* reads to the ileum than the cecum samples. Thus, we focused on the most abundant transcripts within the ileum with both treatments in hopes that the *C. parvum* community can use this *in vivo* data for comparisons with *in vitro* systems. By discovering *C. parvum* genes that are more abundant during infection of animals that lack IFNγ signaling, we are defining possible alternatives to control infection

Methods

Generation of RNA and RNA Sequencing

We used the University of Wisconsin – Madison Biotechnology Center's Gene Expression Center Core Facility (Research Resource Identifier - RRID:SCR_017757) for RNA isolation, RNA library preparation, and the DNA Sequencing Facility (RRID:SCR_017759) for sequencing and demultiplexing of reads. Libraries were prepared for polyA enrichment (Illumina TruSeq

Stranded mRNA). Samples were run in duplicate in two lanes of a 2x100bp S1 Flowcell (Novaseq6000). On average a total of 41.5 million reads (min: 36 million, max: 49.6 million) paired-end 150-bp reads per sample were generated. The quality of the reads was determined (FastQC v0.11.9 (95), a threshold of 34 was selected, and only reads that met the threshold were used for further analysis.

Transcriptome assembly and Differential expression Analysis

We trimmed the data to remove low-quality reads (Trimmomatic, v0.39) (6) Mapping reads to two genomes: *Mus musculus* strain C57BL/6 (GRCm38.p6, release38; NCBI) and *C. parvum* (Iowa II, release 49; CryptoDB) was conducted (Spliced Transcripts Alignment to a Reference program, v2.7.5c) (97,98). Default parameters were selected with the following exceptions: maximum mismatch (2-bps), minimum intro length (20-bps), and maximum intron length (100000-bps). Quantification of mapped reads and the generation of a counts table were conducted (RSEM v1.3.1(99). Counts were imported

into R (tximport v1.16) (100), and differential expression analysis was conducted (DESEq2 v1.28.1) (101). The log-transformed DESeq2 values were used for the generation of PCA plots. For reads mapped to the host genome, we selected the following thresholds: false discovery rate (10%), adjusted p-value (< 0.05), and an absolute log2fold change (>2). If a differential expression gene met those parameters, we called that gene significantly differentially expressed. (Supplemental CSV file 1-12). Given that the average *C. parvum* Iowa II percentage mapping (ileum= 2.58% and cecum= 0.33%) was significantly lower than the host mapping (ileum= 78.92% and cecum= 77.95%), we selected only two thresholds for *C. parvum* Iowa II significance: false discovery rate (10%), and adjusted p-value (< 0.05). Lists of significant genes were used as input for gene ontology enrichment analysis using the Database for Annotation, Visualization, and Integrated Discovery (DAVID, v6.8 (46,47) for visualization of this enrichment only terms were populated by 3 or more genes were charted ($p < 0.05$).

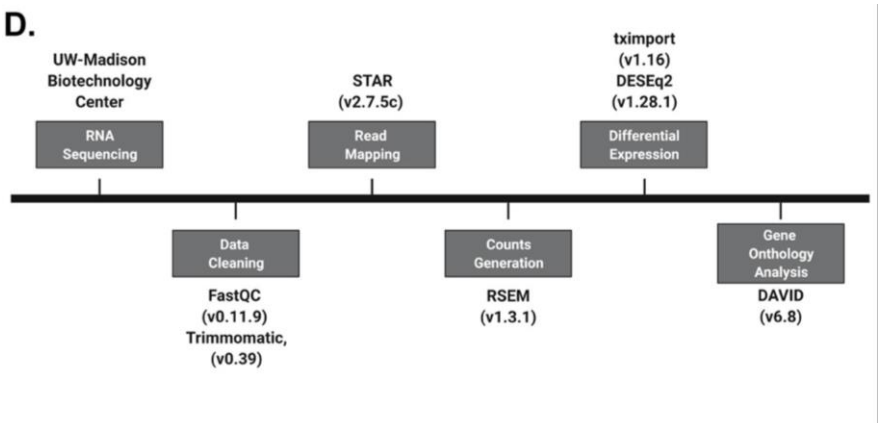

Figure 2. Mice Experimental Design and analysis for RNA sequencing. **D)** RNA sequencing analysis flowchart listing the programs and packages used for reading and analysis. Versions used are indicated in parenthesis.

Cytokine Profile

The concentrations of cytokine IL-6, IL-10, IL-12, TNF, and MCP-1 were measured using a mouse inflammation cytokine bead array kit (552364; BD Biosciences). Blood serum was collected for cytokine analysis on 6 and 9 dpi, following the manufacturer's instructions. Samples were analyzed by flow cytometry with a ThermoFischer Attune at the UW-Madison Flow Cytometry Core (Grant P30 CA014520) and concentrations were calculated using FlowJo.

List of abbreviations

IFNγ = Interferon gamma; Nluc = Nano luciferase; STAg= soluble *Toxoplasma gondii* Antigen; RNA= ribonucleic Acid; PolyA= poly adenylation; DEGs= differential expressed genes; OAS= oligoadenylate synthetase; qPCR = quantitative Polymerase Chain Reaction; IVIS = *in vivo* imaging system; AUC = are under the curve; DPI: Days postinfection; GO: Gene ontology; PBS: Phosphate buffered saline; PCA: Principal component analysis; RNAseq: High-throughput RNA sequencing; STAR: Spliced Transcripts Alignment to a Reference program; Gapdh = Glyceraldehyde-3-Phosphate Dehydrogenase; SLFN = Schlafen gene family ; ATP = adenosin Triphosphate; padj = P value adjusted. DAVID = Database for Annotation, Visualization, and Integrated Discovery. FDR = false discovery rate; CC = Go term integral component of membrane; MF = Go Term Molecular Function; BP= Go Term Biological Process

Availability of data and materials

All of the data is available. All raw RNA sequencing data have been deposited in the NCBI Sequence Read Archive Link under the accession number PRJNA726295

RNA sequencing data have been supplied for public availability to HostDB.org and CryptoDB.org. Differential expression analysis output and counts of mapped reads per individual biological replicate are available (Supplemental files 1-12).

Ethics approval

All animal studies were carried out in compliance with the Animal Research: Reporting of In Vivo Experiments (ARRIVE) guidelines and approved by the Institutional Animal Care and Use Committee (IACUC) of the University of Wisconsin School of Medicine and Public Health. The University of Wisconsin is accredited by the International Association for Assessment and Accreditation of Laboratory Animal Care. All methods and all experimental protocols were approved by the University of Wisconsin IACUC (protocol M005217) as well as the Office of Biological Safety (protocol B00000086).

Funding: This work was funded by the National Institutes of Health (R21AI122898 RMO, LJK; R01AI144016 LJK; T32007215 CMC), SciMed Graduate Research Scholars Fellowship UW-Madison (CMC), Foster Wisconsin Distinguished Fellowship from the Food and Research Institute (CMC), The Hartwell Foundation postdoctoral fellowship (ALG), and Morgridge Postdoctoral Fellowship supported by the Morgridge Institute for Research (GMGL). Funding bodies had no role in the design of the study and collection, analysis, and interpretation of data and in writing the manuscript.

Figures legends not generated by CMC

Figure 1. **Infection time course of *C. parvum* infected mice treated with STAg or PBS. (A)** Oocyst shedding per dpi in experiment #1 over 14 dpi; *p=0.020. Oocyst shedding was calculated by qPCR, as described in the methods section. **(B)** Oocyst shedding per dpi in experiment #2 over 14 dpi; **p=0.0058 and *p= 0.0457. Oocyst shedding was calculated by expression of nanoLuciferase, as described in the methods section. Each circle represents a mouse (Blue=PBS and Red=STAg). Open circles represent uninfected animals while filled circles represent infected animals. Statistic differences were determined using R using ANOVA testing. The mean of each group is represented with a line. **(C)** Bioluminescent imaging of *C. parvum* in IFNγ-KO mice throughout the intestinal tract: the intestinal tract of mice infected for 9 days with Nluc *C. parvum* Iowa II strain at $1x10^5$ showed a higher signal in the ileum and cecum regions compared to the duodenum, jejunum, and colon sections. Radiance scale bar (p/sec/cm2/s).

Figure 2. Mice Experimental Design and analysis for RNA sequencing. **(A)** For the RNAseq analysis, 12 mice, 6 infected and 6 non-infected were treated with PBS or STAg. The treatment was administered 4 hours before infection (2.5×10^5 Nluc *C. parvum* Iowa II strain oocyst by oral gavage) and 1, 3, and 5 dpi. Fecal samples were collected every other day and the infection was quantified by nanoLuciferase expression. IFNγ-KO mice were euthanized on 9 dpi and ileum and cecum samples were collected. **(B)** Oocyst shedding per dpi in experiment 3 over 9 dpi. Oocyst shedding was calculated by expression of nanoLuciferase, as described in the methods

section. Significance was determined using R using ANOVA testing. The mean of each group is represented with a line. Open circles represent uninfected animals while filled circles represent infected animals **(C)** Relative quantification of C. *parvum* by qPCR using 18S rRNA primers P4 normalized to mouse Gapdh in ileum samples. Mean of two independent experiments. Fold change was calculated relative to the reference PBSinfected group at day 6. Significance was determined using R using ANOVA testing **p =0.0079 (Infected STAg D6 vs D9). Each circle represents a mouse (Blue=PBS and Red=STAg).

Supplemental Figure S1. Quantification of *C. parvum* in the ileum at 6 and 9 dpi. **(A)** Relative quantification of *C. parvum* in ileum samples by qPCR using 18S rRNA P4 primers. 1/CT ratio was calculated with Ct value for *C. parvum* 18S rRNA gene over Ct of mouse housekeeping gene Gapdh for the same sample. Each graph represents the mean of two independent experiments. Statistical analyses were performed by the Anova Kruskal-Walls test and significant differences between multiple comparisons were calculated by Dunn's test. **(B)** Relative quantification of *C. parvum* in ileum samples by qPCR using 18S rRNA P5 primers normalized to mouse housekeeping gene Gapdh. Fold change was calculated relative to the reference PBS group of the respective day. **(C)** Relative quantification of *C. parvum* in ileum samples by qPCR using 18S rRNA P5 primers. 1/CT ratio was calculated with Ct value for *C. parvum* 18S rRNA gene over Ct of mouse housekeeping gene for the same sample.

Supplemental Figure S7. qPCR analysis of host genes at 6 and 9 dpi. (A & C) Relative gene expression of Ifi44 and Oas-3 in mice ileum samples by qPCR. Ct values were

normalized to mouse housekeeping gene Gapdh. Fold change was calculated relative to the reference PBS group of the respective day. (B & D) Relative gene expression of Ifi44 and Oas-3 in mice ileum samples by qPCR. 1/CT ratio was calculated with Ct value for each gene over Ct of mouse Gapdh housekeeping gene for each sample. (E & G) Relative gene expression of Fbp1 and Lct in mice ileum samples by qPCR. Ct values were normalized to mouse housekeeping gene Gapdh. Fold change was calculated relative to the reference PBS group of the respective day. (F & H) Relative gene expression of Lct and Fbp1 in mice ileum samples by qPCR. 1/CT ratio was calculated with Ct value for each gene over Ct of mouse Gapdh housekeeping gene for each sample. The graphs represent the mean of two independent experiments. Statistical analyses were performed by the Anova Kruskal-Walls test and significant differences between multiple comparisons were calculated by Dunn’s test.

Chapter 3. *Entamoeba muris*

Recapitulating the life cycle of the global pathogen *Entamoeba* in mice

The text in this chapter is a reformatted version of an article submitted to PLOS Neglected Tropical Diseases on June 23, 2022.

Citation

To be determined

Author contributions

Design of experiments: CMC, MYH, LAO & LJK. Conceptualization: CMC & LJK; Funding acquisition: CMC & LJK; Investigation: CMC, MYH, LAO; Methodology: CMC, LAO & MYH; Project administration: LJK. Resources: LJK; Supervision: LJK. Visualization: CMC, LAO, MYH; Writing: CMC, LAO, MYH; Writing – review & editing: CMC, MYH, LAO & LJK. All authors read and approved the final manuscript.

Acknowledgments

We sincerely thank Upinder Singh and her lab for advice, and Jerry Cangelosi and his lab for the 1A4 anti-Jacob2 antibodies. We would like to thank researchers from across the US for providing mouse fecal samples. We also thank members of the Knoll lab (Nicole M. Davis, Billy J. Erazo Flores, and Carlos J. Ramirez Flores) for assistance

with experiments, software, as well as scientific advice. We thank Apoorva P. Maru and Sarah K. Wilson for their critical reading and editing of this manuscript.

Abstract

There are several *Entamoeba* species that colonize humans, but only *Entamoeba histolytica* causes severe disease. *E. histolytica* is transmitted through the fecal-oral route to colonize the intestinal tract of 50 million people worldwide. The current mouse model to study *E. histolytica* intestinal infection directly delivers the parasite into the surgically exposed cecum, which circumvents the natural route of infection and infectious fecal cysts are not produced. To develop a fecal-oral mouse model, we screened our vivarium facility for a natural murine *Entamoeba* colonizer via a pan-*Entamoeba* PCR targeting the 18S ribosomal gene. We determined that C57BL/6 mice were chronically colonized with an *Entamoeba muris.* This amoeba is closely related to *E. histolytica,* as determined by 18S sequencing and cross-reactivity with an *E. histolytica*-specific antibody. In our screen, we discovered that our outbred Swiss Webster (SW) mice were not chronically colonized with *E. muris.* We challenged SW mice with $1x10^5$ *E. muris* and discovered they were susceptible to infection, with a peak of cyst shedding between 5-7 days postinfection. Most SW mice did not have significant weight loss but there was a trend for less weight gain throughout the experiment as compared to mock-infected controls. Within the intestinal tract, *E. muris* localizes to the cecum and colon, but no *E. muris* is detectable within the small intestine. When purified *E. muris* cysts were treated with bile acids*,* mobile pre-trophozoite stages could be seen excysting from their chitin-rich shells*.* Overall, this work describes a novel fecal-oral mouse model for the important global pathogen *E. histolytica.*

Author's Summary

Infection with parasites from the *Entamoeba* genus are significantly underreported causes of diarrheal disease that disproportionally impact tropical regions. There are several species of *Entamoeba* that infect humans to cause a range of symptoms from asymptomatic colonization of the intestinal tract to invasive disease with dissemination to the soft tissue organs. All *Entamoeba* species are spread via the fecal-oral route in contaminated food and water. Studying the life cycle of *Entamoeba* species, from colonization of their host to infectious cyst production in the feces, can provide targets for vaccine and drug development. Because there is not an oral challenge rodent model, we screened for a mouse *Entamoeba* within our vivarium and identified *Entamoeba muris* as a naturally occurring colonizer. We determine the peak of infection after an oral challenge as well as the localization within the intestinal tract and the cues that trigger excystation *in vitro*. This oral infection mouse model will be valuable for the development of novel therapeutic options for *Entamoeba* infections.

Introduction

Parasitic diseases are underappreciated causes of morbidity and mortality because disease outcomes are variable (1), cases are often underreported (2), and disease disproportionately impacts geographical locations experiencing poverty (94-96). Diarrheal diseases are a significant and underreported cause of child mortality in tropical regions (97, 98). Such infections are exacerbated by factors such as resource availability, lack of sanitation infrastructure, and malnutrition (99). For these reasons,

diarrheal diseases represent a long-standing and significant burden, particularly in Latin America, Southeast Asia, and sub-Saharan Africa (99). Diarrheal diseases are caused by a range of pathogens, such as bacteria, viruses, and parasites including the *Entamoeba* genus*. E. histolytica* is an extracellular parasite that causes human infection with variable outcomes ranging from asymptomatic colonization to diarrhea, invasive colitis, liver abscess, and metastatic infection. Amebiasis from *E. histolytica* is the second leading parasitic cause of death globally but remains classified as a neglected disease (3). Globally 50 million cases are reported per year, resulting in 2.2 million disability-adjusted life years and 55-100 thousand deaths annually (reviewed in (100)).

Entamoeba infection starts with the ingestion of the cyst stage from contaminated food or water. Presumably in the small intestine, the *Entamoeba* cyst molts from its chitinous shell and differentiates into the metabolically active trophozoite form through a process known as excystation. Trophozoites then attach to the intestinal epithelium where they undergo asexual reproduction and encystation. The infectious fecal cysts are shed and contaminate the environment to complete the parasite life cycle. Trophozoites can either stay contained within the intestinal tract or may disseminate to soft tissue organs like the liver, the lungs, or the brain (101-104), although in ~90% of the cases, the infection remains in the intestinal lumen (105, 106). The current murine intestinal infection model surgically delivers trophozoites into the cecum of animals and has provided immense insight into host-pathogen interactions but produces no cysts (107). Thus, modeling the critical developmental stage interconversion that *E. histolytica* undergoes between ingestion and colonization of the cecum is not yet possible (108). A model that includes

the developmental changes of excystation and encystation would allow the field to understand the transmission of the pathogen and find targets for intervention (reviewed in (109)) as only viable parasites completely encysted and shed via the fecal-oral route can contaminate food and water and infect a new host.

The parasitology field has used species that naturally colonize animals to expand the knowledge of infectious diseases that are fastidious to culture or model in the laboratory. Murine pathogens like *Plasmodium chabaudi* have been pivotal to studying the *in vivo* pathology of malaria. For the *Entamoeba* field, *Entamoeba invadens,* a reptile-specific pathogen, has provided critical insights related to developmental changes like encystation. Here, we screened for a natural murine *Entamoeba* colonizer and developed an oral infection model using Swiss Webster (SW) mice. We further determine infection location within the intestinal tract and excystation cues for the purified fecal cysts.

Results

C57BL/6 but not Swiss Webster mice are chronically colonized with a naturally occurring *Entamoeba* organism

We screened transgenic and wild-type animals within our vivarium facility (Fig 1A) using a Pan-*Entamoeba* PCR (Fig S1). We screened fecal material from males and females with ages ranging from newly weaned to mice that spent up to a 1 year in our facility.

Eighty percent of the mice from the C57BL/6 background were colonized with an *Entamoeba* organism. To address if an *Entamoeba* is naturally occurring in other vivariums, we requested fecal samples from C57BL/6 mice from five collaborators around the country (n=18). We detected *Entamoeba* using a single-step PCR in samples from one other institution while in another we only detected the parasite using a 2-step, nested PCR. However, colonization was by no means ubiquitous as the majority of these institutions were PCR negative even when using the nested approach (Table S1). In contrast, all the SW mice from our vivarium tested were PCR negative, regardless of age or sex (Fig 1A).

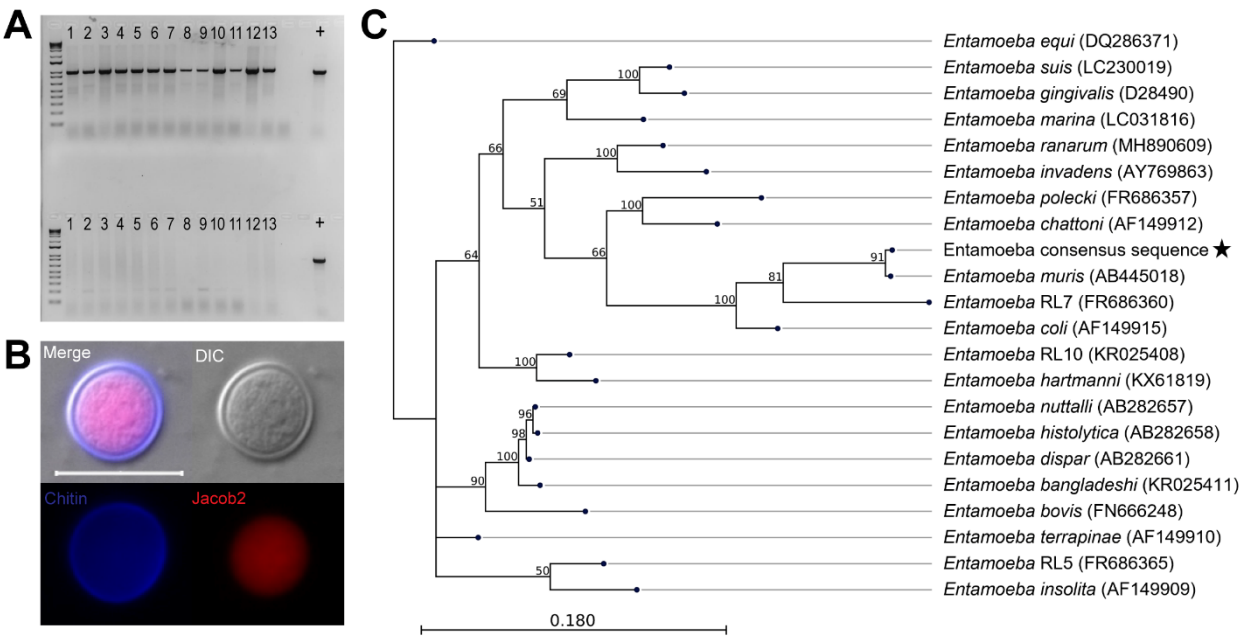

Fig 1. Identification of *Entamoeba* species. (A) Representative Pan-*Entamoeba* PCR for C57BL/6 mice (top) and Swiss Webster mice (bottom) within our vivarium. The loading control was murine GAPDH (data not shown). Each lane number represents a mouse cage. Positive control (+) is isolated genomic DNA from axenic *Entamoeba histolytica* culture. (B) Immunofluorescence assay staining for chitin (calcofluor-white), Jacob2 (1A4 antibody), scale bar represents 20µm. (C) 18S phylogeny is based on a 1,033 bp alignment including 27 published *Entamoeba* sequences, labeled as species name (NCBI accession), plus the *Entamoeba* found in our vivarium, indicated by a star. Numbers on branches are bootstrap values (%) based on 1,000 replicates (values >50% are shown). The scale bar indicates nucleotide substitutions per site.

Fig S1. Pan-*Entamoeba* primer design. Full-length Entamoeba 18S rRNA sequences (n=63, 25 Entamoeba species) were downloaded from NCBI GenBank, aligned in CLC Genomics Workbench v20.0.4 (Qiagen, Hilden, Germany), and conserved regions were the target for the placement of the forward and reverse primers, which together amplify a 1 kb product.

Forward: 5'-AGATACCGTCGTAGTCCT-3'

Reverse: 5'-ACGACTTCTCCTTCCTCTAA-3'

Table S1. Colonization rates at vivarium facilities around the United States.

Institution Location	B6 Samples	% Positive (40 cycle PCR)	% Positive (Nested PCR)
Arizona	N= 4	0%	25%
California	N= 2	100%	100%
Pennsylvania	N= 2	0%	0 %
Texas	N=1	0%	0%
Vermont	N=10	0%	0%

To confirm the PCR findings in our animals, we developed a sucrose density gradient protocol based on fecal isolation methods from the *Entamoeba* literature (110) (Fig S2) and conducted phenotypic characterization of the isolated cysts (Fig S3). We processed feces of PCR-positive mice within a sucrose gradient of 1.33 specific gravity and isolated structures of 15 - 20µm in diameter. These structures were cyst-like and stained with calcofluor white, indicating the presence of chitin (Fig 1B). We further characterized these cysts by immunofluorescence detection of a previously published *Entamoeba*-specific antibody targeting the lectin Jacob2 (48). The sucrose gradient results for B6 and SW mice were 100% replicative of the Pan-*Entamoeba* PCR; SW mice did not display cyst-like structures in their fecal samples, while the B6 fecal samples contained 15 - 20µm-diameter cysts that stained positive for both chitin and Jacob2 (Fig 1B).

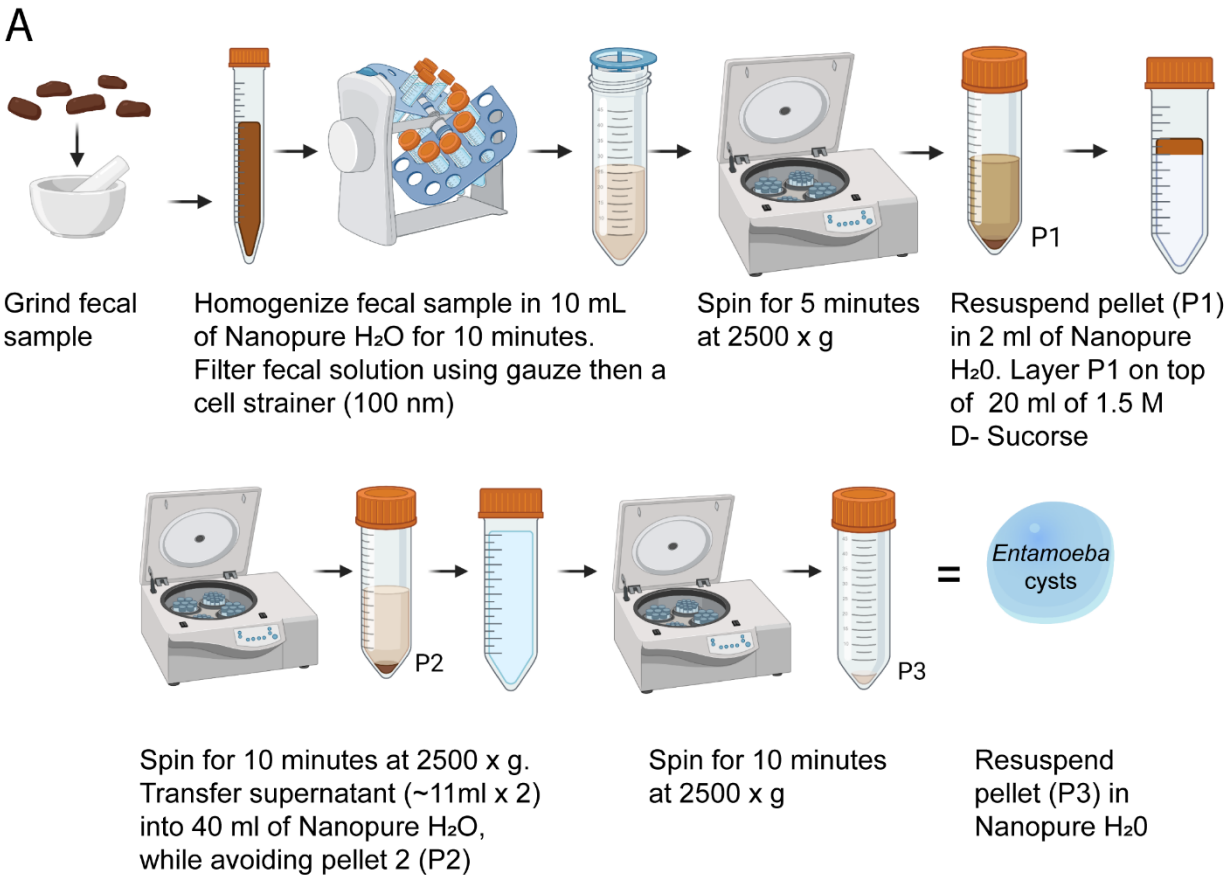

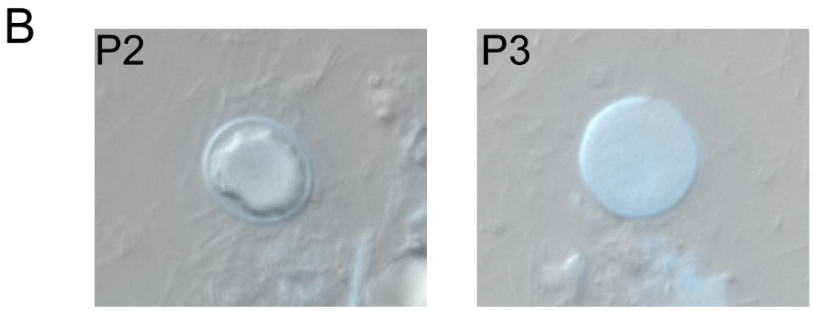

Fig S2. Sucrose gradient isolation protocol. (A) Fecal samples (0.25 – 5g) that were collected overnight were processed as indicated above. Briefly, fecal samples were ground to a fine powder using a mortar and pestle then shortly homogenized with Nanopure water for 15 minutes using a Mini Rotator (Glas-Col) at 60 rpm. The resulting solution was filtered through four-ply cotton gauze, and samples were pelleted for 10 minutes at 2500 x g. The resulting pellet was layered on top of 1.5M sucrose solution. The mid-layer was washed with Nanopure water and pelleted again at the same speed. Pellet 3 was suspended in Nanopure water, and the isolated un-fixed cysts were used as the input for oral infection. (B) While cysts can be found in the P2 pellet during the winter months, they have a dehydrated appearance compared to the cysts in the P3 pellet, likely due to the low humidity of the vivarium.

Fig S3. Representative phenotypic characterization of the number of nuclei of *E. muris* cysts (>4 nuclei). Scale bar represents 10µm.

To determine the species of *Entamoeba* present in our mice, we gel-purified and Sanger-sequenced the 1 kb pan-*Entamoeba* PCR product from cecum, colon, and fecal samples from 8 mice (n=24 total). The resulting reads were 100% identical to each other and most closely matched *Entamoeba muris* (GenBank accession number AB445018) with 98% query coverage at 92% identity and an E value of 0.00. We then performed phylogenetic analysis to further confirm this preliminary species identification. Alignment of 21 published *Entamoeba* 18S sequences from NCBI GenBank along with our consensus Sanger sequence yielded a final alignment length of 1,033 bp. A maximum-likelihood phylogeny built from this alignment shows our organism to cluster with *E. muris,* as expected from the BLASTn results, and form a clade with *Entamoeba* RL7 and *E. coli* (Fig 1C). Pairwise comparison of the *E. muris/coli* clade based on the 18S phylogenetic tree across the entire length of the alignment shows our organism to be 91.63% identical to *Entamoeba muris* with 9 total alignment gaps (0.87%) as compared to 81.82% identity and 42 gaps (4.1%) with it's next-closest relative, *Entamoeba* RL7 (Table S2). Thus, we will refer to this organism as *E. muris* hereafter.

Table S2. Pairwise comparison of *Entamoeba muris/coli* clade. Comparison is based on 1,033 base pair alignment. Percent nucleotide identity is shown above the diagonal and number of gaps are shown below the diagonal.

	Entamoeba coli	*Entamoeba* RL7	*Entamoeba muris*	Consensus sequence
Entamoeba coli		77.9	77.6	76.1
Entamoeba RL7	51		82.6	81.7
Entamoeba muris	44	37		91.6
Consensus sequence	49	42	9	

Swiss Webster mice are susceptible to *Entamoeba muris* oral challenge

As SW mice were not currently colonized, we determined if these mice were suitable for *E. muris* infection and characterization using an oral challenge model. When orally challenged with a low cyst dosage ($1x10^5$ isolated from B6 mice), SW mice were able to host a patent infection, as evidenced by fecal cyst shedding, but displayed asymptomatic infections in all cases. We monitored changes in weight during the infection but observed no significant differences between uninfected animals and animals orally challenged with *E. muris* cysts, although there was a trend for infected animals to have less weight gain when compared to uninfected controls (Fig 2A). Weight loss was only observed for one of the biological replicates (Fig S4A) and was not correlated to cysts shedding (Fig S4B). Fecal samples showed cysts as early as 3 days postinfection (dpi) via sucrose gradient. When using this method, we determined the peak of infection to be 7 dpi based on average cysts counts across four independent

infection replicates (n=27 mice, 17 infected and 10 uninfected controls). Shedding per biological replicates does not show significant differences between biological replicates (Fig S4B). We detected a significant decrease in cyst shedding by 11 dpi, and very few *E. muris* cysts were detected using this method by 28 dpi.

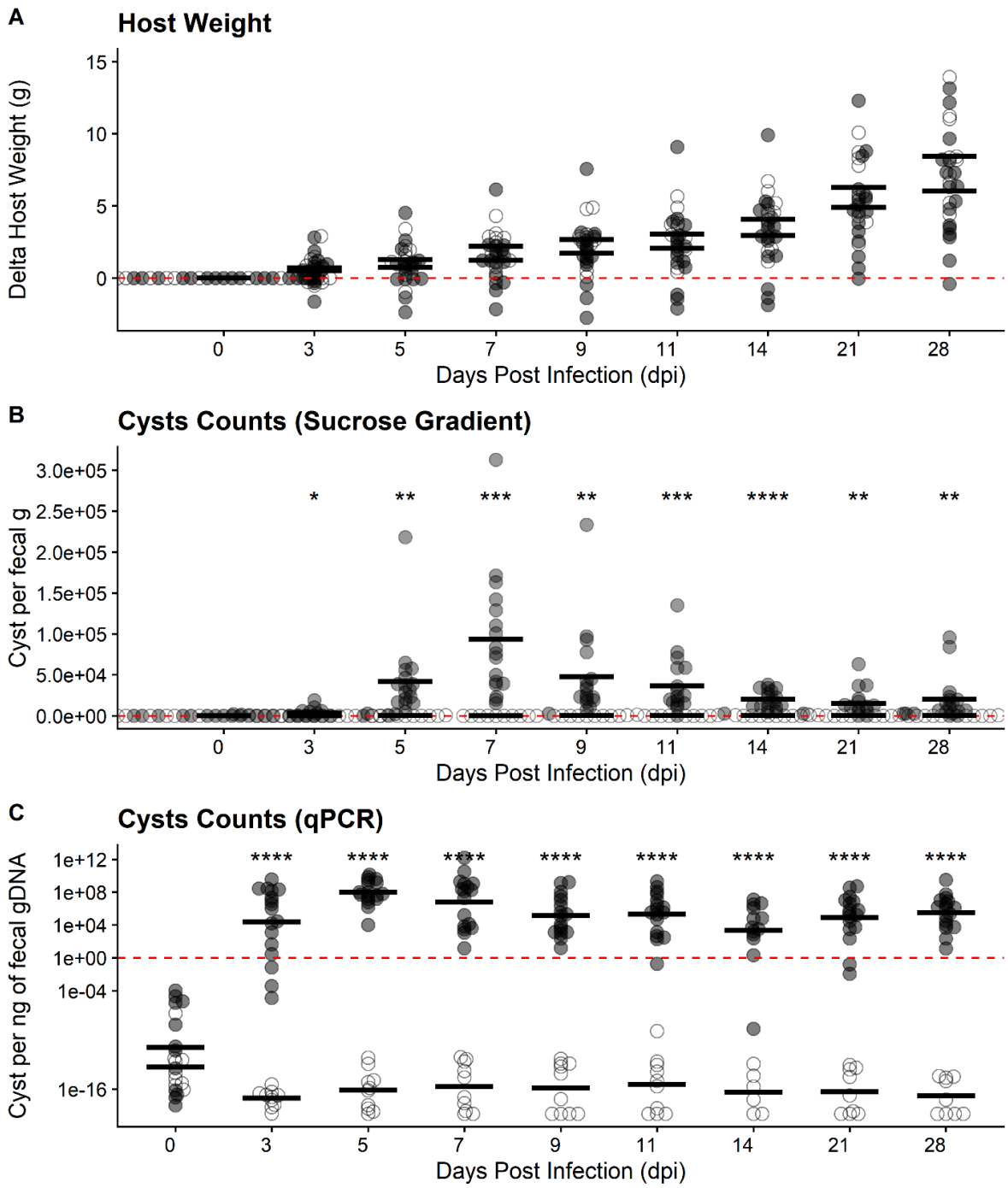

Fig 2. Swiss Webster are susceptible to *Entamoeba muris* oral challenge. (A) Host weight was monitored through the course of infection. (B) Quantification of cysts isolated by sucrose gradient from Swiss Webster's fecal samples (normalized by fecal weight). Peak of infection was determined to be 7 dpi. (C) Quantification of cysts in fecal samples via qPCR isolated from Swiss Webster's fecal samples (normalized by gDNA per qPCR reaction). Each dot represents a single mouse (n=27 mice, 17 infected and 10 uninfected controls). Open circles represent uninfected mice while grey circles represent infected mice. Significance was determined using a two-tailed t-test between the uninfected vs. infected average per DPI. Data combines four independent biological replicates (see supplement Fig S4 for individual biological replicate (n=4) plotting).

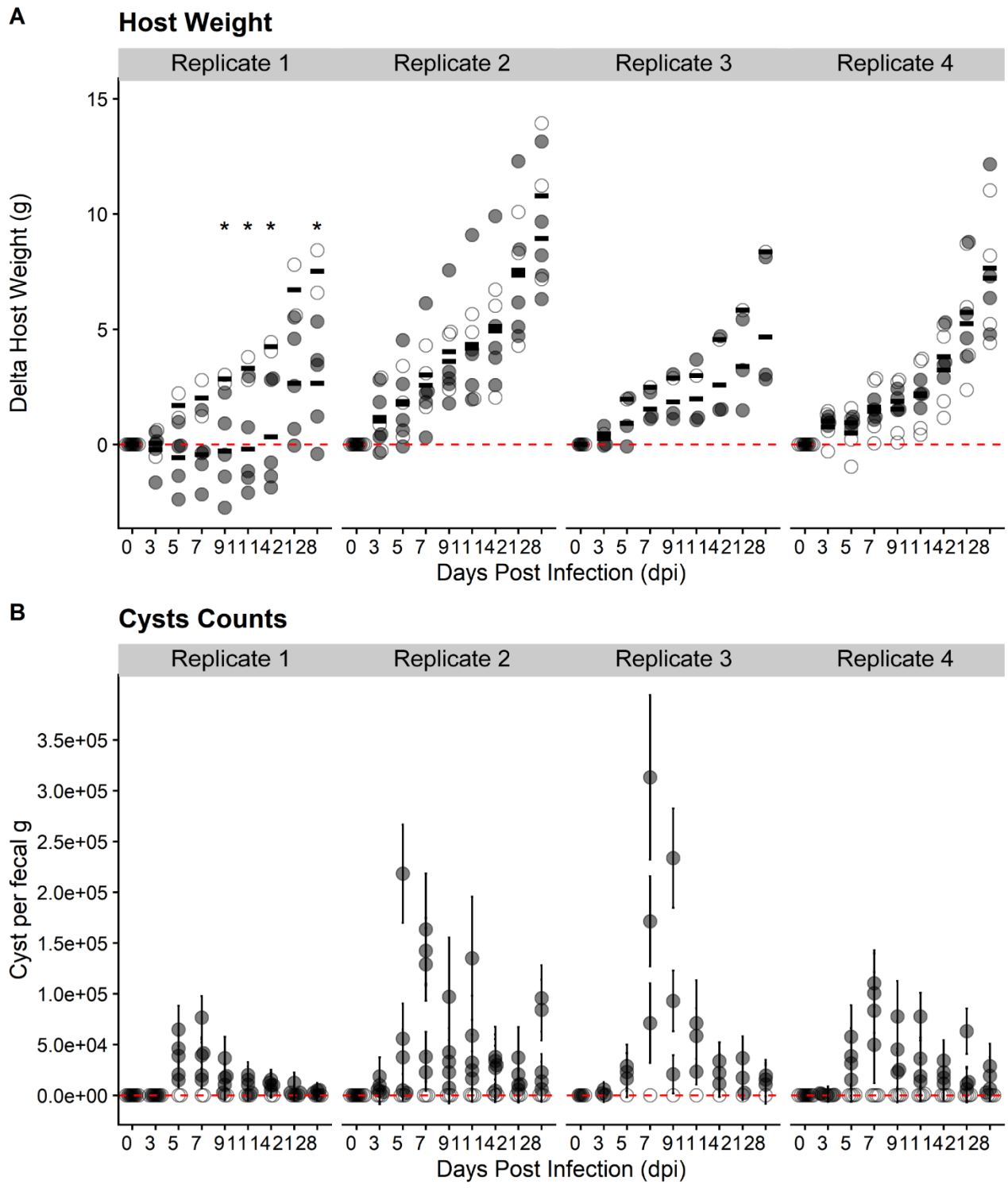

Fig S4. Swiss Webster mice are susceptible to *Entamoeba muris* oral challenge, per biological replicate. (A) Host weight was monitored through the course of infection. (B) Quantification of cysts isolated by sucrose gradient from Swiss Webster's fecal samples (normalized by fecal weight).

Using a similar approach to the Pan-*Entamoeba* screen, we designed qPCR detection primers that amplified a 200-bp amplicon, to quantify *E. muris* shedding. We generated a standard curve using cyst samples of known concentrations based on counts, ranging from 1,562 cysts to 100,000 cysts in a 2-fold scale (Fig S5). Our qPCR results determined that *E. muris* was detectable as early as 3 dpi, in accordance with the sucrose gradient isolation. However, the peak of infection was at 5 dpi and a significant reduction was evident by 9 dpi. Taken together, these results suggest that qPCR detection occurs prior to peak viable cysts isolation.

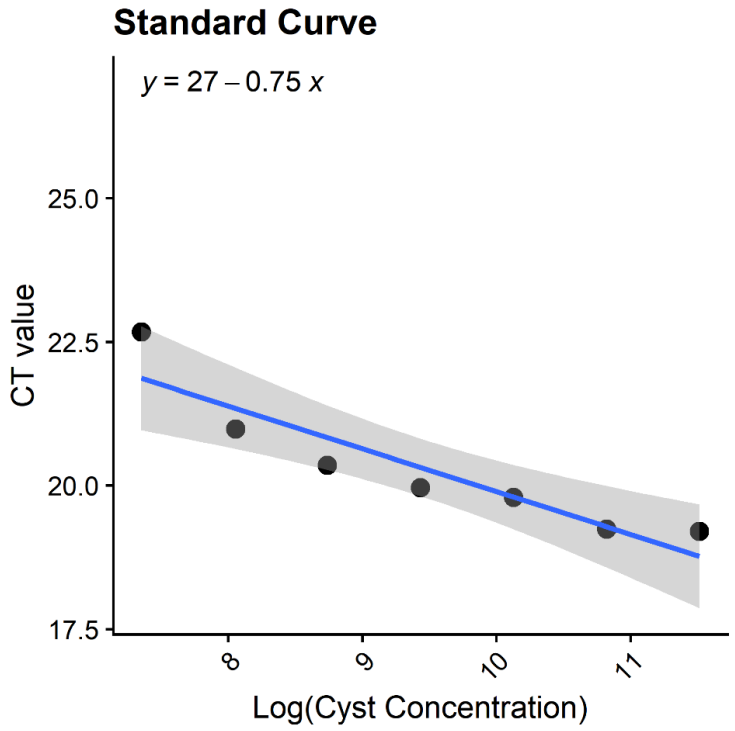

Fig S5. Standard curve for qPCR cyst quantification. Primers were designed as described above for pan-*Entamoeba* PCR (Fig S1), except here they were chosen to amplify a 200 bp product (see primers below). We generated a standard curve using cyst samples of known concentrations, ranging from 1,562 cysts to 100,000 cysts (2-fold scale). Concentrations for Fig 2 were calculated using the cycle threshold (CT) values of the experimental samples and the linear trendline equation presented above.

Forward: 5'-TCGAGATAAACGAGAGCGAAAG-3'

Reverse: 5'-GTCAGGACTACGACGGTATCTA-3'.

Entamoeba muris resides in the large intestine at 5 days postinfection

E. histolytica is thought to replicate in the colon and has been found during diagnostic colonoscopies (111). As our model uses the natural oral route of infection, we aimed to determine where *E. muris* is located during primary infection. We infected SW mice with 10^5 cysts by oral gavage and collected the intestinal content and mucus layer of murine gastrointestinal sections at 5 dpi, when the overwhelming majority of the animals were shedding cysts by qPCR detection (Fig 2). The small intestine was sectioned into three parts: duodenum (D), jejunum (J), and ileum (I). The cecum (Ce) and the colon (Co) correspond to the large intestine (Fig 3A). As a positive control for the presence of cysts, we included two fresh fecal pellets (F) and we used a standard loading control, murine GAPDH (Fig 3B, lower panel). As expected from clinical data (reviewed in (112)), *Entamoeba* localizes within the large intestine (Fig 3B, upper panel). While we found mouse to mouse variability between levels of *E. muris* detection within the cecum, colon, and fecal samples, no *Entamoeba muris* gDNA was isolated from the small intestine (Fig 3B, upper panel).

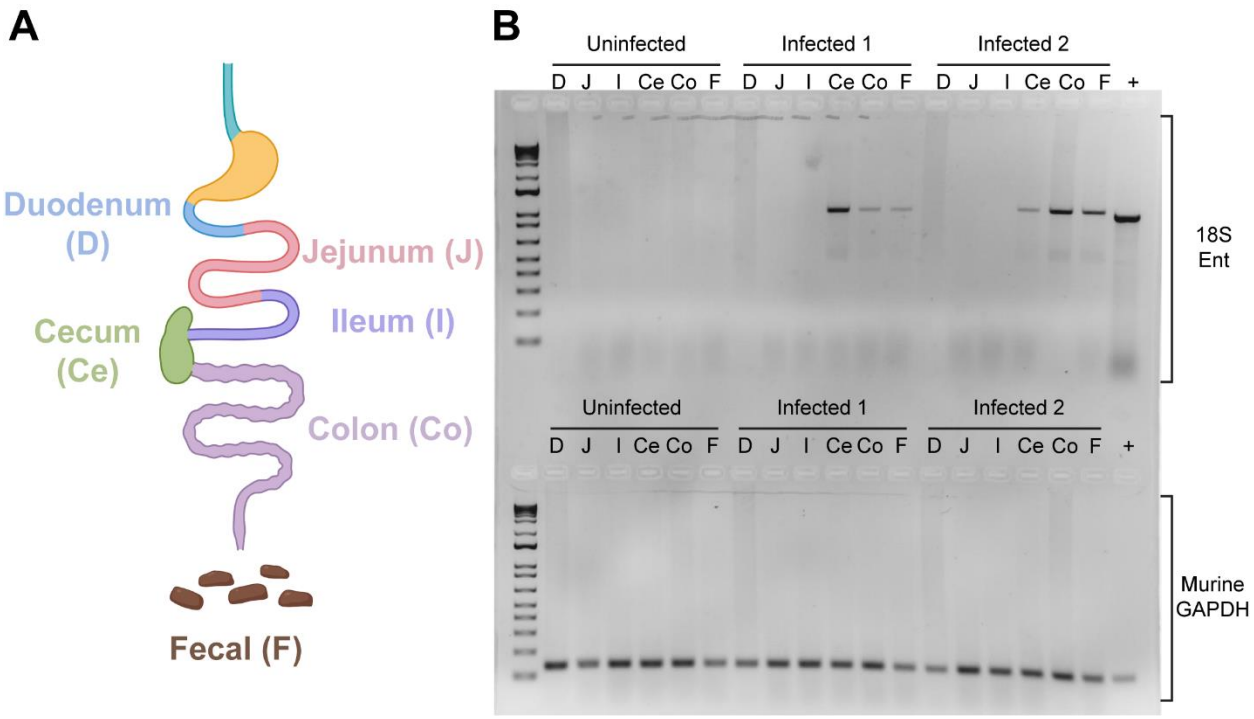

Fig 3. *Entamoeba muris* localizes to the large intestine of infected animals. (A) Schematics of the murine intestine. (B) The *Entamoeba* 18S gene was amplified from gastrointestinal sections (gel top). The positive control is genomic DNA extracted from an *Entamoeba histolytica* axenic culture. Loading control for targeting murine GAPDH from gastrointestinal various sections, positive control is genomic gDNA isolated mice tail snips (gel bottom). Gel image is a representative of two independent biological replicates (n=6, 4 infected and 2 uninfected controls).

Bile extract triggers *Entamoeba muris* excystation *in vitro*

To determine if the previously published *E. invadens* cues could trigger consistent *E. muris* excystation *in vitro*, we incubated the isolated cysts with Nanopure water, 80 mM sodium bicarbonate, 1% bovine bile, or a combination of both treatments for 24 hours (22). We scored excystation efficiency based on the percentage of the parasite that was outside of the chitin shell. An intact cyst was given a score of 0 (Fig 1B). We scored an open cyst with less than 50% of the trophozoite-mass excysted as a 1, cysts where 50% or more of the parasite was outside of the chitin shell as a 2, and empty chitin shells were given a score of 3 (Fig 4A). We observed excystation to be an asynchronous

process, as scores ranged within each condition (Fig S6). Treatment of cysts with only 1% bovine bile resulted in greater than 70% excystation by 24 hours, which was statistically higher than the excystation rate of the Nanopure water treatment ($p = 0.0040$). This excystation rate was not enhanced by the addition of the sodium bicarbonate, and sodium bicarbonate alone did not significantly enhance excystation compared to water only. These results strongly indicate that 1% bile is sufficient to trigger excystation, which implies that excystation of *E. muris* is occurring in the small intestinal tract as we would expect.

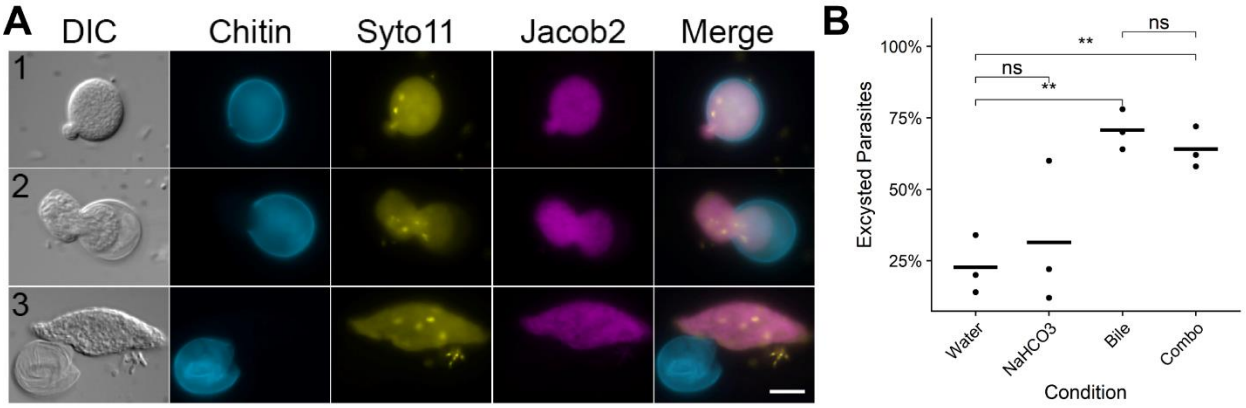

Fig 4. *Entamoeba muris* shows reliable excystation *in vitro* when treated with upper gastrointestinal tract components. Fecal cysts were purified by sucrose density gradient and then acid washed (0.1 M HCl). Cysts were inoculated into excystation conditions (1 mg/ml bile, 80 mM sodium bicarbonate, or a combination of both), then incubated for 24 hours at room temperature. (A) Cysts were scored from 0 to 3, where 0 represented an intact cyst and 3 is an empty chitin shell. Chitin (calcofluor-white), Jacob2 (1A4 antibody (17)), and nuclei (Styo11). Scale bar represents 10 μm. (B) Excystation rates (score >= 1) were quantified in these conditions. Significance was determined using a two-tailed t-test. Only significant pairwise comparisons are shown; Bile ($p=0.004$) and, $NaHCO_3$ + Bile ($p=0.0064$). Each dot represents a biological replicate (n=3 independent experiments), black horizontal line is the average of the three biological replicates.

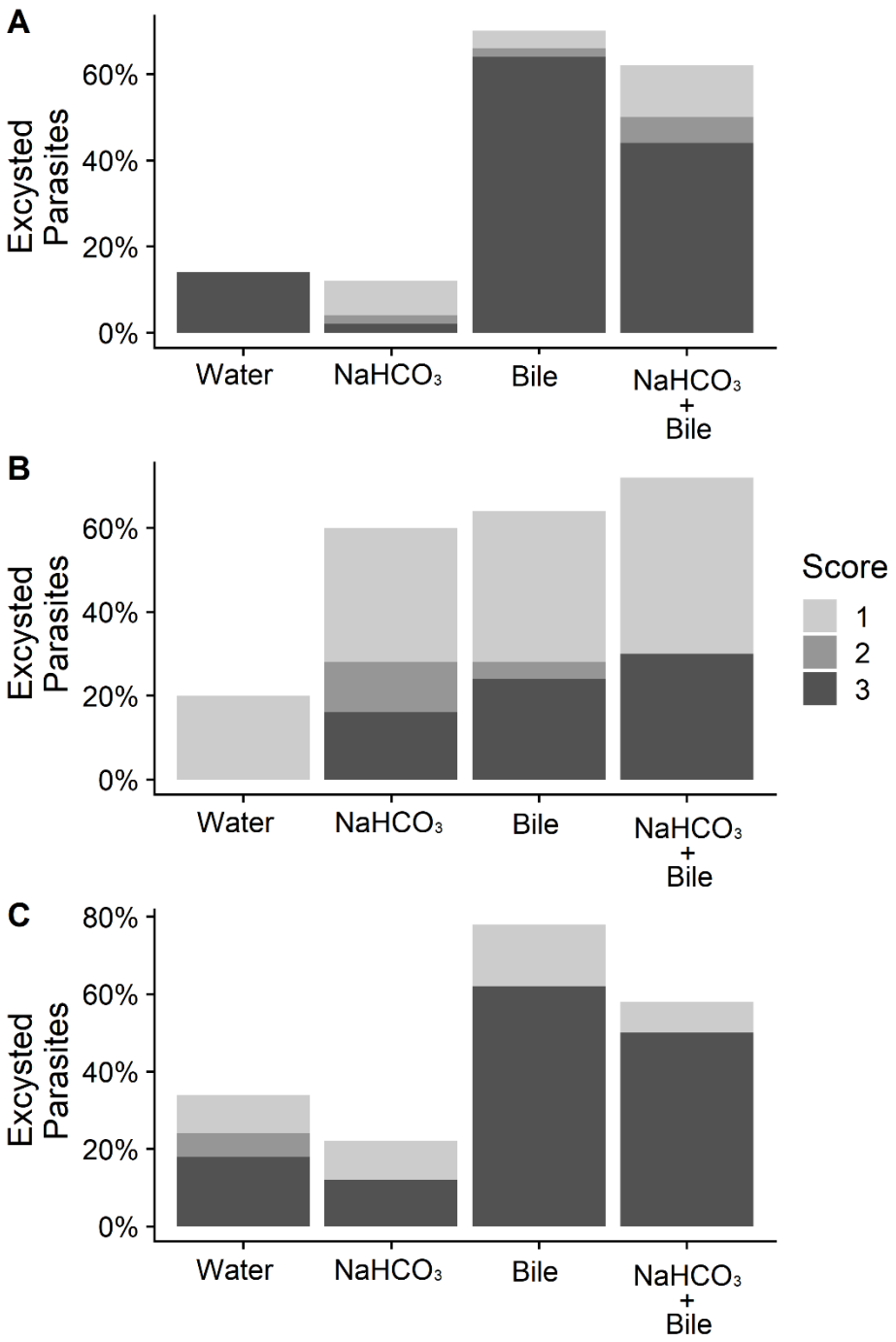

Fig S6. *Entamoeba muris* excystation is an asynchronous process. Fecal cysts were purified by sucrose density gradient and then acid washed (0.1 M HCl). Cysts were inoculated into excystation conditions (1 mg/ml bile, 80 mM sodium bicarbonate, or a combination of both), then incubated for 24 hours at room temperature. Cysts were scored from 0 to 3, where 0 represented an intact cyst and 3 is an empty chitin shell. Each panel (A-C) represents the individual biological replicates averaged in Fig 4.

Discussion

To the best of our knowledge this work is the first to demonstrate that C57BL/6 mice can be chronically colonized with *E. muris.* C57BL/6 mice have been previously described as naturally resistant to *E. histolytica* when injecting trophozoites directly into a surgically exposed cecum (113). However, other protozoans like *Tritrichomonas musculis* have been reported to chronically colonize many colonies on the East Coast of the United States (71). *T. musculis* was found to change the immune response to protect against pathogens in mice with chronic colonization, and *E. muris* may also be changing the immune responses. Understudied intestinal protozoans may account for the variability of results between research institutions. Many of the fecal samples from C57BL/6 mice across the US did not amplify *Entamoeba,* but this lack of amplification is not due to low gDNA isolated from the feces, as we can still detect host gDNA in *Entamoeba* negative samples when using a primer set for murine GAPDH. One of the limitations of this study is that the *Entamoeba* identification is based on the 18S gene (Fig 1C and Table S2) and phenotypic characterization of the number of nuclei (>4) via microscopy (Fig S3), thus further characterization might be required.

One surprising result was the positive Jacob2 staining for the *E. muris* cysts. The 1A4 antibody was previously described to distinguish *E. histolytica* cysts without cross-reacting either to *E. dispar* or *E. bangladeshi* cysts. The 1A4 antibody was generated against the flexible, serine-rich spacer of the Jacob2 lectin in *E. histolytica* (48), so perhaps this region is similar in *E. muris*. It is also interesting that the *E. Muris* cyst

Jacob2 staining is associated with the pre-trophozoite during excystation and not the chitin-rich wall (Fig 4), as previously shown in stool samples and xenic cultures with another anti-Jacob2 antibody (114).

We demonstrated that previously uninfected SW mice can be infected with *E. muris* via oral gavage. We were especially interested in the natural route of infection as it has been established that the route of infection impacts disease progression for oral parasites like *Toxoplasma gondii* (39, 115). Because SW are outbred mice, they have been used for the evaluation of vaccines due to their unbiased immune response (116). In contrast, inbred mice of various genetic backgrounds exhibit different immune responses to an infectious challenge (117), specifically for parasitic infections that are intracellular (118) or extracellular (119). Inbreeding within human populations has been linked to protection against malaria (120) but inbreeding in wild European badgers intensified sex- and age-dependent tuberculosis disease (121). Future studies will examine *E. muris* oral infection in other inbred and outbred mice as well as immune deletion strains to determine the inflammatory responses necessary for *Entamoeba* control.

Contrary to our expectations, about 20% of cysts isolated from unfixed fecal material via a sucrose gradient undergo asynchronous excystation when stored overnight at 4°C in Nanopure water. These results are surprising because, for axenic *Entamoeba invadens*, a combination of cues encountered in the upper gastrointestinal tract are required for

comparable levels of excystation (22). Perhaps chemical signals present in the fecal samples, not eliminated during the sucrose gradient purification and not present in *E. invadens* literature, are triggering excystation in the isolated cysts. The experimental induction of excystation with the bile treatment alone was also surprising because for *E. invadens,* bile alone yields less than 40% excystation (22). We did not perform the water pre-treatment as described in the *E. invadens* protocol. Perhaps our isolation process (Fig S2) might act as a water pretreatment, given the excystation yield of the bile alone treatment is comparable to the combination treatment previously reported (22).

There was a significant difference in the number of parasites quantified when using qPCR detection versus sucrose gradient isolation. This result is an important limitation that might be explained by the nature of the two selected assays. The sucrose isolation protocol selects for healthy cysts with a specific gravity of 1.33. A parasite that is in the trophozoite state, currently excysting, or that has a suboptimal cyst wall would be lost during the density gradient protocol. Meanwhile, the qPCR assay detects parasites in any state regardless of viability. In addition, each cyst can contain more than 4 nuclei, further increasing the amount of detectable *E. muris* gDNA in fecal samples.

During this project, we discovered the importance of humidity on cyst viability, which has been characterized previously in other diarrhea causing parasites (122). Vivarium records indicate that there are drastic differences in humidity between the winter (20%)

and summer (50%). The number of cysts isolated that were “healthy” and presumably viable at the specific gravity of 1.33 (Fig S2B, pellet 3) was dramatically reduced during the winter months. When we examined the waste sections of the gradient, where the material of different density would be expected, we found many cysts with a desiccated appearance (Fig S2B, pellet 2). Thus, room humidity will be important for researchers to monitor as they develop this model in their own facilities. Humidity may also play an important role in the seasonality that is seen with increases in human *E. histolytica* infections (123-125).

We foresee our model to be useful in *Entamoeba* stage interconversion research as well as drug efficiency testing. We hope for improvement in the methodology of detection by targeting moieties present specifically in the cyst stage. Lastly, we have confidence that with further studies, by our and other groups, the establishment of a robust culturing protocol is attainable to study parasite-microbiome interactions *in vitro*. We are excited to present these results, which allow for a myriad of new research avenues focusing on parasite physiology and transmission.

Materials and Methods

All mice were treated according to the guidelines established by the Institutional Animal Care and Use Committee (IACUC) of the University of Wisconsin School of Medicine and Public Health (protocol #M005217). The institution adheres to the regulations and guidelines set by the National Research Council.

Screen for colonized mice

Fecal samples were collected from various institutions within the continental United States Table S2), as well as our own vivarium facility.

Genomic DNA (gDNA) was isolated following previously published protocols with the following modifications (126, 127): briefly, whole feces (~0.10g) were placed on a solvent-resistant screw-cap tubes containing 0.1mm zirconia/silica beads (BioSpec Products 11079101z) and 1 large stainless steel bead (BioSpec Products 11079132ss) suspended in 20% SDS buffer (200 mM Tris·HCl, pH 8.0/200 mM NaCl/20 mM EDTA), and UltraPure Phenol/Chloroform/Isoamyl alcohol, pH 7.9, 25:24:1 (Invitrogen 15593-049). Samples were bead beat on high for 3 minutes at room temperature, and gDNA was precipitated with 3M sodium acetate and isopropanol overnight. gDNA was cleaned using DNA Clean & Concentrator 5 (Zymo Research D4004). For identification of *Entamoeba muris* a set of pan-*Entamoeba* primers were designed by downloading full-length *Entamoeba* 18S rRNA sequences (n=63, 25 *Entamoeba* species) from NCBI GenBank, aligning them in CLC Genomics Workbench v20.0.4 (Qiagen, Hilden, Germany), and identifying conserved regions to target forward and reverse primers (Forward: 5'-AGATACCGTCGTAGTCCT-3' and Reverse: 5'-ACGACTTCTCCTTCCTCTAA-3') which together amplify a 1 kb product (Fig S1, reaction 1). A total of 500ng per PCR reaction were the genetic template for reaction 1, while for some samples a 2-step, nested PCR, was performed using 5ul of reaction 1 as genetic template, using the same primer set and thermocycler conditions

Cysts Purification

Cysts counts: Fecal samples were processed used sucrose gradients as previously described with some modifications (128). Briefly, fecal samples (0.25 – 5g) were ground to a fine powder using a mortar and pestle then shortly homogenized with Nanopure water for 15 minutes using a Mini Rotator (Glas-Col) at 60 rpm. The resulting solution was filtered through four-ply cotton gauze, and samples were pelleted for 10 minutes at 2500 x g. The resulting pellet layered on top of 1.5M sucrose solution. The mid-layer was washed with Nanopure H_2O and pelleted again at same speed. Isolated un-fixed cysts were used as the input for oral infection.

Immunofluorescence Assays

Fresh fecal sample was used to isolate cysts as described above then fixed in 10% formalin washed twice and resuspended. Isolated cysts were blocked for 5 minutes in 3% normal goat serum at room temperature with rotation. After washing, primary antibody 1A4 (48) was added at 1:1000 dilution (2.9µg/ml concentration) and incubated for 2 hours with rotation. As the secondary antibody we utilized a goat anti-mouse IgG conjugated to Alexa Fluor 594 (Thermo Fischer Scientific) and incubated in the same conditions overnight. A set of washes in between antibodies was conducted. Lastly, the samples were stained with 0.1% Calcofluor White Stain (Sigma-Aldrich) according to manufacturer instructions. To target nucleic acids, 0.025% Syto11 stain (Thermo Fisher Scientific) was used. Equal parts of sample and VECTASHIELD Mounting Media (Vector Laboratories) were utilized. Samples were visualized using an Axio Imager 2

microscope (Zeiss). Images were captured at 40X and 100X magnification using the DAPI, DIC, GFP and TexRed channels.

Sanger sequencing and phylogenetic analysis

~1 kb products from the Pan-*Entamoeba* PCR above were gel purified using a Zymoclean Gel DNA Recovery Kit (Zymo Research) and submitted to the UW-Madison Biotechnology Center for Sanger Sequencing using the amplification primers described above. Sanger reads were manually inspected and edited using Sequencher v10.1 (Gene Codes Corporation) and queried against NCBI GenBank using Megablast (129) and default parameters. Twenty-seven full-length 18S *Entamoeba* sequences were downloaded from NCBI GenBank and aligned, along with our consensus Sanger sequence, using CLC Genomics workbench v20.0.4 (final length 1033 positions). A phylogenetic tree was inferred from the alignment with PhyML v.1.8.1 (130) using the general time reversible (GTR) substitution model and 1000 bootstrapped data sets were used to estimate statistical confidences of clades. To quantify nucleotide-level distances within the clade containing our organism, a pairwise distance matrix was constructed with the 4 clade members in CLC Genomics Workbench v20.0.4.

Mouse Infections

House-bred male and female JAX Swiss Webster Outbred mice were used to characterize *Entamoeba muris* infection for biological replicate 1. Male and female JAX Swiss Webster Outbred mice, purchased from Charles Rivers, were used to

characterize *Entamoeba muris* infection for biological replicates 2-4 (Fig 2). Mice were 6-8 weeks of age at the time of oral challenge, individually caged, and provided enrichment for the duration of the experiments. All animals were gavage-fed cysts ($1x10^5$) or 1X PBS as a control.

Localization: House-bred male and female JAX Swiss Webster Outbred mice were infected and euthanized at 5 dpi. The entire murine intestine was isolated and placed in 1X PBS. The small intestine was divided into three sections. Starting from the stomach, the first third was determined to be the duodenum, the following section was labeled as the jejunum, and the most proximal to the cecum was labeled ileum. For the large intestine, the entire cecum pouch and colon were used as independent sections. Intestinal contents of each section and a generous scraping of the host epithelial layer were pelleted at 2500 x g at room temperature for 5 minutes. The pellet was then processed in the previously described gDNA extraction protocol.

Cyst Quantification

Sucrose Gradient: Cysts were purified as described above. For sucrose gradients ~0.25g of fecal sample were used to isolate cysts. The cysts were then counted using a hemocytometer and fecal weight was used to normalize counts.

qPCR: For quantification of *Entamoeba muris* a standard curve was generated with known concentrations of cysts (1,562 cysts – 100,000 cysts) and intercalated dye (Bio-Rad iTaq Universal SYBR Green Supermix) using a QuantStudio™ 7 Flex Real-Time

PCR System. Primers were designed as described above for pan-*Entamoeba* PCR (Fig S1), except here they were chosen to amplify a 200 bp product The following primers were used: Forward: 5'-TCGAGATAAACGAGAGCGAAAG-3' and Reverse: 5'-GTCAGGACTACGACGGTATCTA-3'. Fecal samples were collected and ~0.10g of whole feces were used as the starting material for gDNA isolation as described above. Per qPCR well, 100ng of gDNA per sample were analyzed. Concentrations where then calculated using the CT values of the experimental samples and the linear trendline equation of the standard curve to calculate the total number of cysts present by nanogram of gDNA (100ng per reaction).

Excystation assay

Assays were conducted as previously described for *Entamoeba invadens* (22). Briefly, isolated cysts were acid washed with 0.1 M HCl for 10 minutes, followed by a second wash with Nanopure water. Cysts were then inoculated into each excystation treatment condition at a final amount of 10,000 cysts per condition: Nanopure water, 1% bovine bile, 80 mM sodium bicarbonate, or a combination of both bovine bile and sodium bicarbonate. Samples were incubated for 24 hours at room temperature, washed with Nanopure water, and fixed in 10% formalin. Fixed cysts were stained with 0.1% Calcofluor White. Cysts were mounted and visualized as described for immunofluorescence assays. A total of 50 cysts per biological replicate were scored per tested condition.

Financial Disclosure: This work was funded by the National Institutes of Health (R21AI150957 (US&LJK); T32007215 (CMC); T32 AI007414 (LAO)), SciMed Graduate

Research Scholars Fellowship UW-Madison (CMC&MYH), Foster Wisconsin Distinguished Fellowship from the Food and Research Institute (CMC). Funding bodies had no role in the design of the study and collection, analysis, and interpretation of data, and in writing the manuscript.

Chapter 4. Future Directions

Entamoeba muris

In Chapter 3 I presented a new model for the study of non-invasive *Entamoeba* oral infection. We identified *Entamoeba muris* in our vivarium naturally colonizing the majority of our B6 mice. We isolated cysts from B6 mice and used them as inoculum to characterize the infection of SW mice, a strain that was uncolonized at the time of infection. The SW mice infection display a non-invasive infection, which at 5 days post infection resides in the large intestine. Our model works as expected when treated with paromomycin, as we observe 100% efficacy in treating *Entamoeba muris*. Lastly, cysts can be triggered to undergo excystation when treated with bovine bile. Much of my work has focused on tool development, and the murine model for oral infection presented in Chapter 3 opens a myriad of research questions. This chapter will discuss some of the approaches I wish future students can continue during their Ph.D. work while using my model.

Host Approaches

According to the literature, *E. histolytica* infections using trophozoites directly delivered to the surgically exposed cecum range from $1x10^6$ to $1x10^8$. A colonization curve might be required to assess if a higher dosage ($>1x10^5$) of *E. muris* results in symptomatic infection or even invasive pathology.

Modeling Invasive Disease

Dextran sulfate sodium (DSS) can induce colitis in mice (131). A possible immediate future direction could be inducing an inflammatory environment to assess if this commensal *Entamoeba muris* can undergo invasiveness. Other commensal organisms, like *Clostridium difficile*, require environmental changes to make the transition to their pathogenic state (reviewed in (132)). Assuming the induced colitis is similar to *E. histolytica* driven inflammation, there are various assays to determine if invasiveness can occur. The experimental design consists of animals pre-treated with DSS (2-4%). A subset of animals can be infected with a high dose of *Entamoeba muris (>1x10^5*), while a subgroup remains as uninfected controls.

Immunocompromised individuals, especially those diagnosed with HIV, are known to have severe infections and are at higher risk of invasive disease (133-135). Thus, a valuable future direction is to determine if immunocompromised mice are susceptible to invasive disease following an *E. muris* oral challenge (136). A similar experimental design to the DSS treatment can be followed. Animals can be immunocompromised through various methods, including radiation (at WMIR's Cancer Center) or drug treatment (such as dexamethazone). Both avenues can be performed under the current Knoll lab protocol. Another possible approach, not currently under the Knoll lab animal protocol, is the Severe Combined Immuno-Deficiency (SCID) mouse model. A subset of animals can be infected with a high dose of *E. muris* (>1x10^5), while a subgroup remains uninfected as controls with or without immunocompromised treatment.

E. muris shedding and weight loss should be monitored throughout infection. Whole blood serum samples through a time course, possibly a longer one than two weeks based on the clinical manifestation in patients(137). The whole blood can be used for PCR detection of parasite gDNA, while cytokine levels in the serum can be used to quantify proinflammatory cytokines(138). If there is any indication that the parasite is located within blood samples, the liver of these animals shall be immediately examined as the trophozoites first travel through the hepatic portal vein. Morphological signs of an infection such as enlargement of the organ (hepatomegaly), visible abscesses (most likely the right lobe), or liver discoloration are some examples of invasive disease pathology. A molecular approach would determine if parasite gDNA is present within the liver.

Murine Immune Response to *E. muris* oral challenge

Future studies can focus on characterizing the host immune response *E. muris* induces in the SW host. Animals can be infected with a higher dose of *Entamoeba muris* than those presented in Chapter 3 (>1x10^5). Two infection outputs are to be characterized at the peak of infection or throughout infection: histological inflammation scores and cytokine profile.

The histological evaluation focuses on inflammation and immune cell recruitment and has been published elsewhere (50, 107). Briefly, numbers of *Entamoeba* can be scored from 0–5 (where 0 means no ameba to 5, virtually complete occupation of the lumen by ameba). The extent of tissue ulceration can be scored on a scale from 0–100%. The degree of inflammation can also be scored using a 0–5 scale (where 0 means normal

tissue to 5 where there is the complete destruction of tissue architecture by inflammation). On the day of tissue collection, sera can also be collected and processed with a commercially available cytokine bead array. A combination of the two kits currently used by the lab can aid in determining whether the immune response is skewed towards Th1, Th2, or Th17 response (IL-2, IL-4, IL-6, IL-10, IL-12p70, IL-17A, IFN-γ, TNF, and MCP-1). Patients experiencing an asymptomatic infection have lower levels of IL-10 when compared to patients undergoing invasive disease or amebic liver abscesses (138).

Another observation noted but not included in the published article was the detection of Jacob2 staining in cysts isolated from B6 mice versus SW mice. Freshly isolated cysts from chronically infected B6 mice were always clearly positive for Jacob2 staining while using the 1A4 antibody (48). However, cysts isolated from SW mice at the shedding peak had an array of staining. Most of those cysts were weakly stained; some cysts were positive, while others had no staining at all. These results suggest that the expression of the Jacob2 protein might be different between cysts from B6 and SW mice.

A possible explanation for changes in Jacob2 expression is the immune pressure the two murine backgrounds are exerting during an acute versus chronic infection (117). A possible way to evaluate if prolonged host stress is what is driving Jacob2 expression is to perform IFAs late in the course of SW infection (>28 dpi). Alternatively, if there is enough gene homology, relative quantification of Jacob2 expression can be pursued in

cysts isolated from both murine strains via qPCR while using the 18S gene as a housekeeping gene control.

Colonization/Reinfection based on adaptive immune response

B6 were chronically colonized with *E. muris* while SW mice remained PCR negative before experimental colonization. A hypothesis to explain this phenomenon is that colonization is mouse strain-specific, based on the strain innate and adaptive immune response. To test this hypothesis, future experiments can focus on infecting and co-housing young animals from various genetic backgrounds associated with different adaptive immune responses. Based on the B6 and SW mice colonization rates, I suspect that tamed Th2 response is responsible for long-term colonization/reinfection (117). If this hypothesis is correct, Balb-c mice would also be able to clear *E. muris* oral challenge, similarly to SW mice. An alternative hypothesis concerns the basal availability of iron in blood and tissues. *E. histolytica* has a high need for iron. *E. histolytica* has various hemoglobin-degrading proteases used upon phagocytosed erythrocytes to acquire the iron necessary for its survival when invasive (139). In fact, axenic culture media needs to be supplemented with Ferric Ammonium Citrate. It has been reported that B6 and Balb/c mice significantly differ in blood iron levels during normal physiological and inflammatory conditions (140). If colonization is dependent on physiological iron levels, Balb/c mice are expected to have higher levels of *E. muris* upon oral challenge. If the iron hypothesis happens to be correct, there is an argument to try the DSS experiment mentioned above with Balb/c mice, instead of SW mice.

Arginine Surplus Paradox

Arginases catabolize arginine hydrolysis and the consequent production of urea and ornithine; expression of the isoforms is tissue-dependent in mammals. Notably, arginine is the sole substrate used for nitric oxide (NO) synthesis (141) which is a host resource to kill pathogens. Animals lacking arginases should have a large among of arginine to use for NO synthesis and therefore clear the parasite by macrophage cytotoxicity (142). However, the murine genotype that most reliably provided large quantities of *E. muris* cyst were mice lacking arginases genes (Arg1 and Arg2 KO).

A possible explanation can be that *E. muris.* possesses and arginase like *Entamoeba histolytica's* essential metalloenzyme arginase (EhArg). This enzyme catalyzes the breakdown of L-arginine to L-ornithine and urea. Consumption of L-arginine mediated by EhArg inhibits amoebicidal activity and nitric oxide production by activated host macrophages (143). In fact, there are been efforts to target this enzyme as a potential anti-amoebic (144). An alternative hypothesis is that large arginine availability is allowing for higher levels of *Entamoeba* replication. *E. histolytica* energy generation depends on glycolysis and fermentation (145). Asparagine and arginine supplementation of axenic *E. histolytica* enhance growth in simple and complex media and this effect is greater when glucose concentration is low (146). These results have been observed *in vitro* only. *In vivo* studies have elucidated that dietary arginine supplementation of mice changes the intestinal microbiota, which results in the activation of intestinal innate immunity through various signaling pathways (147).

Arg 2 is highly expressed in the human small intestine (148) and nitric oxide in the gastrointestinal tract has various roles (149). High NO synthesis during intestinal inflammatory conditions can result in aggravated ulcer colitis and mucosal destruction (150) or it can have a protective effect against drug-induced lesions (151). The lack of the host Arg2 enzyme results in the higher levels of arginine for competing pathways: host NO production or parasite breakdown of arginine.

Mammalian Arg1 is highly expressed in the bone marrow as well as in the liver (148). However, as the liver is highly skewed arginine catabolism towards the urea cycle, thus little to no net arginine is available for NO's production, making the liver a suitable environment for *E. histolytica* abscesses. In fact, NO is required for the control of amebic liver abscess in immunocompetent mice (152). To test if the lack of Arg2 enhances *E. muris* replication, we first have to determine if the cysts phenotype is genetically linked or microbiome dependent as we started this colony of mice recently, they might not have the same microbiome as the rest of our B6 animals. We could test the genetic hypothesis by breading littermates that yield every possible genotype. Homozygote WT B6, heterozygous Arg2 (one allele is a WT and one allele is a KO), and homozygous Arg2 KO mice. Fecal cysts can be quantified and determine if there are significant differences between the three genotypes.

Another experimental approach would be to use the three genotypes' littermates listed above, to determine if dietary arginine supplementation has an impact on *E. muris*

replication. We could quantify the cysts shedding and analyze if there are significant differences between supplemented and non-supplemented animals. We would assume that all mice share the same microbiome at the beginning of the experiment as they are littermates. If the arginine supplementation is the reason why *E. muris* has high replication, we would expect the cysts shedding of Arg2 KO mice to resemble the WT supplemented mice. We could also determine if the microbiota of these two animals is more similar after the supplementation treatment.

E. muris **co-infection**

A big question I did not get to answer but I think it would be very valuable, is to determine if individual parasitic phenotypes are exacerbated by co-infection. *Toxoplasma gondii* is an obligated intracellular parasite while *Entamoeba muris* is an extracellular parasite. Both parasites naturally colonize via the oral route while in the gastrointestinal tract they might compete or cooperate to scavenger limited resources within the same niche.

We observed that the majority of B6 mice are colonized by *Entamoeba muris,* thus when experimental *Toxoplasma* infection are conducted *Entamoeba muris* is already colonizing the gut. We also know that animals chronically infected with *Toxoplasma* might be protected against secondary infections via IFN-g signaling (NK, T cells, etc) or IFN-g independent pathways (as seen in Chapter 2).

Chronically *Toxoplasma* infected mice display cachexia, an altered metabolism state that results in lean weight loss characterized by acute anorexia, systemic inflammation, and loss of 20% body mass. Mice fail to regain muscle mass or visceral adipose depots (153). However, there has been reports of positive association between chronic *Toxoplasma gondii* and obesity (154). Unpublished data from our lab shows that chronically infect mice excrete high levels of fat within their feces. The parasitology field has reported that changes in lipid profile occur in patients having active infections with most of the parasites (155).

Entamoeba histolytica is an auxotroph for cholesterol, while the pathogenicity of invasive disease is exacerbated by malnutrition (156). Based the Arg2 KO mice phenotype, I would expect that the high levels of fat within the feces will result in a higher colonization rate of *E. muris.* Thus, animals chronically colonized with *T. gondii* would have higher levels of *E. muris* when compared to age match controls. The gut microbiome has been proposed to be a modulator of parasitic pathology (157). Changes to the microbiome towards a “harmful-state” occur when mice are orally infected with *Toxoplasma gondii* at 13 dpi in Balb/C mice but their microbiome at 21 dpi is similar to healthy mice (158).

Inflammatory microbiomes are known as dysbiosis environment and *Entamoeba histolytica* might flourish there. This even has been observed before with other opportunistic pathogens like *Clostridium difficile.* Co-incidence between *E. histolytica*

and *C. difficile* has been previously reported (159). Thus, using our model we could explore co-infection studies to determine if *C. difficile* exacerbates or protects against *E. muris* infection. One hypothesis is that *Entamoeba muris* could exacerbate *C. difficile* infection by predation of "healthy" microbiome residents (34). On the other hand, *Entamoeba muris* could act similar to other eukaryotic microbes like *Blastocyst spp,* which has been associated with a healthy microbiota and thus prevent *C. difficile* infection (61).

E. muris colonization and quantitative trait loci (QTL) analysis

Susceptibility to *E. histolytica* and infection progression has been linked to some host genetic factors like host polymorphism in leptin receptors (15), intergenic insertion in the cAMP Responsive Element Modulator (16) gene, and microbiome-mediated immune cell recruitment (19). For a more global approach to determine other genetic factors, we could utilize the diversity outbred (DO) mouse population and QTL analysis (160). This endeavor is quite ambitious and should be a team effort due to the large amount of work it entails. The major challenges are listed below: (1) *Entamoeba* infection still needs optimization (2) The recommended sample size is between 200-800 mice. (3) Founder strains must display heterogeneity in colonization and/or pathology with a naturally occurring organism. Having said that, if a student up to the task and funding comes along, performing QTL analysis could yield a high scale global characterization of mammalian genetic factors that are linked to *E. histolytica* infection susceptibility. DO mice are the genetically diverse mouse resource available and thus allows researchers

to model the human population more accurately. The founders are 8 inbreed mouse strains (A/J, C57BL/6J, 129S1/SvImJ, NOD/ShiLtJ, NZO/HlLtJ, CAST/EiJ, PWK/PhJ, and WSB/EiJ) that are subsequentially inbreed to develop unique recombination yielding 36 possible haplotypes.

First the susceptibility of the founder strains must be determined. I am assuming that there will be a range of colonization between the 8 founder strains. Then, the selected sample size must be challenged with an appropriate dosage. Another potential challenge is to determine what biological markers should be is collected throughout the infection. Metabolites have recently emerged as important controllers of infection pathophysiology (145).

The Rey laboratory has already collected samples from about 500 DO mice expanding 6 timepoints. The mice were housed in the Biochemistry vivarium for the duration of the experiment. The Rey group collected biological markers data and fecal samples. The experiment was performed a while ago and limited amount of fecal sample is available, so *Entamoeba muris* quantification must be done via qPCR. This DO approach is a can serve to test if there are genetic factors that are highly correlated to *Entamoeba muris* colonization with already collected data.

Microbiome-Host-Parasite Interactions

Now that we have a murine model, we could start exploring the tangled relationship between microbe-host-parasite interactions. One most interesting topics regarding this three way relationship involves short chain fatty acids (SCFA) produced by the bacterial microbiome, which can inhibit encystation of *E. invadens in vitro* (35) presumably by restriction of ploidy (161). It would be of great interest to test if SFCA production have the same effect on *E. muris* within our SW model. An important note is that not all SFCA might have the same impact on *Entamoeba* encystation, but rather a signal of where within the intestine the microbe is located. For example, *E. histolytica* survives on glycolysis and the two major products are ethanol and acetate. Acetate concentration peaks in the cecum while reduces along the colon (162). A simple way to regulate SFCA production is by the modulation of the members of the mouse microbiome. This modulation can occur via introduction of microbial communities that vary on the number of SFCA producers and further enhanced by dietary changes. A subset of animals can be infected with a high dose of *Entamoeba muris (>1x10^5)*, while a subgroup remains as uninfected controls. Animals would be fed chow diets that vary in the level of fiber and the colonization (and hopefully invasiveness) can be monitored in these animals to determine if there is an impact on *E. muris* by SFCA concentration. If high production of SFCA is inhibitory of encystation we could aim to lower *Entamoeba* transmission by only changing diet behaviors and without medication.

Parasite Approaches

A previous publication reported that di-xenic culture is possible(163). Viability of these new trophozoites to establish a culture remains to be observed in our laboratory. We

discovered certain cues can induce excystation *in vitro* (Chapter 3), and a avenue to persue is to combine these two approaches.

The first future direction for *Entamoeba muris* would be to develop culturing techniques from fresh fecal samples, to have as close to an axenic culture as possible. There is plenty of literature documenting the isolation of *Entamoeba histolytica* and other *Entamoeba* species directly from fecal samples. Initial piloting for these endeavors was conducted by undergraduate summer projects that had some success in terms of growing *Escherichia coli*, one of two of the bacteria needed for the intermediate dixenic culture, in R medium. The next step from this piloting would be to grow the dixenic bacterial culture by introducing *Bacillus fragilis* (provided by the The Hryckowian Lab) to the *E. coli* culture in R medium. Having a trophozoite culture would allow for the study of encystation cues.

Whether from a pure culture or a highly concentrated fecal sample, a future direction for the parasite itself, would be to obtain sequencing at the genome level. The genome size of the currently sequenced Entamoeba species ranges between 12 to 41 Mb belonging to *E. histolytica* to *E. invadens,* respectively (Table 1). The most resent whole genome sequencing was in 2019 for *Entamoeba nuttalli,* a species that colonizes wild macaques and its genetically closest species to *E. histolytica* in current phylogenetic analyses. (164). Sequencing the genome of the *E. muris* will most likely be a *de novo* assembly that might require a combination of long (PacBio) and short (Ilumina) reads. In campus we have access to the Biotechology Center and both of these platforms are offered. The *E. nuttalli* genome publication can serve as a framework for this work. Of note is to

determine a suitable substitute for the primary assembly (Celera 7.0) The genome size of *E. nutalli* is more similar to *E. histolytica.* Perhaps instead a newer approach such as Fast Hybrid Assembly of Long Reads (HASLR) might be more appropriate for a potentially larger genome (165).

Table 1. *Entamoeba* genomes available at Amoeba DB sorted by genome size.

Organism	Strain	Size (Mb)
E. histolytica	HM1: IMSS-A	12
E. histolytica	HM1 IMSS-B	13
E. histolytica	HM-3: IMSS	14
E. nuttalli	P19	14
E. histolytica	KU27	15
E. histolytica	KU48	17
E. histolytica	DS4-868	20
E. histolytica	HM-1: IMSS	21
E. dispar	SAW760	23
E. moshkovskii	Laredo	25
E. invadens	IP1	42

Dual Transcriptomic Approaches

If a more global characterization of the host immune response is desired, I recommend a murine transcriptomic approach. The pipeline that I coded for the transcriptomics presented in Chapter 2, can immediately be used to analyze the SW host immune response to an *Entamoeba muris* challenge. A challenge of note is the heavy bacteria load associated with the isolated parasite and how to discern the host immune response to bacteria within the inoculum and the parasite, thus the additional cleaning step seen on Appendix B will be a most. A possible control for bacteria load can be to mock infect control mice with their own feces. These samples would not contain *Entamoeba muris* but would need to be processed in a similar sucrose gradient and sarkosyl washed.

SW mice that have been colonized with *Entamoeba muris* and control animals can be infected for a given time post infection. A subset of infected and control mice can be euthanized to isolate RNA from the gastrointestinal tract from the intestinal content and a light scrapping of the intestine. Prior to this work, there was no animal model for oral infection thus the current hypothesis that excystation occurs in the small intestine can be directly tested. The cecum and the colon sections are the regions of the intestine that seem to have the higher likelihood of colonization (Chapter 3), thus sending these sections for sequencing might be the best approach to track developmental changes such as encystation and excystation.

To determine what makes B6 susceptible to chronic infection, but not SW mice, a genetic approach could also be taken. Uncolonized WT B6 mice and SW mice can be house bred (parental) and generate a heterozygous generation (F1). The parental and F1 mice can then be challenge with *Entamoeba muris* and. I would expect the F1 generation to have an intermediate phenotype of susceptibility to the parasite. Differential expression analysis can be used to propose host genes responsible of parasite clearance.

What are the responsible pathways for infection clearance? Using publicly available data, could we determine if the immune factors responsible for clearing surgically delivered *E. histolytica* are similar to those activated via *E. muris* oral challenge? A transcriptomics approach that has a time component would provide data to answer these questions. A dual approach is completely dependent on the availability of a parasite genome. However, host questions can still be pursued in either scenario. This type of experiment could support the mechanism that the host immune response utilizes during oral infection. If the parasite genome is available by this time or is similar enough to currently available data for the 11 *Entamoeba* genomes deposited into Amoeba DB, future project can characterize the developmental changes that the parasite undergoes throughout the gastrointestinal tract. In other words, a combination of the projects presented in this dissertation.

Cryptosporidium parvum

My intellectual contributions to this project were on the bioinformatics portion. I have taken the liberty to also write, my own ideas, that resulted from the literature searches required to make interpretations for the RNA-seq data presented in Chapter 2.

Improving Murine and Parasite Transcriptomic

After discovering that our B6 mice were naturally colonized with *E. muris*, I checked if the animals that we used for the Chapter 2 study were also colonized with *E. muris* using the Pan-Entamoeba PCR screen. I was able to detect *E. muris* gDNA in 83% of the infected samples (See Appendix E). Although I did not perform a quantification for E. muris the size of the bands in the Pan-*Entamoeba* PCR might suggest different colonization levels. Thus, the presence of *E. muris* might have impacted the mouse transcriptomics we presented in the published article. In the future, I suggest screening all animals that are going to be used for transcriptomics. The screening might suggest that animals should be treated to eliminate *E. muris* prior to sequencing.

One of the main limitations of this project was the coverage for the parasite's transcriptome. The day of parasite isolation was selected based on the highest level of parasite shedding and might not need optimization. However, the isolation of the parasite and coverage can both be improved. For the data presented on Chapter 2, we did not concentrated parasites from each sectional sample, we also used only one murine intestinal sample. If our goal switches to determine the transcriptome of the

parasite, we might opt for the combination of murine samples and do a cyst isolation prior to the RNA isolation and library preparation. From the data we observed a maximum of 6% mapped reads, meaning we only obtained 3.7 million reads. Thus, the amount of coverage was also an area of opportunity. The genome size of *C. parvum* is 10Mb according to Crypto DB. Thus, the goal would be to obtain the appropriate amount of reads for a given research question. If we would like to perform comparison of medium to highly expressed genes, 10-20M would be sufficient. While if we want to find rare transcripts, SNPs, or novel splice junctions, around 50-100M would be necessary.

Host Approaches (Immune Response)

An immediate future direction is the study of Type I interferon pathway using mice IFN-γ KO mice that also lack the Type I interferon receptor (IFNAR) or the individual ligands IFN-α and IFN-β. The Sauer Lab currently has IFNAR KO mice within our vivarium. Of note, we would need to generate a IFN-g/IFNAR KO animal. Alternatively, pharmacological inhibition of the type I interferon pathway can be achieved using commercially available polyclonal anti IFN α/β neutralizing antibodies. Thus, this approach can be implemented right now with our current mice to validate that Type I interferon pathway is conferring protection against *C. parvum* infection. According to the results presented in Chapter 2, I would hypothesize mice lacking Type I interferon response to be more susceptible to *C. parvum* infection. Weight loss and parasite quantification can be used as readout of infection. If type I interferon response is indeed conferring protection and then it is blocked (genetically or pharmacologically), I would

expect no significant differences in infection between PBS and STAg treated animals. In other intracellular parasites like *Plasmodium berghei* and *Toxoplasma gondii* infection, infection of IFNAR KO mice results in higher parasite load and lower survival (166). However, this response is not ubiquitous as human macrophages lacking IFNR infected with *Leishmania major* have higher survival with lower lesions.

One of the downstream targets of the Type I interferon pathways that was significantly upregulated was the Schlafen family, which are induced in an inflammation setting. Three Schlafen proteins (Schlafen-2, Schlafen-4, and Schlafen-5) were the highest expressed transcripts in infected mice that were treated with STAg. Previously, Slfn4 was reported to promote leukocyte recruitment to the spleen (167) while macrophage response is crucial for *C. parvum* infection clearance (168). To evaluate the role of Slfn4 in *C. parvum* clearance, Slfn4 KO mice can be infected. I expect Slfn4 KO mice to be more susceptible to *C. parvum* oral challenge, higher parasite counts due to lower macrophage and granulocyte recruitment, leading to higher parasitemia and lower host survival. Of those immune cells recruited, it would be interesting to determine differentiation status by quantifying the following myeloid markers: Bst2 (Mature B cells), Ifi204 (Macrophage differentiation), CD274 (Activated T and B cells), CCRL2 (Activated Neutrophil).

If a culture approach is preferred, overexpression or knock down approaches have been used before to determine the role of Slfn13 (169) and Slfn14 (170). Commercially available siRNA targeting mouse Slfn4 are available (Thermo-Fischer). I am hesitant of this approach as the role of Slfn4 has been reported in immune recruitment. Thus,

instead of single tissue culture, organoid derived monolayers from IFN-γ KO mice intestines should be used.

Parasite Approaches (Metabolomics)

The long-term goals would be to develop a drug capable of preventing cysts shedding.

Our data suggest that *C. parvum* is inhibiting gluconeogenesis to push glucose towards glycolysis, the pentose phosphate pathway (PPP), or the TCA cycle. To pursue this endeavor two types of cell lines have been used in *C. parvum in vitro* assays: HCT8 (Adenocarcinoma on Ileocecal Colorectal) and COLO 680N (Squamous cell carcinoma of the esophagus). Metabolites derived from the PPP can be distinguished from metabolites derived directly from glycolysis using 13C Glucose labeling (171). An alternative approach is to measure the transcription levels of the enzymes responsible for glycolysis, gluconeogenesis, pentose phosphate pathway, or the TCA cycle (172). Interestingly, purine nucleotide biosynthetic processes are upregulated when infected and STAg treated. Why would the host upregulate a pathway involved in purine synthesis during an infection? Could it be that *C. parvum* is manipulating the host? We expect that the rates of glycolysis in infected sample will be higher than uninfected controls and that gluconeogenesis is lower in infected than uninfected controls. *C. parvum* scavenges their purines from the host, as genetic ablation of purine salvage in *C. parvum* does not impair infection (173), thus I would expect purine synthesis to also be upregulated. These results can further be corroborated by using Liquid chromatography–mass spectrometry (LC-MS) to determine the concentrations of intermediate metabolites for all these pathways.

Appendix A

Humidity has an impact on *Entamoeba muris* viability

Entamoeba histolytica is considered endemic in tropical regions and much of the literature focuses on the inadequate hygiene and access to sanitation (135). Access to sanitation is a factor, but one characteristic the tropics have is constant high humidity levels due to temperature, vegetation, and average rainfall. The highest number of diarrhea cases are correlated with higher temperature, humidity, and rainfall in Bangladesh (125). The physiology of the *Entamoeba spp* cysts was affected by environmental humidity. Significant differences in the animal's cages were due to two reasons: 1) supply chain issues resulted in compressed paper (CP) bedding instead of the usual corncob (CC) and 2) seasonal humidity changes. CP bedding has been shown to be advantageous due to the reduced need to conduct early cage changes in a individually ventilated caging system due to its absorption capacity (174). We were unaware of the differences between CC and CP bedding when the supply chain issues led to this forced change in bedding. The striking reduction of humidity between summer and winter was around 20-30% according to our daily mouse room records.

The phenotype was seasonally observed but was really apparent during the winter (2021 to 2022) when we introduced CP bedding. There was a drastic reduction on the number of cysts isolated that were "healthy" and presumably viable at the specific gravity of 1.33 (Figure A, left). I examine the waste sections of the gradient, where material of different density would be expected, and I found cysts that looked desiccated (Figure A, right). When the animals' cages were strategically placed next to a store-

bought humidifier and with very reduced bedding, we observed a 3-fold increase in cyst yield (data not shown). The cyst total was not ever as high as the summer yields, but enough to continue some *in vivo* pilot experiments. My advice for the next graduate student is to focus on pilots and in vitro work during winters (Dec-March) and on experiments involving cysts viability for the rest of the year.

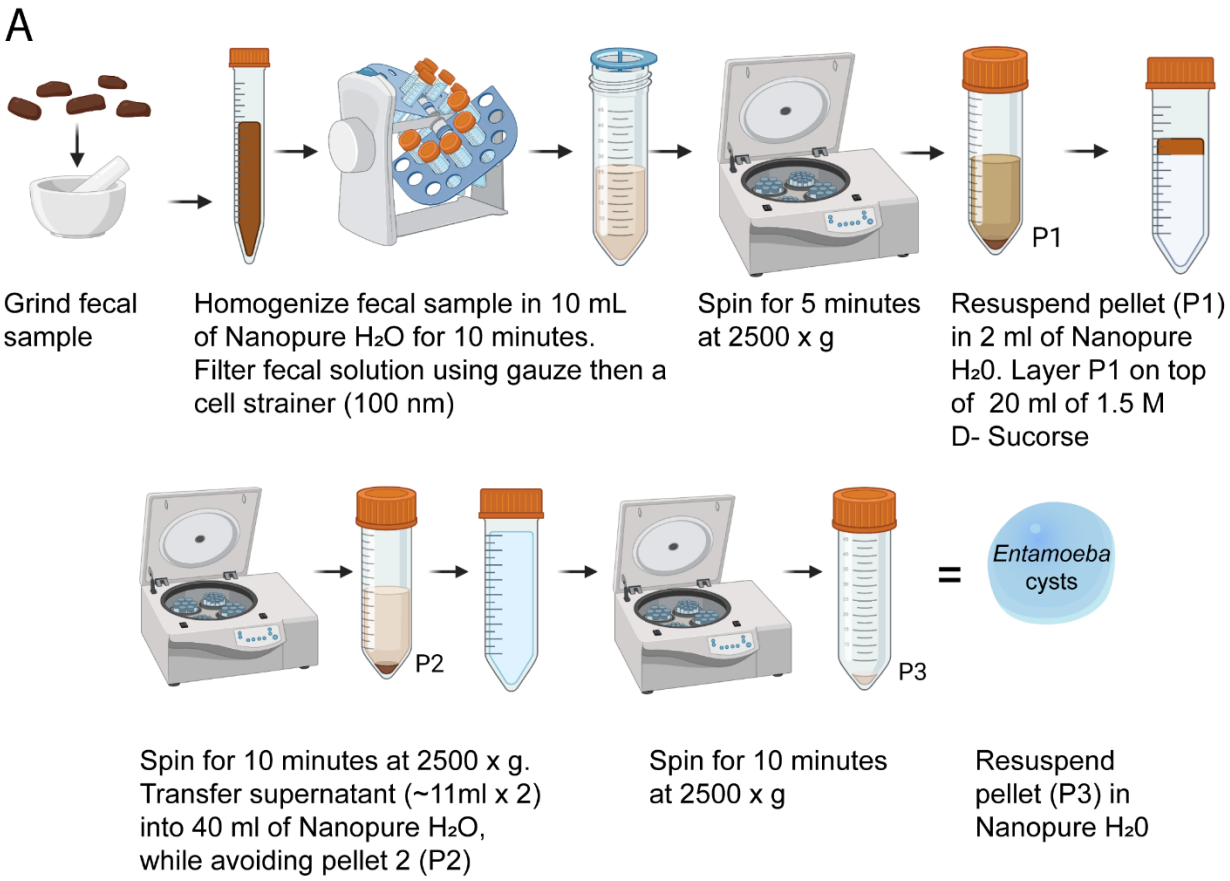

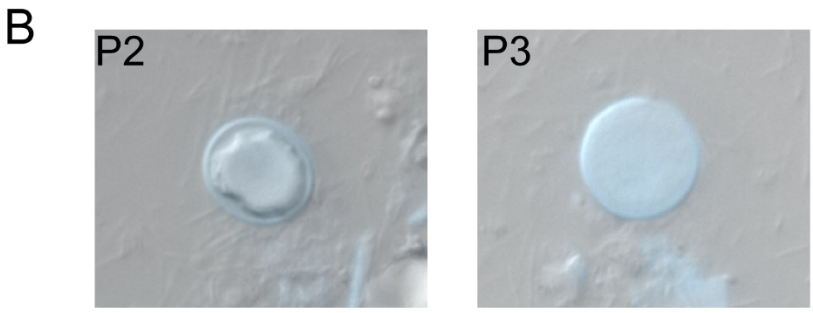

Fig A. Sucrose gradient isolation protocol. (A) *Entamoeba* isolation protocol. (B) While cysts can be found in the P2 pellet during the winter months, they have a dehydrated appearance compared to the cysts in the P3 pellet, likely due to the low humidity of the vivarium.

Appendix B

A 0.1 % Sarkosyl solution significantly reduced bacterial contamination without compromising cysts viability

Sodium lauroyl sarcosinate, herin after called sarkosyl, is an amphiphilic compound as it is formed by a hydrophobic 12-carbon chain and a hydrophilic carboxylate. It is commonly used as a foaming agent in personal hygiene products and the *Entamoeba* field has use this compound to determine cysts viability. The assumption is that cysts that have an intact cyst wall would be sarkosyl resistant, while cysts with compromised cyst wall would completely lyse in the presence of this mild detergent. We tested a 0.1% sarkosyl solution wash on ice for 30 minutes after the cysts isolation protocol (Appendix A) to determine if bacterial load was reduced. We observed significantly cleaner samples via immunofluorescence assays (IFA).

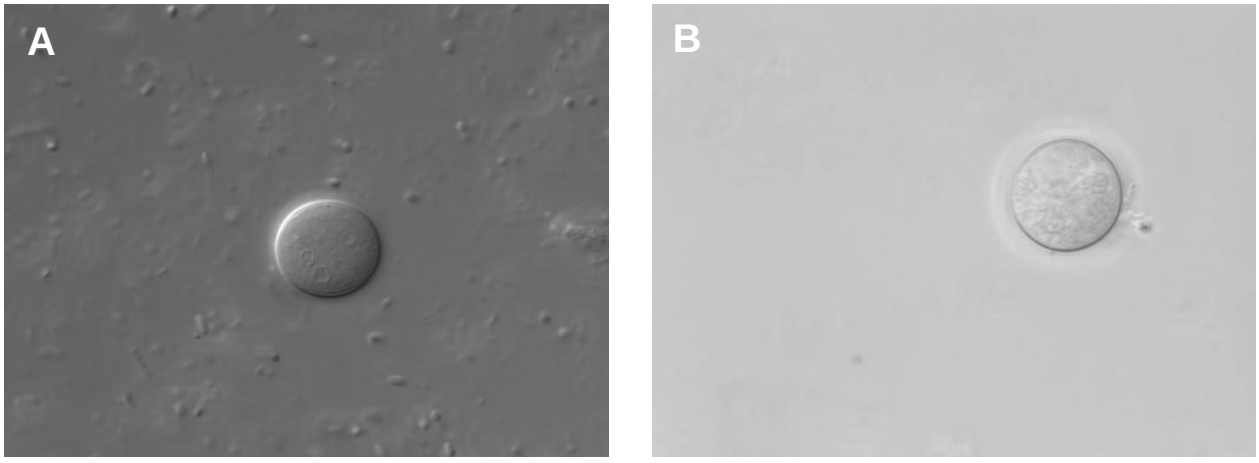

Fig B. Efficiency of a 30 minute 0.1 % Sarkosyl wash on ice. (A) *Entamoeba muris* cysts using the isolation protocol shown in Fig A. (B) *Entamoeba muris* cysts using the isolation protocol shown in Fig A in addition to a 30 minute 0.1% sarkosyl wash on ice.

Appendix C

Entamoeba muris shedding seems to be cyclical

Rodents and rabbits, among other animals, are coprophagic (93). B6 animals most likely encounter the primary infection of *Entamoeba muris* when they start being coprophagic. Male mice display high levels of coprophagy early in their lives peaking around t 5 to 6 weeks of age, then feces ingestion decreases with age (175). For female mice, higher levels of coprophagy are observed during pregnancy and lactation than when the animals are not pregnant or nursing (176). However, to our surprise we observed shedding to have a cyclical pattern (Figure C). Animals first shedding peak was weaning, then around 13 weeks of age (3 months), and a third peak was observed at 25 weeks (6 months), suggesting animals can still shed a decent number of cysts throughout their lifetime. Future characterization of this periodicity can be address as a lab undergraduate project. The student would monitor the shedding of various age-matched litters or various strains since weaning to 6 months of age. A possible hypothesis for this cyclical behavior is antigenic variation as seen in *Plasmodium* (177).

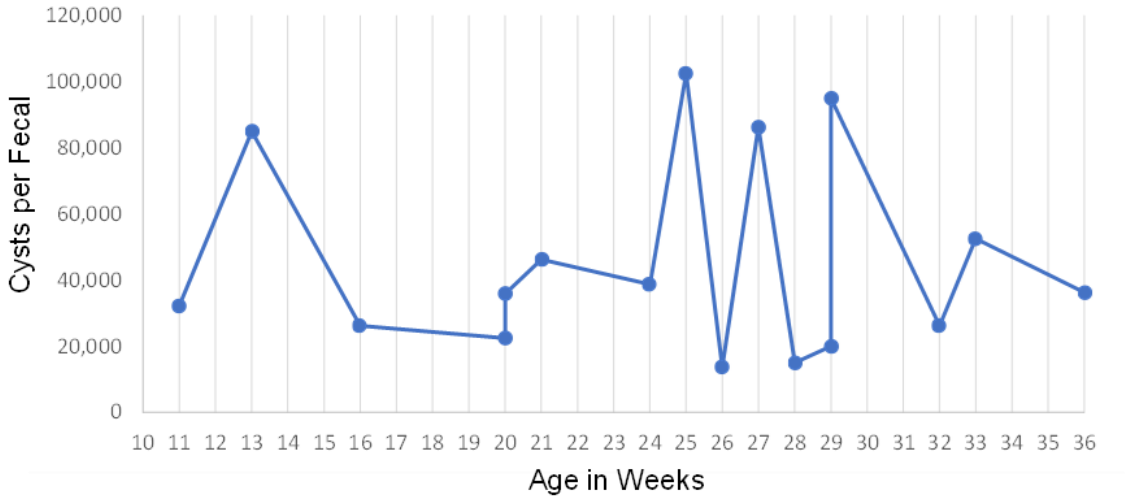

Fig C. Characterization of cysts shedding over time by naturally colonized Arg2 KO mice. *Entamoeba muris* cysts were isolated from 0.5 g of fecal sample from (n=4 cages) at various time points to determine periodicity of shedding.

Appendix D

E. histolytica oral challenge does not exacerbate *Entamoeba muris* shedding in WT mice nor ZBP1 KO mice

Prior to discovering that our facility had a resident *Entamoeba*, my main thesis objective was to determine the importance of the Z-DNA Binding Protein 1 gene was conferring against *E. histolytica* infection. E*. histolytica* induces cell death upon contact with host cells based on various *in vitro* and *in vivo* experiments (reviewed in (178)). Trophozoites have been demonstrated to attach to host cells and within minutes induce program cell death (PCD) via apoptosis (179) or necroptosis (180). Work on delimiting what type of PCD was occurring in amoebic liver abscess (ALA) concluded that it was in a non-FAS and non-TNF-alpha pathways (181). Later, it was determined this killing in a caspase-dependent manner and PCD results in a more invasive-like phenotype (182, 183). More recently, it was discovered that *E. histolytica* consumes living cells via trogocytosis, in order to avoid host detection, and results in PCD of the host cells *in vitro* (17, 184). Based on the importance of cell death in *E. histolytica* invasive disease, we hypothesized that the lack of a crucial protein upstream of various types of PCD, such as Z-DNA binding protein 1 (ZBP1), would result in a switch from tissue invasion towards a non-invasive replication pattern. PCD in the form of apoptosis has been shown to during invasive disease in the gut (182) and the liver (181) of current animal models. ZBP1 and its role in programmed cell death has been heavily studied during viral infections like influenza A virus (185), murine cytomegalovirus (186), and West Nile Virus (187) in part due to its capacity to bind to nucleic acids. Research to determine nucleic acid independent functions, in the absence of ZBP1 regulators, describes

rampant activation of ZBP1 which leads to high levels of necroptosis during early stages of embryonic development (188, 189). Lastly, PCD regulators such as RIPK1, maintain epithelial homeostasis by inhibiting apoptosis and necroptosis (190), but the involvement of ZBP1 in intestinal homeostasis, remains to be elucidated. Transcriptional regulation of the ZBP1 has been linked to chronic intracellular parasites infections like *Toxoplasma gondii* (191) and *Neospora caninum* (192). Our laboratory developed a ZBP1 KO mice strain in which the entire coding region of the ZBP1 gene was removed utilizing CRISPR targeting as recent reports state that the previous ZBP1 KO model to have a mix of genetic background (193). Additionally, ZBP1 KO mice have been reported to support the sexual stages of *Toxoplasma gondii* when the enzyme delta-6-desaturase is inhibited, phenotype not reproducible with C57BL/6 mice (194). As ZBP1 KO mice had been reported to be susceptible to parasitic oral infection and can support developmental changes that WT mice have previously been resistant, this study was aim to test the susceptibility of the ZBP1 KO mice when orally challenged with *E. histolytica* trophozoites (strain HM-1: IMSS). Having a natural occurring *Entamoeba*, provided a confounding variable to this project and efforts for the *Entamoeba* model focused then on *E. muris.* We decided to test if *E. histolytica* impacted *E. muris* shedding in two murine strains WTs or ZBP1 KOs. We co-housed animals for two weeks to ensure that all mice were colonized with similar levels of *E. muris.* We infected animals with *E. histolytica* trophozoites (red), TYI media supplemented with antibiotics (green), or mock infected (blue) and measured cysts shedding via qPCR. There were no differences in the shedding, regardless of the treatment they received (Figure D1) and this remain true in both murine strains. To determine if there was genetic protection

conferred by the ZBP1 gene, we compared *E. muris* shedding between the WT and the ZBP1 KO strains (Figure D2). However, no significant differences between the WT and ZBP1 KO mice were observed suggesting that the ZBP1 gene is not essential for *E. muris* colonization.

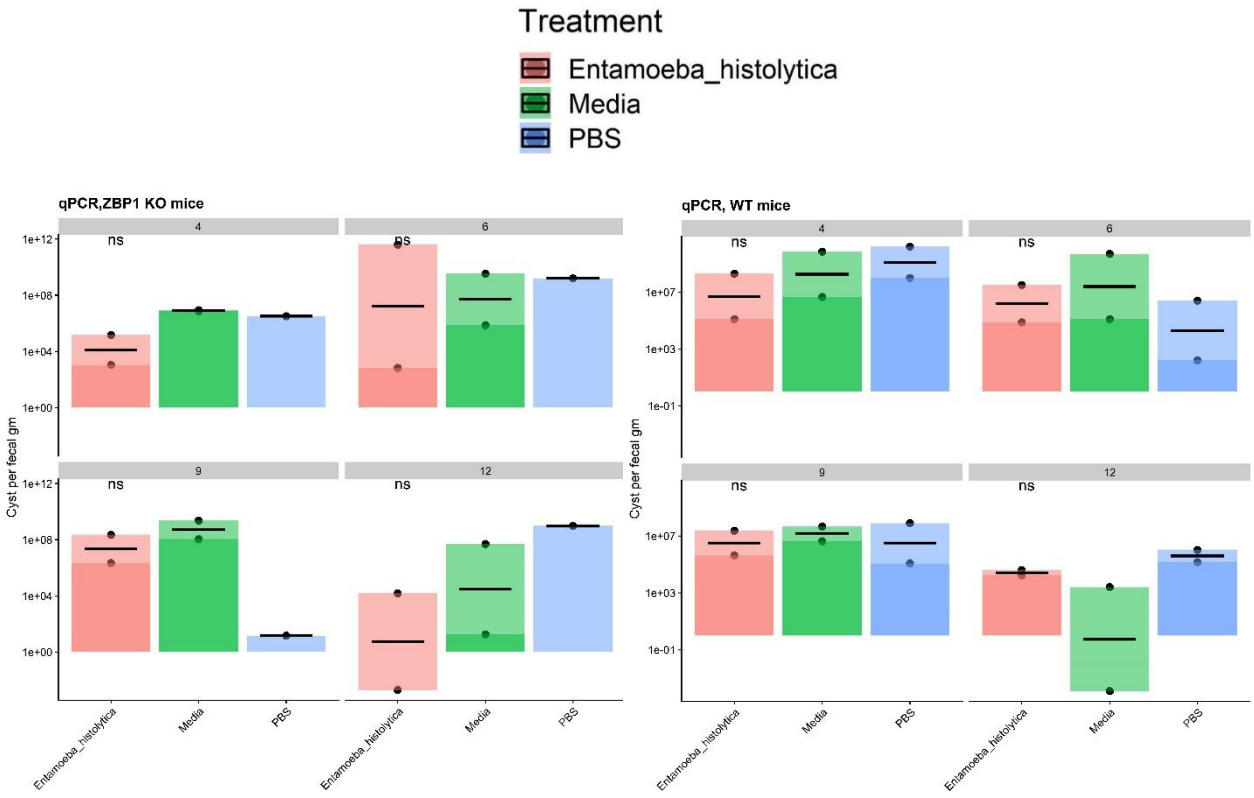

Fig D1. *Entamoeba muris* cyst shedding upon trophozoite *E. histolytica* oral challenge (Treatment Comparison). Mice were challenged via oral gavage with *E. histolytica* (red bar), TYI media (green bar), or PBS (blue). *E. muris* cysts shedding was quantified via qPCR for 12 days post infection. Significance was determined by an ANOVA test.

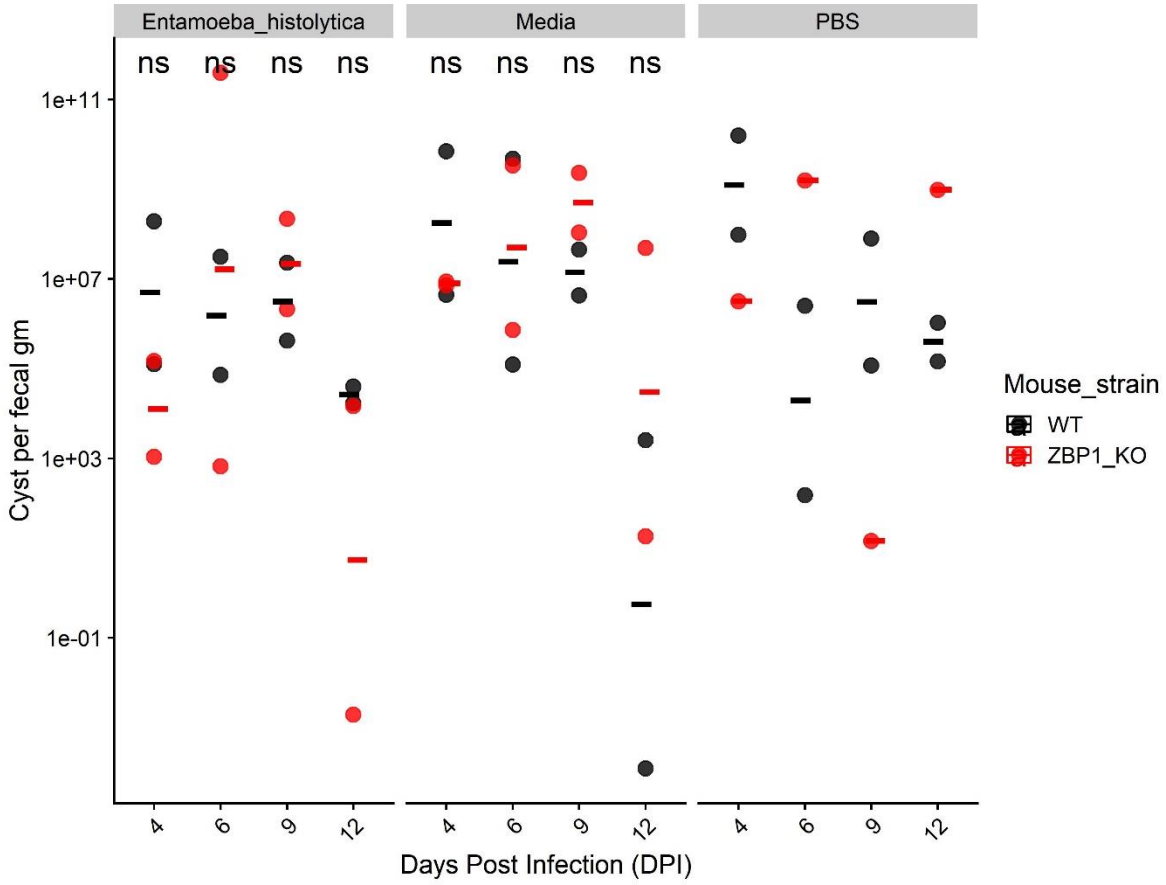

Fig D2. *Entamoeba muris* cyst shedding upon *E. histolytica* trophozoite oral challenge in various murine strains. Mice were challenged via oral gavage with *E. histolytica*, TYI media, or PBS. *E. muris* cysts shedding was quantified via qPCR for 12 days post infection. Significance was determined by a two-tail t-test between the murine strains per day among the three tree treatments.

The ZBP1 KO project had various flaws that we became aware once we realized we had *E. muris* within our vivarium. If the ZBP1 KO project wants to be explored mice must be cleared from *E. muris* first via drug treatment, then challenged with the same number of cysts (without microbiota differences). Our newest *Entamoeba* graduate student is currently evaluating the efficacy of paromomycin, a drug use to treat the luminal stage of *E. histolytica* infection.

To test if *E. muris* colonization has an impact on the natural resistance against *E. histolytica,* Swiss Webster (SW) mice can be colonized with *E. muris* then infected with *E. histolytica.* I am assuming there is a redout of pathology from *E. histolytica* trophozoite oral challenge, perhaps weight loss or decline in health scores. Thus, the first pilot experiments must focus on the characterization of *E. histolytica* challenge in outbred mice.

Appendix E

Cryptosporidium parvum infected mice were colonized with *Entamoeba muris*

To determine if there was *Entamoeba* colonization in the IFN-g KO mice used in Chapter 2, I performed the Pan-*Entamoeba* PCR on fecal samples collected for the *Cryptosporidium* publication. A total of 6 fecal samples from day 9 post infection were processed using the same gDNA isolation protocol attached in Appendix G. I performed two reactions (RXN 1= 300ng and RXN 2 = 5 µl of RXN 1 as genetic template) and *Entamoeba* gDNA was detected in (5/6) 83% of the tested samples. Next, I purified each band (Qiagen Gel Extraction Kit) and sent for sequencing at the UW-Madison Biotechnology Center using same primers as the amplification step (Forward: 5'-AGATACCGTCGTAGTCCT-3' and Reverse: 5'-ACGACTTCTCCTTCCTCTAA-3') which together amplify a 1 kb product. The resulting reads were 100% identical to each other and most closely matched *Entamoeba muris* (GenBank accession number AB445018) with 98% query coverage at 92% identity and an E value of 0.00.

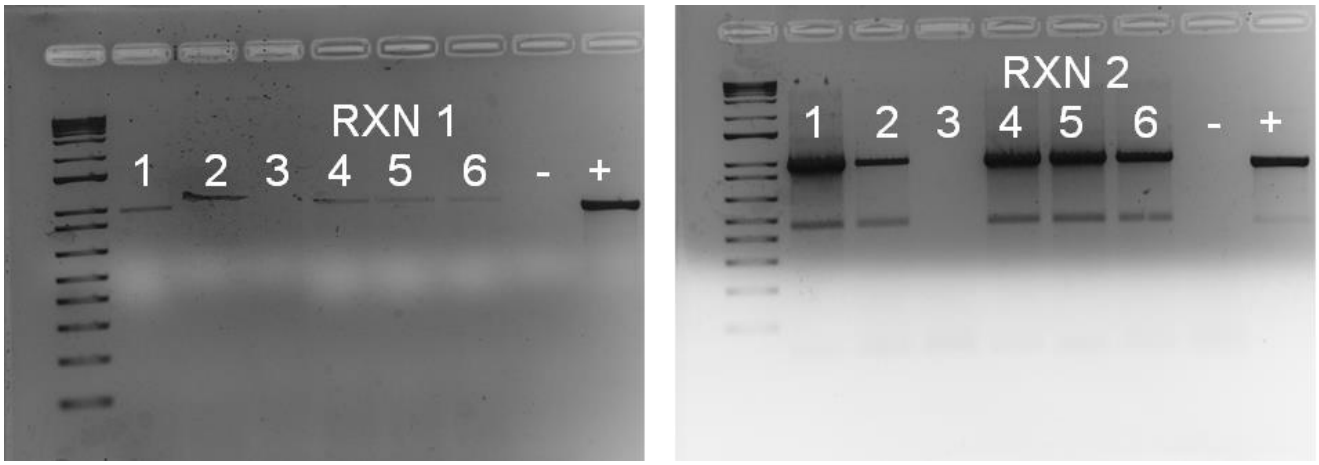

Figure E. Fecal samples from Cryptosporidium infected mice display Entamoeba colonization 9 dpi. Samples 1-3 were treated with PBS and Samples 4-6 received the STAg treatment. All animals were infected with *C. parvum* (1×10^7).

Appendix F

Analysis scripts for CBA

The following script is for the analysis for the commercially available BD kit “Mouse Inflammation Panel (552364)”

For the Knoll lab members, a copy of this script and the template excel file to include your data are located in the shared P:/ drive using the following path

P:Carolina>Cytokine_Anlaysis_Script.R

P:Carolina> Cytokine_Analysis_Template.xlsx

```
#Needed packages
library(tidyr)
library(dplyr)
library(ggplot2)
library(scales)
library(ggpubr)
library(ggbeeswarm)
library(readxl)

#Other useful but not necessary here
#library(ggpmisc),
#library(forcats)
#library(stringr)
#library(patchwork)

#set working directory to where your raw data is located, currently set for the Knoll Lab Shared Drive (P)
setwd("P:/Carolina")

#load the control data to generate the standard curves
#in the template they are located in the metadata_controls
cytokines_curve<- read_excel("Cytokine_Analysis_Template.xlsx", sheet="metadata_controls")
cytokines_curve<- cytokines_curve %>%
  gather(cytokine_type, PE_signal, IFNg:TNFa)

#graph standard curves per cytokine, check the trendlines make sense here
ggplot(cytokines_curve, aes(x=Concentration, y=PE_signal)) + geom_point() +
  facet_wrap(~cytokine_type) + theme_pubr() +
  geom_smooth(method='lm', se=FALSE)
  #If you can to show the equation and R squared values load #library(ggpmisc)
  #stat_poly_eq(aes(label = after_stat(eq.label))) +
  #stat_poly_eq(label.y = 0.9)

#subdivide the data per cytokine, so the program can create a table of the each cytokine's trendlines
#You can also use the function lapply if desired
(https://www.rdocumentation.org/packages/base/versions/3.6.2/topics/lapply)
IFNg<- cytokines_curve %>%
  filter(cytokine_type== "IFNg")
IL10<- cytokines_curve %>%
  filter(cytokine_type== "IL10")
```

```
IL12<- cytokines_curve %>%
  filter(cytokine_type== "IL12")
IL6<- cytokines_curve %>%
  filter(cytokine_type== "IL6")
MCP1<- cytokines_curve %>%
  filter(cytokine_type== "MCP1")
TNFa<- cytokines_curve %>%
  filter(cytokine_type== "TNFa")

#Generates linear model (lm) of each cytokine based on the formula PE_signal ~ Concentration
IFNg_curve<-lm(IFNg$PE_signal~IFNg$Concentration)
IL6_curve<-lm(IL6$PE_signal~IL6$Concentration)
IL10_curve<-lm(IL10$PE_signal~IL10$Concentration)
IL12_curve<-lm(IL12$PE_signal~IL12$Concentration)
MCP1_curve<-lm(MCP1$PE_signal~MCP1$Concentration)
TNFa_curve<-lm(TNFa$PE_signal~TNFa$Concentration)

#Makes a table for each cytokine's slope and intercept value
curves<- list(IFNg_curve, IL6_curve, IL10_curve,
              IL12_curve, MCP1_curve, TNFa_curve)
slopes<- c(IFNg_curve$coefficients['IFNg$Concentration'], IL6_curve$coefficients['IL6$Concentration'],
IL10_curve$coefficients['IL10$Concentration'],
             IL12_curve$coefficients['IL12$Concentration'], MCP1_curve$coefficients['MCP1$Concentration'],
TNFa_curve$coefficients['TNFa$Concentration'])
intercepts <- c(IFNg_curve$coefficients['(Intercept)'], IL6_curve$coefficients['(Intercept)'],
IL10_curve$coefficients['(Intercept)'],
IL12_curve$coefficients['(Intercept)'], MCP1_curve$coefficients['(Intercept)'],
TNFa_curve$coefficients['(Intercept)'])

cytokines_curve_equations<- data.frame(Cytokine= c("IFNg", "IL6", "IL10",
                                        "IL12", "MCP1", "TNFa"), M= slopes, B=intercepts)

#load the experimental data to calculate cytokine concentrations using the standard curves we just
generated
#in the template they are located in the metadata_experimental
cytokines_experimental_info<- read_excel("Cytokine_Analysis_Template.xlsx",
sheet="metadata_experimental")
cytokines_experimental_values<- read_excel("Cytokine_Analysis_Template.xlsx", sheet="rawdata")

cytokines_experimental<- left_join(cytokines_experimental_info,
                                   cytokines_experimental_values,
                                   by = c("Sample" = "Sample"))
cytokines_experimental<- cytokines_experimental %>%
  gather(cytokine_type, PE_signal, IFNg:TNFa)
cytokines_experimental$PE_signal<- as.numeric(cytokines_experimental$PE_signal)

#Creates a table with the experimental values and the calcualted standard curves, will allow us to
calcuate concentration of experimental samples
cytokines_experimental<- left_join(cytokines_experimental,
                                   cytokines_curve_equations,
                                  by = c("cytokine_type" = "Cytokine"))

###HERE YOU CAN MAKE ANY DATA A FACTOR AND USE THEM AS VARIABLES TO GRAPH
YOUR DATA
#Below I change the parasite strain to be a leveled factor so the graphs alwyas show Patental first then
the KO parasite, then the complement
```

```
### RELEVEL BASED ON YOUR OWN DATA
cytokines_experimental$Strain<- factor(cytokines_experimental$Strain,
                                levels=c("WT", "IFN"))
cytokines_experimental$Parasite<- factor(cytokines_experimental$Parasite,
                                levels=c("Parental", "LOX_KO", "Complement"))

cytokines_experimental$DPI<- factor(cytokines_experimental$DPI)

#Calculates concentration you need to solve for x in the following equation
# Y = MX + B, using the data frame "cytokines_curve_equations"
cytokines_experimental$Replicate<- factor(cytokines_experimental$Replicate)

cytokines_experimental<- cytokines_experimental %>%
  group_by(cytokine_type, Replicate) %>%
  summarise(Strain, DPI, Sex, Parasite, PE_signal, M, B, Replicate_Average_PE=(mean(PE_signal)))
%>%
  mutate(Replicate_Average_Concentration= ((Replicate_Average_PE-B)/M))

#Keeps only the average value of the cytokine's concentration
cytokines_experimental<- distinct(cytokines_experimental,
            Replicate_Average_Concentration, .keep_all = TRUE)



#GRAPHS
### CHANGE THE DIRECTORY TO SAVE YOUR GRAPHS
setwd("P:/Carolina")

### FILTER YOUR DATA IN A WAY IT MAKES SENSE FOR YOUR DESIRED GRAPH
### GO BONKERS WITH GGPLOT HERE
### BELOW IS ONE EXAMPLE

#PER cytokine, day 7, sex difference???
IL6_only_dp7<- cytokines_experimental%>%
  filter(cytokine_type =="IL6") %>%
  filter(DPI == "7")
ggplot(IL6_only_dp7, aes(x=Strain, y=Replicate_Average_Concentration,color=Sex)) +
  geom_beeswarm(size=3, alpha=0.5) + facet_wrap(~Parasite) +#, scales = "free") +
  labs(title= "IL-6", x= "Mouse Strain", y= "Concentration") +
  stat_summary(fun=mean, geom='crossbar', width=0.6, alpha=0.5, position =
position_dodge(width=0.25)) +
  #facet_wrap(Parasite)+
  #here you are comparing M vs F cytokine level, per parasite strain
  stat_compare_means(method = "t.test", label =  "p.signif", size=5, hide.ns = TRUE) + theme_pubr()
#ggsave("change_this_name.jpg", width = 5, height =4, scale= 2, dpi=300)
```

Appendix G

Protocols

gDNA Isolation (Rey Lab)

Protocol based but not the same as previous microbiome publications (126, 127)

A) Prepare 2 ml solvent-resistant screw-cap tubes + 500 µl (~1.2 g) 0.1mm zirconia/silica beads (BioSpec Products 11079101z) + 1 large ss bead (BioSpec Products 11079132ss); autoclave (caps loose, cover with foil + autoclave tape) 20 min (dry cycle preferable).

B) 20% SDS in Nanopure water: Will go into solution O/N at ~32°C; DO NOT autoclave.

C) Sterile Buffer A (aka "2× Buffer A"): 200 mM Tris·HCl, pH 8.0 / 200 mM NaCl / 20 mM EDTA. For 150 mL: 30 mL of Tris·HCl, pH 8.0, 30 mL of NaCl [1M], 30 mL of EDTA [100mM], and 60 mL of Nanopure water.

>> Check SDS in solution, check microfuge at 4°C <<

Add frozen samples [~20-50 mg (< 200 mg) keep on wet ice] to sterile 2 ml tubes (see "A", above);

if this if for qPCR, don't forget to weigh the sample and record.

NOTE: Preload Buffer A + 20% SDS mixture into beads prior to loading fecal sample

1. Add 500 µl Buffer A with 210 µl 20% SDS *(may premix 1 + 2 as needed for multiple samples; add 710 µl)*
    a. If using concentrated pellet resuspend in 420ul of Buffer A + 20% SDS mixture
2. Add 500 µl Phenol / Chloroform / Isoamyl alcohol, pH 7.9, 25:24:1 (Invitrogen 15593-049)
3. Bead beat on high for 3 min at room temperature (be sure the block is firmly secured)
4. Spin, 8,000 RPM (~7200 × *g*), 4°C, 3 min (note speed; higher risks tube breakage; 3 min is usually plenty, but may extend)
5. Transfer aqueous layer (≤600 µl) to a sterile, new 1.7ml tube (do the optional steps for qPCR)
6. Add 500 µl Phenol/Chloroform, mix by inversion
7. Spin, 13,000 RPM (~18,000 × *g*), 4°C, 3 min
8. Transfer aqueous layer to new tube

9. Add 60 µl 3M NaAcetate, mix (assumes 500 – 600 µl aqueous recovery)
10. Add 600 µl isopropanol, mix by inversion
11. Place on ice for 1 h to O/N [OR at −80°C for 12 min (max!), OR store at −20°C indefinitely]
12. Spin, 13,000 RPM (~18,000 × *g*), 4°C, 20 min
13. Decant or remove the supernatant as thoroughly as possible
14. Rinse pellet with ≥500 µl 100% EtOH, remove traces of liquid, (air dry or Speed Vac 1 min)
15. Dissolve pellet in 200 µl sterile $T_{(10)}E_{(1)}$ buffer on ice (for DNA samples only, may temporarily warm to ~30 - 37°C to aid rapid dissolution

Proceed to clean DNA (all 200 µl) using DNA Clean & Concentrator 5 (Zymo Research D4004). Following instructions for plasmid, genomic DNA (>2 kb)

- Be sure to spin dry membrane prior to the start of this protocol
- Elute using 50-100 µl of kit's elution buffer (sterile $T_{(10)}E_{(1)}$ buffer as an alternative), depending on the downstream application. **NEVER ELUTE IN WATER – DNA WILL DEGRADE 10-FOLD IN FREEZER.**
- Quantify using nanodrop (Use 100-500ng per reaction for screen, use 100ng per reaction for qPCR)

Immunofluorescence Assay for Jacob2 staining

This protocol was based on the publication associated with the α-Jacob-2 antibody (48).

All samples were processes in 1.75 mini-centrifuge tubes. Incubations were at room temperature for 5 minutes and with 1 ml volumes each unless otherwise stated.

Sample Prep

- Fresh poop or isolated cysts via sucrose gradient treated with 0.1% sarkosyl wash (skip to fixation)
    - **USE FRESH POOP, poop that has been stored in the -20 will not have strong Jacob2 in staining**
- About ~0.10 to 5 g of frozen fecal samples were ground to a fine powder using a mortar and pestle then homogenized with 5 to 15 mls of nanopure water for 5 minutes using the poop rotator at 60 rpm
- Sample was filtered through two two-ply cotton gazes. Optional nylon mesh plastic filters (100, 70, and 40 µm)
- Sample was incubated on ice on 0.1% sarkosyl solution for 30 minutes
- Sample was pelleted for 5 min at 250g (note the slower speed)

Fixation Step

- Pellet was fixed by adding 1mL of 10% formalin
    - Incubate for 5-10 minutes at room temperature while rotating
- Wash with nanopure water

Blocking Step

- Sample was blocked using 3% goat serum (diluted in nanopure water)
    - NOTE use serum of the same species as the secondary antibody
    - For cleaner results might need to use serum plus BSA
    - Per 1 ml, add 10 ul of serum
    - Incubate for 5 min
- Wash with nanopure water

Primary Antibody Incubation

- Primary antibody (1A4) was added (2.9 ug/ml, 1:1000 dilution from stock)
    - Use Nanopure water, not the goat-blocking buffer
    - Incubated 2 hours with rotation
- Wash with Nanopure water

Secondary Antibody and Nucleic Acid Stain Incubation (KEEP COVERED FROM LIGHT USING FOIL)

- Secondary antibody (Alexa Fluor 594, goat anti-mouse IgG) was added (20 µg/mL, 1:1000 goat anti-mouse
    - Use 0.1% triton in nanopure water, not the goat-blocking buffer
    - Incubate for 2 hours **(overnight is really not encouraged for whole feces, if sucrose gradient is fixed you may extend overnight. Again, it doesn't look great)**
- Wash 0.1 % (calcofluor-white and 10% KOH) in nanopure water,
- Wash with nanpure water
    - ***ONLY IF ISOLATED CYSTS TREATED WITH 0.1% SARKOSYL ARE BEING USED****, Add Syto 11 stain (# S7573) AT 1:5000 dilution. DO NOT USE FOR WHOLE FECES*
        - No need for incubation
- Resuspend in 50 ul of nanopure H2O

Mounting

- Add 2 ul Vectashield and 8 ul of sample
- Place a circular coverslip on top of mix
- Seal with nail polish
- Store at 4° C for short term, -20° C for long term

Fluorescence Detection

- Take images using DIC, DAPI (calc), GFP (Syto11), and Texas-Red (1A4).

References

1. WHO. Entamoeba taxonomy. Bull World Health Organ. 1997;75(3):291-4.
2. Carrero JC, Reyes-López M, Serrano-Luna J, Shibayama M, Unzueta J, León-Sicairos N, et al. Intestinal amoebiasis: 160 years of its first detection and still remains as a health problem in developing countries. Int J Med Microbiol. 2020;310(1):151358.
3. Shirley DT, Watanabe K, Moonah S. Significance of amebiasis: 10 reasons why neglecting amebiasis might come back to bite us in the gut. PLoS Negl Trop Dis. 2019;13(11):e0007744.
4. Manna D, Ehrenkaufer GM, Singh U. Regulation of gene expression in the protozoan parasite Entamoeba invadens: identification of core promoter elements and promoters with stage-specific expression patterns. Int J Parasitol. 2014;44(11):837-45.
5. Mi-ichi F, Miyamoto T, Takao S, Jeelani G, Hashimoto T, Hara H, et al. Entamoeba mitosomes play an important role in encystation by association with cholesteryl sulfate synthesis. Proc Natl Acad Sci U S A. 2015;112(22):E2884-90.
6. Singh M, Sharma S, Bhattacharya A, Tatu U. Heat Shock Protein 90 regulates encystation in Entamoeba. Front Microbiol. 2015;6:1125.
7. D M, CS L, GM E, S S, A B, U S. An NAD +-dependent Novel Transcription Factor Controls Stage Conversion in Entamoeba. eLife. 2018;7.
8. D M, U S. Nuclear Factor Y (NF-Y) Modulates Encystation in Entamoeba via Stage-Specific Expression of the NF-YB and NF-YC Subunits. mBio. 2019;10(3).
9. Quach J, St-Pierre J, Chadee K. The future for vaccine development against Entamoeba histolytica. Hum Vaccin Immunother. 2014;10(6):1514-21.
10. Burgess SL, Petri WA. The Intestinal Bacterial Microbiome and E. histolytica Infection. Curr Trop Med Rep. 2016;3:71-4.
11. Nakada-Tsukui K, Nozaki T. Immune Response of Amebiasis and Immune Evasion by Entamoeba histolytica. Front Immunol. 2016;7:175.
12. Ghosh S, Padalia J, Moonah S. Tissue Destruction Caused by Entamoeba histolytica Parasite : Cell Death, Inflammation, Invasion, and the Gut Microbiome. Current Clinical Microbiology Reports. 2019;6(1):51-7.
13. Diamond LS. Axenic cultivation of Entamoeba hitolytica. Science. 1961;134(3475):336-7.
14. Cobo ER, Holani R, Moreau F, Nakamura K, Ayabe T, Mastroianni JR, et al. Entamoeba histolytica Alters Ileal Paneth Cell Functions in Intact and Muc2 Mucin Deficiency. Infect Immun. 2018;86(7).
15. Mackey-Lawrence NM, Guo X, Sturdevant DE, Virtaneva K, Hernandez MM, Houpt E, et al. Effect of the leptin receptor Q223R polymorphism on the host transcriptome following infection with Entamoeba histolytica. Infect Immun. 2013;81(5):1460-70.
16. Wojcik GL, Marie C, Abhyankar MM, Yoshida N, Watanabe K, Mentzer AJ, et al. Genome-Wide Association Study Reveals Genetic Link between Diarrhea-Associated Entamoeba histolytica Infection and Inflammatory Bowel Disease. MBio. 2018;9(5).
17. Ralston KS, Solga MD, Mackey-Lawrence NM, Somlata, Bhattacharya A, Petri WA. Trogocytosis by Entamoeba histolytica contributes to cell killing and tissue invasion. Nature. 2014;508(7497):526-30.
18. Shimokawa C, Kabir M, Taniuchi M, Mondal D, Kobayashi S, Ali IK, et al. Entamoeba moshkovskii is associated with diarrhea in infants and causes diarrhea and colitis in mice. J Infect Dis. 2012;206(5):744-51.
19. Burgess SL, Leslie JL, Uddin MJ, Oakland DN, Gilchrist CA, Moreau GB, et al. Gut microbiome communication with bone marrow regulates susceptibility to amebiasis. J Clin Invest. 2020.

20. Watanabe K, Gilchrist CA, Uddin MJ, Burgess SL, Abhyankar MM, Moonah SN, et al. Microbiome-mediated neutrophil recruitment via CXCR2 and protection from amebic colitis. PLoS Pathog. 2017;13(8):e1006513.
21. Santi-Rocca J, Rigothier MC, Guillén N. Host-microbe interactions and defense mechanisms in the development of amoebic liver abscesses. Clin Microbiol Rev. 2009;22(1):65-75, Table of Contents.
22. Mitra BN, Pradel G, Frevert U, Eichinger D. Compounds of the upper gastrointestinal tract induce rapid and efficient excystation of Entamoeba invadens. Int J Parasitol. 2010;40(6):751-60.
23. Chauhan, Das. Simultaneous caecal and liver infections in hamster, mouse and guinea-pig by oral feeding of Entamoeba histolytica cysts. Current Science. 1987;56(23):1223–4.
24. Owen DG. Attempts at oral infection of rats and mice with trophozoites of Entamoeba histolytica. Trans R Soc Trop Med Hyg. 1984;78(2):160-4.
25. Quadri GSA, Saleem Y, Ishaq M, Habibullah CM. Experimental hepatic amoebiasis in immunosuppressed mice fed orally with cysts of Entamoeba histolytica. IRCS Medical Science. 1985;13(7):590-1.
26. Owen DG. A mouse model for Entamoeba histolytica infection. Lab Anim. 1985;19(4):297-304.
27. Owen DG. The effect of orally administered Entamoeba histolytica on Wistar and athymic (rnu rnu) rats observed during a 12-month period. Trans R Soc Trop Med Hyg. 1987;81(4):621-3.
28. Lushbaugh WB, Kairalla AB, Loadholt CB, Pittman FE. Effect of hamster liver passage on the virulence of axenically cultivated Entamoeba histolytica. Am J Trop Med Hyg. 1978;27(2 Pt 1):248-54.
29. Bos HJ, van de Griend RJ. Virulence and toxicity of axenic Entamoeba histolytica. Nature. 1977;265(5592):341-3.
30. Leon-Coria A, Kumar M, Moreau F, Chadee K. Defining cooperative roles for colonic microbiota and Muc2 mucin in mediating innate host defense against Entamoeba histolytica. PLoS Pathog. 2018;14(11):e1007466.
31. Guo X, Roberts MR, Becker SM, Podd B, Zhang Y, Chua SC, et al. Leptin signaling in intestinal epithelium mediates resistance to enteric infection by Entamoeba histolytica. Mucosal Immunol. 2011;4(3):294-303.
32. Partida-Rodríguez O, Serrano-Vázquez A, Nieves-Ramírez ME, Moran P, Rojas L, Portillo T, et al. Human Intestinal Microbiota: Interaction Between Parasites and the Host Immune Response. Arch Med Res. 2017;48(8):690-700.
33. Sicard JF, Le Bihan G, Vogeleer P, Jacques M, Harel J. Interactions of Intestinal Bacteria with Components of the Intestinal Mucus. Front Cell Infect Microbiol. 2017;7:387.
34. Iyer LR, Verma AK, Paul J, Bhattacharya A. Phagocytosis of Gut Bacteria by *Entamoeba histolytica*. Front Cell Infect Microbiol. 2019;9:34.
35. Byers J, Faigle W, Eichinger D. Colonic short-chain fatty acids inhibit encystation of Entamoeba invadens. Cell Microbiol. 2005;7(2):269-79.
36. Leon-Coria A, Kumar M, Chadee K. The delicate balance between Entamoeba histolytica, mucus and microbiota. Gut Microbes. 2020;11(1):118-25.
37. Verma AK, Verma R, Ahuja V, Paul J. Real-time analysis of gut flora in Entamoeba histolytica infected patients of Northern India. BMC Microbiol. 2012;12:183.
38. Yanagawa Y, Arisaka T, Kawai S, Nakada-Tsukui K, Fukushima A, Hiraishi H, et al. Case Report: Acute Amebic Colitis Triggered by Colonoscopy: Exacerbation of Asymptomatic Chronic Infection with. Am J Trop Med Hyg. 2019;101(6):1384-7.
39. Pittman KJ, Cervantes PW, Knoll LJ. Z-DNA Binding Protein Mediates Host Control of Toxoplasma gondii Infection. Infect Immun. 2016;84(10):3063-70.

40. Barreto-de-Albuquerque J, Silva-dos-Santos D, Pérez AR, Berbert LR, de Santana-van-Vliet E, Farias-de-Oliveira DA, et al. Trypanosoma cruzi Infection through the Oral Route Promotes a Severe Infection in Mice: New Disease Form from an Old Infection? PLoS Negl Trop Dis. 2015;9(6):e0003849.
41. Zimmermann P, Curtis N. Factors That Influence the Immune Response to Vaccination. Clin Microbiol Rev. 2019;32(2).
42. Burgess SL, Gilchrist CA, Lynn TC, Petri WA. Parasitic Protozoa and Interactions with the Host Intestinal Microbiota. Infect Immun. 2017;85(8).
43. Luna-Nácar M, Navarrete-Perea J, Moguel B, Bobes RJ, Laclette JP, Carrero JC. Proteomic Study of Entamoeba histolytica Trophozoites, Cysts, and Cyst-Like Structures. PLoS One. 2016;11(5):e0156018.
44. Mukherjee C, Clark CG, Lohia A. Entamoeba shows reversible variation in ploidy under different growth conditions and between life cycle phases. PLoS Negl Trop Dis. 2008;2(8):e281.
45. Marie C, Petri WA. Regulation of virulence of Entamoeba histolytica. Annu Rev Microbiol. 2014;68:493-520.
46. Regan CS, Yon L, Hossain M, Elsheikha HM. Prevalence of Entamoeba species in captive primates in zoological gardens in the UK. PeerJ. 2014;2:e492.
47. Aguilar-Díaz H, Carrero JC, Argüello-García R, Laclette JP, Morales-Montor J. Cyst and encystment in protozoan parasites: optimal targets for new life-cycle interrupting strategies? Trends Parasitol. 2011;27(10):450-8.
48. Spadafora LJ, Kearney MR, Siddique A, Ali IK, Gilchrist CA, Arju T, et al. Species-Specific Immunodetection of an Entamoeba histolytica Cyst Wall Protein. PLoS Negl Trop Dis. 2016;10(5):e0004697.
49. Nayeem MA, Habibullah CM, Saleem Y, Quadri GS, Ishaq M. In vitro encystation and excystation of Entamoeba histolytica trophozoites. Indian J Exp Biol. 1993;31(6):562-3.
50. Houpt E, Vines R, Camerini V, Lockhart L, Petri W. The mucosal immune response in a mouse model of amebic colitis. Arch Med Res. 2000;31(4 Suppl):S89.
51. Scanlan PD, Stensvold CR, Rajilić-Stojanović M, Heilig HG, De Vos WM, O'Toole PW, et al. The microbial eukaryote Blastocystis is a prevalent and diverse member of the healthy human gut microbiota. FEMS Microbiol Ecol. 2014;90(1):326-30.
52. Parfrey LW, Walters WA, Lauber CL, Clemente JC, Berg-Lyons D, Teiling C, et al. Communities of microbial eukaryotes in the mammalian gut within the context of environmental eukaryotic diversity. Front Microbiol. 2014;5:298.
53. Rook GA. Hygiene hypothesis and autoimmune diseases. Clin Rev Allergy Immunol. 2012;42(1):5-15.
54. Ley RE, Lozupone CA, Hamady M, Knight R, Gordon JI. Worlds within worlds: evolution of the vertebrate gut microbiota. Nat Rev Microbiol. 2008;6(10):776-88.
55. Laforest-Lapointe I, Arrieta MC. Microbial Eukaryotes: a Missing Link in Gut Microbiome Studies. mSystems. 2018;3(2).
56. Ehret T, Torelli F, Klotz C, Pedersen AB, Seeber F. Translational Rodent Models for Research on Parasitic Protozoa—A Review of Confounders and Possibilities. Front Cell Infect Microbiol. 2017;7.
57. Chabé M, Lokmer A, Ségurel L. Gut Protozoa: Friends or Foes of the Human Gut Microbiota? Trends Parasitol. 2017;33(12):925-34.
58. Bär AK, Phukan N, Pinheiro J, Simoes-Barbosa A. The Interplay of Host Microbiota and Parasitic Protozoans at Mucosal Interfaces: Implications for the Outcomes of Infections and Diseases. PLoS Negl Trop Dis. 2015;9(12):e0004176.
59. Stensvold CR, Tan KSW, Clark CG. Blastocystis. Trends Parasitol. 2020;36(3):315-6.
60. Beghini F, Pasolli E, Truong TD, Putignani L, Cacciò SM, Segata N. Large-scale comparative metagenomics of Blastocystis, a common member of the human gut microbiome. ISME J. 2017;11(12):2848-63.

61. Audebert C, Even G, Cian A, Loywick A, Merlin S, Viscogliosi E, et al. Colonization with the enteric protozoa Blastocystis is associated with increased diversity of human gut bacterial microbiota. Sci Rep. 2016;6:25255.
62. Yakoob J, Jafri W, Beg MA, Abbas Z, Naz S, Islam M, et al. Irritable bowel syndrome: is it associated with genotypes of Blastocystis hominis. Parasitol Res. 2010;106(5):1033-8.
63. Jimenez-Gonzalez DE, Martinez-Flores WA, Reyes-Gordillo J, Ramirez-Miranda ME, Arroyo-Escalante S, Romero-Valdovinos M, et al. Blastocystis infection is associated with irritable bowel syndrome in a Mexican patient population. Parasitol Res. 2012;110(3):1269-75.
64. Billy V, Lhotská Z, Jirků M, Kadlecová O, Frgelecová L, Parfrey LW, et al. Colonization Alters the Gut Microbiome and, in Some Cases, Promotes Faster Recovery From Induced Colitis. Front Microbiol. 2021;12:641483.
65. Sarkar S, Heise MT. Mouse Models as Resources for Studying Infectious Diseases. Clin Ther. 2019;41(10):1912-22.
66. Ericsson AC, Davis JW, Spollen W, Bivens N, Givan S, Hagan CE, et al. Effects of vendor and genetic background on the composition of the fecal microbiota of inbred mice. PLoS One. 2015;10(2):e0116704.
67. Sivan A, Corrales L, Hubert N, Williams JB, Aquino-Michaels K, Earley ZM, et al. Commensal Bifidobacterium promotes antitumor immunity and facilitates anti-PD-L1 efficacy. Science. 2015;350(6264):1084-9.
68. Theriot CM, Koenigsknecht MJ, Carlson PE, Hatton GE, Nelson AM, Li B, et al. Antibiotic-induced shifts in the mouse gut microbiome and metabolome increase susceptibility to Clostridium difficile infection. Nat Commun. 2014;5:3114.
69. Yang J, Park J, Park S, Baek I, Chun J. Introducing Murine Microbiome Database (MMDB): A Curated Database with Taxonomic Profiling of the Healthy Mouse Gastrointestinal Microbiome. Microorganisms. 2019;7(11).
70. Mims TS, Abdallah QA, Stewart JD, Watts SP, White CT, Rousselle TV, et al. The gut mycobiome of healthy mice is shaped by the environment and correlates with metabolic outcomes in response to diet. Commun Biol. 2021;4(1):281.
71. Chudnovskiy A, Mortha A, Kana V, Kennard A, Ramirez JD, Rahman A, et al. Host-Protozoan Interactions Protect from Mucosal Infections through Activation of the Inflammasome. Cell. 2016;167(2):444-56.e14.
72. Bonner M, Fresno M, Gironès N, Guillén N, Santi-Rocca J. Reassessing the Role of *Entamoeba gingivalis* in Periodontitis. Front Cell Infect Microbiol. 2018;8:379.
73. Elsheikha HM, Regan CS, Clark CG. Novel Entamoeba Findings in Nonhuman Primates. Trends Parasitol. 2018;34(4):283-94.
74. García G, Ramos F, Pérez RG, Yañez J, Estrada MS, Mendoza LH, et al. Molecular epidemiology and genetic diversity of Entamoeba species in a chelonian collection. J Med Microbiol. 2014;63(Pt 2):271-83.
75. Komatsu T, Matsubayashi M, Murakoshi N, Sasai K, Shibahara T. Retrospective and Histopathological Studies of Entamoeba spp. and Other Pathogens Associated with Diarrhea and Wasting in Pigs in Aichi Prefecture, Japan.
76. Li WC, Geng JZ, Chen C, Qian L, Zhang T, Liu JL, et al. First report on the occurance of intestinal Entamoeba spp. In pigs In China. Acta Trop. 2018;185:385-90.
77. Matsubayashi M, Kanamori K, Sadahiro M, Tokoro M, Abe N, Haritani M, et al. First molecular identification of Entamoeba polecki in a piglet in Japan and implications for aggravation of ileitis by coinfection with Lawsonia intracellularis. Parasitol Res. 2015;114(8):3069-73.
78. Matsubayashi M, Matsuura Y, Nukata S, Daizi Y, Shibahara T, Teramoto I, et al. First detection and molecular identification of Entamoeba bovis from Japanese cattle. Parasitol Res. 2018;117(1):339-42.

79. Ai S, Zhang Z, Wang X, Zhang Q, Yin W, Duan Z. The first survey and molecular identification of Entamoeba spp. in farm animals on Qinghai-Tibetan Plateau of China. Comp Immunol Microbiol Infect Dis. 2021;75:101607.
80. Al-Habsi K, Yang R, Ryan U, Jacobson C, Miller DW. Morphological and molecular characterization of an uninucleated cyst-producing Entamoeba spp. in captured Rangeland goats in Western Australia. Vet Parasitol. 2017;235:41-6.
81. Valdéz-Cruz MP, Hernández-Gil M, Galindo-Rodríguez L, Alonso-Díaz MA. Gastrointestinal nematode burden in working equids from humid tropical areas of central Veracruz, Mexico, and its relationship with body condition and haematological values. Trop Anim Health Prod. 2013;45(2):603-7.
82. Kingston N, Stabler RM. Two species of Entamoeba from white-tailed deer, Odocoileus virginianus, from Georgia. J Parasitol. 1978;64(1):14-6.
83. Huaman JL, Pacioni C, Kenchington-Evans L, Doyle M, Helbig KJ, Carvalho TG. First Evidence of Entamoeba Parasites in Australian Wild Deer and Assessment of Transmission to Cattle.
84. Mirzapour A, Kiani H, Mobedi I, Spotin A, Seyyed Tabaei SJ, Rahimi M. Frequency of Intestinal Parasites among Zoo Animal by Morphometric Criteria and First Report of the Bivitellobilharzia nairi from Elephant (Elephasmaximus maximus) in Iran. Iran J Parasitol. 2018;13(4):611-7.
85. Lau YL, Jamaiah I, Rohela M, Fong MY, Siti CO, Siti FA. Molecular detection of Entamoeba histolytica and Entamoeba dispar infection among wild rats in Kuala Lumpur, Malaysia. Trop Biomed. 2014;31(4):721-7.
86. Hofmann AF, Hagey LR, Krasowski MD. Bile salts of vertebrates: structural variation and possible evolutionary significance. J Lipid Res. 2010;51(2):226-46.
87. Pai HH, Ko YC, Chen ER. Cockroaches (Periplaneta americana and Blattella germanica) as potential mechanical disseminators of Entamoeba histolytica. Acta Trop. 2003;87(3):355-9.
88. Kawano T, Imada M, Chamavit P, Kobayashi S, Hashimoto T, Nozaki T. Correction: Genetic diversity of Entamoeba: Novel ribosomal lineages from cockroaches. PLoS One. 2019;14(5):e0217215.
89. Alderslade R. The Public Health Act of 1848. The Act's qualities of imagination and determination are still needed today. Bmj. 1998;317(7158):549-50.
90. Cui Z, Li J, Chen Y, Zhang L. Molecular epidemiology, evolution, and phylogeny of Entamoeba spp. Infect Genet Evol. 2019;75:104018.
91. Oliveira FM, Neumann E, Gomes MA, Caliari MV. Entamoeba dispar: Could it be pathogenic. Trop Parasitol. 2015;5(1):9-14.
92. Naiyer S, Bhattacharya A, Bhattacharya S. Advances in *Entamoeba histolytica* Biology Through Transcriptomic Analysis. Front Microbiol. 2019;10:1921.
93. Soave O, Brand CD. Coprophagy in animals: a review. Cornell Vet. 1991;81(4):357-64.
94. KD K, RG L, DD J, JM R, HC S. Intestinal parasitism in the United States: update on a continuing problem. The American journal of tropical medicine and hygiene. 1994;50(6).
95. R S, TH X, LNS H, MJ V, KM F, PJ H, et al. Prevalence of Intestinal Parasites in a Low-Income Texas Community. The American journal of tropical medicine and hygiene. 2020;102(6).
96. Hotez PJ. Neglected Parasitic Infections and Poverty in the United States. 2022.
97. Liu L, Johnson HL, Cousens S, Perin J, Scott S, Lawn JE, et al. Global, regional, and national causes of child mortality: an updated systematic analysis for 2010 with time trends since 2000. Lancet. 2012;379(9832):2151-61.
98. Kotloff KL, Platts-Mills JA, Nasrin D, Roose A, Blackwelder WC, Levine MM. Global burden of diarrheal diseases among children in developing countries: Incidence, etiology, and insights from new molecular diagnostic techniques. Vaccine. 2017;35(49 Pt A):6783-9.

99. Collaborators GDD. Estimates of the global, regional, and national morbidity, mortality, and aetiologies of diarrhoea in 195 countries: a systematic analysis for the Global Burden of Disease Study 2016. Lancet Infect Dis. 2018;18(11):1211-28.
100. Turkeltaub JA, McCarty TR, Hotez PJ. The intestinal protozoa: emerging impact on global health and development. Curr Opin Gastroenterol. 2015;31(1):38-44.
101. Skappak C, Akierman S, Belga S, Novak K, Chadee K, Urbanski SJ, et al. Invasive amoebiasis: a review of Entamoeba infections highlighted with case reports. Can J Gastroenterol Hepatol. 2014;28(7):355-9.
102. Lichtenstein A, Kondo AT, Visvesvara GS, Fernandez A, Paiva EF, Mauad T, et al. Pulmonary amoebiasis presenting as superior vena cava syndrome. Thorax. 2005;60(4):350-2.
103. Wuerz T, Kane JB, Boggild AK, Krajden S, Keystone JS, Fuksa M, et al. A review of amoebic liver abscess for clinicians in a nonendemic setting. Can J Gastroenterol. 2012;26(10):729-33.
104. Petri WA, Haque R. Entamoeba histolytica brain abscess. Handb Clin Neurol. 2013;114:147-52.
105. Stanley SL. Amoebiasis. Lancet. 2003;361(9362):1025-34.
106. Haque R, Huston CD, Hughes M, Houpt E, Petri WA. Amebiasis. N Engl J Med. 2003;348(16):1565-73.
107. Houpt ER, Glembocki DJ, Obrig TG, Moskaluk CA, Lockhart LA, Wright RL, et al. The mouse model of amebic colitis reveals mouse strain susceptibility to infection and exacerbation of disease by CD4+ T cells. J Immunol. 2002;169(8):4496-503.
108. Debnath A, Rodriguez MA, Ankri S. Editorial: Recent Progresses in Amebiasis. Front Cell Infect Microbiol. 2019;9:247.
109. Mendoza Cavazos C, Knoll LJ. Entamoeba histolytica: Five facts about modeling a complex human disease in rodents. PLoS Pathog. 2020;16(11):e1008950.
110. Jyothi R, Foerster B, Hamelmann C, Shetty NP. Improved method for the concentration and purification of faecal cysts of Entamoeba histolytica for use as antigen. J Trop Med Hyg. 1993;96(4):249-50.
111. Lee KC, Lu CC, Hu WH, Lin SE, Chen HH. Colonoscopic diagnosis of amebiasis: a case series and systematic review. Int J Colorectal Dis. 2015;30(1):31-41.
112. Kantor M, Abrantes A, Estevez A, Schiller A, Torrent J, Gascon J, et al. Entamoeba Histolytica: Updates in Clinical Manifestation, Pathogenesis, and Vaccine Development. Can J Gastroenterol Hepatol. 2018;2018:4601420.
113. Hamano S, Asgharpour A, Stroup SE, Wynn TA, Leiter EH, Houpt E. Resistance of C57BL/6 mice to amoebiasis is mediated by nonhemopoietic cells but requires hemopoietic IL-10 production. J Immunol. 2006;177(2):1208-13.
114. Ghosh SK, Van Dellen KL, Chatterjee A, Dey T, Haque R, Robbins PW, et al. The Jacob2 lectin of the Entamoeba histolytica cyst wall binds chitin and is polymorphic. PLoS Negl Trop Dis. 2010;4(7):e750.
115. Cervantes PW, Di Genova BM, Erazo Flores BJ, Knoll LJ. RIPK3 facilitates host resistance to oral *Toxoplasma gondii* infection. Infect Immun. 2021.
116. Sunagar R, Kumar S, Namjoshi P, Rosa SJ, Hazlett KRO, Gosselin EJ. Evaluation of an outbred mouse model for Francisella tularensis vaccine development and testing. PLoS One. 2018;13(12):e0207587.
117. Watanabe H, Numata K, Ito T, Takagi K, Matsukawa A. Innate immune response in Th1- and Th2-dominant mouse strains. Shock. 2004;22(5):460-6.
118. Ferreira BL, Ferreira É, de Brito MV, Salu BR, Oliva MLV, Mortara RA, et al. BALB/c and C57BL/6 Mice Cytokine Responses to. Front Microbiol. 2018;9:553.
119. Hartmann W, Blankenhaus B, Brunn ML, Meiners J, Breloer M. Elucidating different pattern of immunoregulation in BALB/c and C57BL/6 mice and their F1 progeny. Sci Rep. 2021;11(1):1536.

120. Denic S, Nicholls MG. Genetic benefits of consanguinity through selection of genotypes protective against malaria. Hum Biol. 2007;79(2):145-58.
121. Benton CH, Delahay RJ, Smith FAP, Robertson A, McDonald RA, Young AJ, et al. Inbreeding intensifies sex- and age-dependent disease in a wild mammal. J Anim Ecol. 2018;87(6):1500-11.
122. A A, IM A, H A, JR R, MK I. Impact of environmental conditions on the survival of cryptosporidium and giardia on environmental surfaces. Interdisciplinary perspectives on infectious diseases. 2014;2014.
123. Pawestri AR, Thima K, Leetachewa S, Maneekan P, Deesitthivech O, Pinna C, et al. Seasonal prevalence, risk factors, and One Health intervention for prevention of intestinal parasitic infection in underprivileged communities on the Thai-Myanmar border. Int J Infect Dis. 2021;105:152-60.
124. Jaran AS. Prevalence and seasonal variation of human intestinal parasites in patients attending hospital with abdominal symptoms in northern Jordan. East Mediterr Health J. 2017;22(10):756-60.
125. Chowdhury FR, Ibrahim QSU, Bari MS, Alam MMJ, Dunachie SJ, Rodriguez-Morales AJ, et al. Correction: The association between temperature, rainfall and humidity with common climate-sensitive infectious diseases in Bangladesh. PLoS One. 2020;15(4):e0232285.
126. Turnbaugh PJ, Hamady M, Yatsunenko T, Cantarel BL, Duncan A, Ley RE, et al. A core gut microbiome in obese and lean twins. Nature. 2009;457(7228):480-4.
127. McNulty NP, Yatsunenko T, Hsiao A, Faith JJ, Muegge BD, Goodman AL, et al. The impact of a consortium of fermented milk strains on the gut microbiome of gnotobiotic mice and monozygotic twins. Sci Transl Med. 2011;3(106):106ra.
128. Walderich B, Müller L, Bracha R, Knobloch J, Burchard GD. A new method for isolation and differentiation of native Entamoeba histolytica and E. dispar cysts from fecal samples. Parasitol Res. 1997;83(7):719-21.
129. Morgulis A, Coulouris G, Raytselis Y, Madden TL, Agarwala R, Schäffer AA. Database indexing for production MegaBLAST searches. Bioinformatics. 2008;24(16):1757-64.
130. Guindon S, Dufayard JF, Lefort V, Anisimova M, Hordijk W, Gascuel O. New algorithms and methods to estimate maximum-likelihood phylogenies: assessing the performance of PhyML 3.0. Syst Biol. 2010;59(3):307-21.
131. Chassaing B, Aitken JD, Malleshappa M, Vijay-Kumar M. Dextran sulfate sodium (DSS)-induced colitis in mice. Curr Protoc Immunol. 2014;104:15.25.1-15.25.14.
132. Schäffler H, Breitrück A. *Clostridium difficile*- From Colonization to Infection. Front Microbiol. 2018;9:646.
133. Hung CC, Ji DD, Sun HY, Lee YT, Hsu SY, Chang SY, et al. Increased risk for Entamoeba histolytica infection and invasive amebiasis in HIV seropositive men who have sex with men in Taiwan. PLoS Negl Trop Dis. 2008;2(2):e175.
134. Zhou F, Li M, Li X, Yang Y, Gao C, Jin Q, et al. Seroprevalence of Entamoeba histolytica infection among Chinese men who have sex with men. PLoS Negl Trop Dis. 2013;7(5):e2232.
135. Shirley DT, Farr L, Watanabe K, Moonah S. A Review of the Global Burden, New Diagnostics, and Current Therapeutics for Amebiasis. Open Forum Infect Dis. 2018;5(7):ofy161.
136. Mabbott NA. The Influence of Parasite Infections on Host Immunity to Co-infection With Other Pathogens. Front Immunol. 2018;9:2579.
137. Salles JM, Moraes LA, Salles MC. Hepatic amebiasis. Braz J Infect Dis. 2003;7(2):96-110.
138. Kocherscheidt L, Agossou A, Gantin RG, Hamm DM, Banla M, Soboslay PT. Cytokine and chemokine responses in adults, newborns and children exposed to Entamoeba histolytica/dispar, Onchocerca volvulus and Plasmodium falciparum. Pediatr Allergy Immunol. 2010;21(4 Pt 2):e756-63.

139. Bruchhaus I, Tannich E. Induction of the iron-containing superoxide dismutase in Entamoeba histolytica by a superoxide anion-generating system or by iron chelation. Mol Biochem Parasitol. 1994;67(2):281-8.
140. Saha P, Xiao X, Li Y, Golonka RM, Abokor AA, Yeoh BS, et al. Distinct iron homeostasis in C57BL/6 and Balb/c mouse strains. Physiol Rep. 2020;8(9):e14441.
141. SM M. Arginine: master and commander in innate immune responses. Science signaling. 2010;3(135).
142. Lin JY, Chadee K. Macrophage cytotoxicity against Entamoeba histolytica trophozoites is mediated by nitric oxide from L-arginine. J Immunol. 1992;148(12):3999-4005.
143. K E, R S-T, S A. Consumption of L-arginine mediated by Entamoeba histolytica L-arginase (EhArg) inhibits amoebicidal activity and nitric oxide production by activated macrophages. Parasite immunology. 2003;25(11-12).
144. A M, V D, S A, S T. Structural insights into Entamoeba histolytica arginase and structure-based identification of novel non-amino acid based inhibitors as potential antiamoebic molecules. The FEBS journal. 2019;286(20).
145. Jeelani G, Nozaki T. Metabolomic analysis of Entamoeba: applications and implications. Curr Opin Microbiol. 2014;20:118-24.
146. Zuo X, Coombs GH. Amino acid consumption by the parasitic, amoeboid protists Entamoeba histolytica and E. invadens. FEMS Microbiol Lett. 1995;130(2-3):253-8.
147. Ren W, Chen S, Yin J, Duan J, Li T, Liu G, et al. Dietary arginine supplementation of mice alters the microbial population and activates intestinal innate immunity. J Nutr. 2014;144(6):988-95.
148. Uhlén M, Fagerberg L, Hallström BM, Lindskog C, Oksvold P, Mardinoglu A, et al. Proteomics. Tissue-based map of the human proteome. Science. 2015;347(6220):1260419.
149. Lanas A. Role of nitric oxide in the gastrointestinal tract. Arthritis Res Ther. 2008;10 Suppl 2:S4.
150. Kimura H, Hokari R, Miura S, Shigematsu T, Hirokawa M, Akiba Y, et al. Increased expression of an inducible isoform of nitric oxide synthase and the formation of peroxynitrite in colonic mucosa of patients with active ulcerative colitis. Gut. 1998;42(2):180-7.
151. Tanaka A, Mizoguchi H, Kunikata T, Miyazawa T, Takeuchi K. Protection by constitutively formed nitric oxide of intestinal damage induced by indomethacin in rats. J Physiol Paris. 2001;95(1-6):35-41.
152. Seydel KB, Smith SJ, Stanley SL. Innate immunity to amebic liver abscess is dependent on gamma interferon and nitric oxide in a murine model of disease. Infect Immun. 2000;68(1):400-2.
153. Hatter JA, Kouche YM, Melchor SJ, Ng K, Bouley DM, Boothroyd JC, et al. *Toxoplasma gondii* infection triggers chronic cachexia and sustained commensal dysbiosis in mice. *PLoS One*. 2018;13(10).
154. Reeves GM, University of Maryland School of Medicine P, Baltimore, 21201, MD, United States, Postolache TT, University of Maryland School of Medicine P, Baltimore, 21201, MD, United States, teopostolache@gmail.com, Mazaheri S, et al. A Positive Association between T. gondii Seropositivity and Obesity. Frontiers in Public Health. 2013;0.
155. Bansal D, Bhatti HS, Sehgal R. Role of cholesterol in parasitic infections. Lipids in Health and Disease. 2005;4(1):1-7.
156. Schaible UE EKS. Malnutrition and Infection: Complex Mechanisms and Global Impacts. 2022.
157. Watanabe K, Petri WA. Learning from the research on amebiasis and gut microbiome: Is stimulation by gut flora essential for effective neutrophil mediated protection from external pathogens? Gut Microbes. 2019;10(1):100-4.
158. DY S, X B, MW T, YY Z, XL L, YH Z, et al. Changes to the gut microbiota in mice induced by infection with Toxoplasma gondii. Acta tropica. 2020;203.

159. CA W, E L, R D, JE S, JD J, ML D. Clostridium difficile and Entamoeba histolytica infections in patients with colitis in the Philippines. Transactions of the Royal Society of Tropical Medicine and Hygiene. 2012;106(7).
160. Churchill GA, Gatti DM, Munger SC, Svenson KL. The Diversity Outbred mouse population. Mamm Genome. 2012;23(9-10):713-8.
161. Byers J, Eichinger D. Entamoeba invadens: restriction of ploidy by colonic short chain fatty acids. Exp Parasitol. 2005;110(3):203-6.
162. Gregory A, Pensinger D, Hryckowian A. A short chain fatty acid–centric view of Clostridioides difficile pathogenesis. PLOS Pathogens. 2022.
163. Kobayashi S, Suzuki J, Takeuchi T. Establishment of a continuous culture system for Entamoeba muris and analysis of the small subunit rRNA gene. Parasite. 2009;16(2):135-9.
164. Tanaka M, Makiuchi T, Komiyama T, Shiina T, Osaki K, Tachibana H. Whole genome sequencing of Entamoeba nuttalli reveals mammalian host-related molecular signatures and a novel octapeptide-repeat surface protein. PLoS Negl Trop Dis. 2019;13(12):e0007923.
165. Haghshenas E, Asghari H, Stoye J, Chauve C, Hach F. HASLR: Fast Hybrid Assembly of Long Reads. iScience. 2020;23(8):101389.
166. Silva-Barrios S, Stäger S. Protozoan Parasites and Type I IFNs. Front Immunol. 2017;8:14.
167. van Zuylen WJ, Garceau V, Idris A, Schroder K, Irvine KM, Lattin JE, et al. Macrophage activation and differentiation signals regulate schlafen-4 gene expression: evidence for Schlafen-4 as a modulator of myelopoiesis. PLoS One. 2011;6(1):e15723.
168. Laurent F, Lacroix-Lamandé S. Innate immune responses play a key role in controlling infection of the intestinal epithelium by Cryptosporidium. Int J Parasitol. 2017;47(12):711-21.
169. Yang J-Y, Deng X-Y, Li Y-S, Ma X-C, Feng J-X, Yu B, et al. Structure of Schlafen13 reveals a new class of tRNA/rRNA- targeting RNase engaged in translational control. Nature Communications. 2018;9(1):1-13.
170. Seong RK, Seo SW, Kim JA, Fletcher SJ, Morgan NV, Kumar M, et al. Schlafen 14 (SLFN14) is a novel antiviral factor involved in the control of viral replication. Immunobiology. 2017;222(11):979-88.
171. Metallo CM, Walther JL, Stephanopoulos G. Evaluation of 13C isotopic tracers for metabolic flux analysis in mammalian cells. J Biotechnol. 2009;144(3):167-74.
172. TeSlaa T, Teitell MA. Techniques to monitor glycolysis. Methods Enzymol. 2014;542:91-114.
173. Pawlowic MC, Somepalli M, Sateriale A, Herbert GT, Gibson AR, Cuny GD, et al. Genetic ablation of purine salvage in *Cryptosporidium parvum* reveals nucleotide uptake from the host cell. Proc Natl Acad Sci U S A. 2019;116(42):21160-5.
174. CC B, GJ M. Absorbencies of six different rodent beddings: commercially advertised absorbencies are potentially misleading. Laboratory animals. 2005;39(1).
175. Ebino KY, Suwa T, Kuwabara Y, Saito TR, Takahashi KW. [Lifelong coprophagy in male mice]. Jikken Dobutsu. 1987;36(3):273-6.
176. Ebino KY, Suwa T, Kuwabara Y, Saito TR, Takahashi KW. Coprophagy in female mice during pregnancy and lactation. Jikken Dobutsu. 1988;37(1):101-4.
177. Rénia L, Goh YS. Malaria Parasites: The Great Escape. Front Immunol. 2016;7:463.
178. Ralston KS, Petri WA. The ways of a killer: how does Entamoeba histolytica elicit host cell death? Essays Biochem. 2011;51:193-210.
179. Ragland B. E*ntamoeba histolytica:* Target Cells Killed by Trophozoites Undergo DNA Fragmentation Which Is Not Blocked by Bcl-2. In: Ashley L, editor. 1994.
180. Berninghausen O, Leippe M. Necrosis versus apoptosis as the mechanism of target cell death induced by Entamoeba histolytica. Infect Immun. 1997;65(9):3615-21.

181. Seydel KB, Stanley SL. Entamoeba histolytica induces host cell death in amebic liver abscess by a non-Fas-dependent, non-tumor necrosis factor alpha-dependent pathway of apoptosis. Infect Immun. 1998;66(6):2980-3.
182. Becker SM, Cho KN, Guo X, Fendig K, Oosman MN, Whitehead R, et al. Epithelial cell apoptosis facilitates Entamoeba histolytica infection in the gut. Am J Pathol. 2010;176(3):1316-22.
183. Huston CD, Houpt ER, Mann BJ, Hahn CS, Petri WA. Caspase 3-dependent killing of host cells by the parasite Entamoeba histolytica. Cell Microbiol. 2000;2(6):617-25.
184. Gilmartin AA, Ralston KS, Petri WA. Inhibition of Amebic Lysosomal Acidification Blocks Amebic Trogocytosis and Cell Killing. MBio. 2017;8(4).
185. Thapa RJ, Ingram JP, Ragan KB, Nogusa S, Boyd DF, Benitez AA, et al. DAI Senses Influenza A Virus Genomic RNA and Activates RIPK3-Dependent Cell Death. Cell Host Microbe. 2016;20(5):674-81.
186. DeFilippis VR, Alvarado D, Sali T, Rothenburg S, Früh K. Human cytomegalovirus induces the interferon response via the DNA sensor ZBP1. J Virol. 2010;84(1):585-98.
187. Rothan HA, Arora K, Natekar JP, Strate PG, Brinton MA, Kumar M. Z-DNA-Binding Protein 1 Is Critical for Controlling Virus Replication and Survival in West Nile Virus Encephalitis. Front Microbiol. 2019;10:2089.
188. Lin J, Kumari S, Kim C, Van TM, Wachsmuth L, Polykratis A, et al. RIPK1 counteracts ZBP1-mediated necroptosis to inhibit inflammation. Nature. 2016;540(7631):124-8.
189. Newton K, Wickliffe KE, Maltzman A, Dugger DL, Strasser A, Pham VC, et al. RIPK1 inhibits ZBP1-driven necroptosis during development. Nature. 2016;540(7631):129-33.
190. Dannappel M, Vlantis K, Kumari S, Polykratis A, Kim C, Wachsmuth L, et al. RIPK1 maintains epithelial homeostasis by inhibiting apoptosis and necroptosis. Nature. 2014;513(7516):90-4.
191. Pittman KJ, Aliota MT, Knoll LJ. Dual transcriptional profiling of mice and Toxoplasma gondii during acute and chronic infection. BMC Genomics. 2014;15:806.
192. Nishimura M, Tanaka S, Ihara F, Muroi Y, Yamagishi J, Furuoka H, et al. Transcriptome and histopathological changes in mouse brain infected with Neospora caninum. Sci Rep. 2015;5:7936.
193. Upton JW, Kaiser WJ, Mocarski ES. DAI/ZBP1/DLM-1 Complexes with RIP3 to Mediate Virus-Induced Programmed Necrosis that Is Targeted by Murine Cytomegalovirus vIRA. Cell Host Microbe. 2019;26(4):564.
194. Martorelli Di Genova B, Wilson SK, Dubey JP, Knoll LJ. Intestinal delta-6-desaturase activity determines host range for Toxoplasma sexual reproduction. PLoS Biol. 2019;17(8):e3000364.